Department of Defense Center for Geosciences/Atmospheric Research under cooperative agreements: #DAAD19-02-2-0005 and DAAD19-01-2-0018 and American Meteorological Society and ITT Industries, Inc. AMS/Industry/Government Graduate Fellowship 2001

THE NUMERICAL SIMULATION OF FOG WITH THE RAMS@CSU CLOUD-RESOLVING MESOSCALE FORECAST MODEL

by Russell J. Chibe

William R. Cotton, P.I.

DEPARTMENT OF ATMOSPHERIC SCIENCE

Paper No. 741

THE NUMERICAL SIMULATION OF FOG WITH THE RAMS@CSU

CLOUD-RESOLVING MESOSCALE FORECAST MODEL

BY

RUSSELL J. CHIBE

DEPARTMENT OF ATMOSPHERIC SCIENCE

COLORADO STATE UNIVERSITY

FORT COLLINS, CO 80523

RESEARCH SUPPORT BY

DEPARTMENT OF DEFENSE CENTER FOR GEOSCIENCES/ATMOSPHERIC RESEARCH

UNDER COOPERATIVE AGREEMENTS #DAAD19-02-2-0005

AND DAAD19-01-2-0018

AND

AMERICAN METEOROLOGICAL SOCIETY AND ITT INDUSTRIES, INC.

AMS/INDUSTRY/GOVERNMENT GRADUATE FELLOWSHIP 2001

JUNE 19, 2003

ATMOSPHERIC SCIENCE PAPER NO. 741

ABSTRACT.

The onset and dissipation of fog can be crucial to military operations. Fog can aid the covert movement of troops or equipment, or it can disrupt aerial maneuvers. Fog also causes accidents on roadways and disrupts air transportation. While many weather phenomena are forecast using numerical models, most mesoscale forecast models do not have the vertical resolution necessary to forecast fog and low-level clouds. Previously-published one-dimensional fog models do not provide valuable information about the spatial characteristics of a fog event. In this study, the RAMS@CSU cloud-resolving mesoscale forecast model is run in a real-time configuration with a sophisticated microphysical package and multiple nested grids, in which the smallest grid has increased vertical resolution in the lower boundary layer. Using this configuration, two specific fog events are simulated in 3-D using initialization data with a horizontal resolution of 40 km. In both cases, fog is simulated in the lowest vertical level. In the first case, a valley fog event in central California, the onset and dissipation of fog are both simulated one hour early. Errors are attributed to slight inaccuracies in the simulation of thermal cooling and moisture evaporation from the surface. In the second case, a radiation fog in eastern Wisconsin, fog is simulated in patches, while observations showed a homogeneous fog layer over the domain of the third grid. Where fog is simulated, the onset of fog is four hours late, while the dissipation is simulated the same hour as observed. The patchy nature of the fog is attributed to errors in the simulated wind field, and the error in the timing of the fog's development is attributed to inaccuracies in the simulated wind field and thermal cooling. The model is shown to simulate fine-scale features observed in the formation of fog, including valley circulations and the development of a dewpoint inversion. The results of the simulations suggest that the RAMS@CSU model can simulate the microphysical processes involved in both the formation and dissipation in fog. Sensitivity studies suggest that the quasi-microscale nature of fog makes the accuracy of a simulation heavily dependent on both the quality and resolution of the initialization data, including soil moisture data. Sensitivity studies also suggest that the accurate simulation of fog requires a vertical resolution greater than 100 m in the lower boundary layer. While the simulation results still offer room for improvement, this study is the first to simulate fog, using a 3-D forecast model, with such accuracy on such a fine scale, both spatially and temporally. The RAMS@CSU model can provide a valuable tool to military, government, and private sector forecasters, offering useful guidance as to the time and location of fog events.

Russell Jason Chibe
Department of Atmospheric Science
Colorado State University
Fort Collins, CO 80523
Summer 2003

ACKNOWLEDGEMENTS.

I would like to acknowledge the following people without whom this research would not have been completed. First and foremost, I wish to thank my advisor, Dr. William Cotton, and my thesis committee members, Dr. Richard Johnson and Dr. David Krueger, for their time and insight. Past and current members of the Cotton research group, particularly Dr. Susan van den Heever, Dr. William Cheng, Ray McAnelly, Travis Ashby, and Stephen Saleeby, have contributed significantly to this research and their assistance is acknowledged and greatly appreciated. Thanks to Dr. Stanley Kidder of the Cooperative Institute for Research in the Atmosphere, who prepared the satellite data presented in this study, and Dr. Jeffrey Collett and Hui Chang of Colorado State University, who provided the CRPAQS data used in this study. Christopher Castro of Colorado State University is acknowledged for providing assistance in integrating soil data into the RAMS model. Thanks also to Rusty Kapela of the Milwaukee National Weather Service Office and Mike Adams of the Wisconsin Department of Transportation for providing data on the impact of fog in Wisconsin. I wish to recognize all those involved in the development of the RAMS@CSU model, particularly Dr. Cotton, Dr. Roger Pielke, and Dr. Robert Walko, as their hard work formed the foundation for this study. I wish to thank Liz Zarovy of the Cotton research group for her thoughtful revisions, and R. Todd Gamber, system administrator for the Cotton group, for his technical assistance. A special thanks to Brenda Thompson, project coordinator of the Cotton research group, for all her assistance over the past two years. Most importantly, I thank the Lord for bringing me to this point in my life. "The mind of man plans his way, but the Lord directs his steps." -- Proverbs 16:9

This study was generously supported by the American Meteorological Society and ITT Industries under an AMS/Industry/Government graduate fellowship and by the Department of Defense Center for Geosciences/Atmospheric Research under cooperative agreements #DAAD19-02-2-0005 and #DAAD19-01-2-0018.

As soon as I got started I took out after the raft, hot and heavy, right down the towhead. That was all right as far as it went, but the towhead warn't sixty yards long, and the minute I flew by the foot of it I shot out into the solid white fog, and hadn't no more idea which way I was going than a dead man.

... I throwed the paddle down. I heard the whoop again; it was behind me yet, but in a different place; it kept coming, and kept changing its place, and I kept answering, till by and by it was in front of me again, and I knowed the current had swung the canoe's head down-stream, and I was all right if that was Jim and not some other raftsman hollering. I couldn't tell nothing about voices in a fog, for nothing don't look natural nor sound natural in a fog.

--Mark Twain, *The Adventures of Huckleberry Finn*

TABLE OF CONTENTS

CHAPTER ONE: INTRODUCTION

1.1 FOG: AN OVERVIEW OF ITS STRUCTURE AND IMPORTANCE

The *Glossary of Meteorology* defines fog as "[w]ater droplets suspended in the atmosphere in the vicinity of the earth's surface that affect visibility" (Glickman, 2000). Researchers have identified three primary processes by which fog forms: the cooling of air to the dewpoint, the addition of water vapor to the air, and the vertical mixing of moist air parcels of different temperatures. While fog generally forms by a combination of processes, one process generally dominates, and a fog event can be categorized into one of four main types: radiation fogs, which are dominated by radiative cooling; frontal fogs, which are dominated by the addition of water vapor; advection fogs, which are dominated by vertical mixing; and ice and snow fogs, which are defined by the physical state of the condensate rather than by the mechanism of the fog's formation (Cotton and Anthes, 1989). For cases of fog deeper than a few meters, Oliver *et al.* (1978) found that radiation almost always plays a significant role, even in cases in which another mechanism is considered dominant. Fog typically lasts for two to six hours (Cotton and Anthes, 1989) and ranges in liquid water content from 0.015 to 0.4 g kg^{-1} (Seinfeld and Pandis, 1998). Fog formation is often

accompanied by weak winds; winds greater than 2 m s^{-1} are often associated with fog dispersal, as they induce the vertical mixing of drier air (Cotton and Anthes, 1989).

Perhaps because fog does not directly harm people or property in the manner that tornadoes, thunderstorms, and hurricanes do, no comprehensive study of the societal impact of fog has been published. However, the indirect effects of fog are undeniable. Fog indirectly impacts the environment in two main ways: by reducing visibility, and by serving as a liquid aerosol which can maintain contact with structures and vegetation for several hours. The effects of reduced visibility are seen quite regularly on our roads and at our airports. While no national statistics are available, the Wisconsin Department of Transportation reports that an average of 2000 fog-related accidents were reported annually in Wisconsin from 1988 to 1999, with 25 deaths and 1000 injuries resulting each year (Adams, 2003). In the Fresno, CA area, five people were killed in four crashes, each of which involved ten or more vehicles, in the year 2002 alone (Fitzenberger, 2003). With regards to the aviation industry, the National Aviation Weather Program Council recently reported that accidents, injuries, delays, and unexpected operating costs resulting from adverse weather cost an estimated $3 billion, with 74% of 109 fatal, weather-related accidents in 1995 resulting from conditions consistent with the presence of fog (Whiffen, 2001). Unfortunately, more specific data on the impact of fog on the aviation industry are unavailable. The lack of visibility associated with fog can have other adverse effects in various regions; in Nigeria, the presence of fog has been linked to piracy and armed robbery against ships and aircraft in the Niger Delta (Ediang, 2001). It is a logical extension of these studies that the presence or absence of fog in a battlefield environment would certainly impact military operations (Seagraves and Szymber, 1995).

The role of fog, viewed by atmospheric chemists as an aerosol in the liquid dispersion phase (Seinfeld and Pandis, 1998), in aqueous-phase chemistry leads to further environmental impacts. Fog has been found to be important in the maintenance of ecosystems (Weathers, 1999); it plays a role in the dispersal of bacteria and fungi (Bauer et al, 2001), and the variation of fog in Chile associated with the El Niño/Southern Oscillation has been found to impact the local zoology (Larrain, 2001). Herckes *et al.* (2001) found fog to play an important role in urban air quality. Fog is even being investigated as a source of drinking water (Ali, 2001; Jaén, 2001). As biological and chemical attacks continue to be a threat, both domestic and abroad, the aforementioned studies suggest that the potential impact of fog as a dispersal mechanism could be even greater in a battlefield environment.

1.2 A HISTORY OF RESEARCH IN THE NUMERICAL MODELING OF FOG

With the importance of fog having been established, one must now turn to the question of how we as a society can mitigate the impact of fog. Like other meteorological phenomena which significantly impact society (hurricanes, blizzards, etc.), two main options emerge: prevent the event, or forecast the event so that the public may prepare for it. In this study, the author will focus on the latter. Operational meteorologists have been issuing heuristic fog forecasts, particularly in geographic locations where it is a common phenomenon, for decades (Croft *et al.*, 1997). However, the accuracy of such forecasts is often dependent on the meteorologist's experience in a given region. Weather offices with high forecaster turnover, such as many military bases, are less likely to consistently predict fog (Tag and Peak, 1996). While meteorologists have relied on numerical forecast models as

a valuable forecasting tool, such guidance has not been available for the forecasting of fog and low-level clouds. This is generally due to two factors: a lack of necessary vertical resolution at the lowest levels, and inadequate microphysical parameterizations. Further complicating the numerical modeling of fog is the fact that the existence of fog in a model often reduces the accuracy of the overall forecast due to a positive feedback with the long-wave radiative cooling (Teixeira, 1999). Recent improvements in these areas, however, have allowed researchers to turn to numerical models for an improved understanding of fog.

Due to computational and data limitations, most early numerical studies of fog employed one-dimensional column models. Early fog simulations focused mainly on radiation fog, though they neglected important physics processes involved in the fog's development. Rohde (1962) and Fisher and Caplan (1963) both neglected the gravitational settling of fog as well as radiative cooling. One of the first studies to integrate a sophisticated radiation scheme into a numerical model was Zdunkowski and Nielsen (1969). Their model's radiation scheme allowed for water vapor and liquid water contributions to radiative fluxes, and included several regimes of exchange coefficients. Zdunkowski and Nielsen found that their model computed liquid water content and temperature profiles that were in general agreement with observations, though the vertical growth of fog usually proceeded too rapidly. Brown and Roach (1976) improved on this model by allowing for the gravitational settling of droplets. Brown and Roach managed to simulate the formation and dissipation of radiation fog to a degree of accuracy never before published. However, the simulated fog events were still off by several hours, and the authors identified several areas for improvement; among these were better turbulence parameterizations and an allowance for the microphysics of the condensation process aside from the optical properties and fall speed of

fog droplets. In a later publication, Brown (1980) added an explicit formulation of the microphysics to their model, and concluded that thermal cooling, turbulent transport, and deposition of water on the soil were the most important physical processes involved in the development of a fog layer.

Following improvements in the treatment of one-dimensional turbulence, Musson-Genon (1987) simulated a radiation fog event with a one-dimensional boundary layer model. Musson-Genon placed new emphasis on the roles of turbulence and thermal radiation, and concluded that a good knowledge of the initial conditions of temperature and moisture, as well as the hydric state of the soil, is necessary for an accurate fog forecast. Musson-Genon also used a large-scale, three-dimensional model to forecast the temperature, wind, and moisture conditions for his one-dimensional boundary layer model. A short time later, Bott *et al.* (1990) introduced a one-dimensional radiation fog model with a detailed treatment of the interaction between radiative transfer and cloud microphysics. Bott *et al*. found a quasi-periodic oscillation in liquid water content (both modeled and observed) with periods of 15-20 minutes, which is believed to be the result of strong interaction between radiatively induced droplet growth and gravitational settling.

While most early fog studies examined radiation fog, several simulations of sea fog were also published. Feit (1972) extended the work of Fisher and Caplan (1963) to simulate fog in a maritime environment. Feit identified the importance of sea surface temperature dynamics in accurate sea fog forecasts. Barker (1977) introduced a two-dimensional boundary layer model, and concluded that low-level moisture is critical to forecasting marine advection fog. As such, the direction of low-level winds and the properties of the upstream air mass must be properly simulated if fog is to form in the right location. Ballard *et al.*

(1991) were the first to utilize a three-dimensional mesoscale model in the prediction of fog. In their study, they concluded that the accuracy of initial conditions are essential to accurate forecasts of "the Haar," sea fog off the coast of Scotland. Ballard *et al.* were also the first to demonstrate that greater vertical resolution increases the accuracy of the model's simulations.

While Ballard *et al.* (1991) were the first to use an operational mesoscale forecast model (the United Kingdom Meteorological Office (UKMO) mesoscale model) to predict fog, improvements in mesoscale modeling led Teixeira (1999) to simulate fog using the European Centre for Medium-Range Weather Forecasts (ECMWF) model with a state-of-the-art prognostic cloud scheme. Teixeira found that major areas of fog and mist were reproduced in high resolution 60- and 72-hour fog forecasts for Europe, though the amount of fog at 12 UTC was generally too low when compared with observations. Recently, Nakanishi (2000) published a large-eddy simulation of radiation fog. In the study, Nakanishi identified three stages of the evolution of fog: the formation, development, and dissipation stages. The formation stage of fog evolution is characterized by longitudinal rolls appearing near the ground surface. In the development stage, an initiation of transverse bands, due to Kelvin-Helmholtz instability and a sudden increase of turbulent kinetic energy, is observed. The dissipation stage of fog evolution sees an organization of longitudinal rolls and polygonal cells due to convective instability.

Bott and Trautmann (2002) recently developed a new efficient forecast model for radiation fog. A modification of the model presented by Bott *et al.* (1990), with parameterized microphysics for numerical efficiency, the model is designed for forecasting at a specific location, and as such is one-dimensional. However, if one desires a spatial fog

forecast, the only two studies to address the need as of this manuscript's completion are Ballard *et al.* (1991) and Teixeira (1999).

1.3 SCIENTIFIC OBJECTIVES

The scientific objectives of this study are threefold. The first objective is to determine whether a mesoscale numerical forecast model (in this case, the Regional Atmospheric Modeling System developed at the Colorado State University, version 4.3; from here on referred to as the RAMS@CSU model), with state-of-the-art microphysics, can produce fog. In order to test such capabilities, the operational RAMS@CSU forecast model first has to be modified. The RAMS@CSU forecast model, as it is run operationally, has its first vertical level at 100m AGL. Meteorological variables are calculated at the halfway point between vertical levels (with the ground technically being the first level), and thus the lowest forecast level is at 50m AGL. Most fog models have their lowest forecast level at 10 to 30m AGL (Teixeira, 1999; Bott and Trautmann, 2002). The RAMS@CSU forecast model runs with three horizontally-nested grids, and in order to simulate fog on the third grid, the lowest vertical levels will be nested such that the lowest vertical level is 33m AGL, with the lowest forecast level being 16m AGL. Comparing our results to observations will help identify those processes that are most integral to the formation of fog. Upon confirming that the model can indeed simulate fog, a second scientific objective needs to be addressed. That objective is to determine to what degree the RAMS@CSU model could be useful in the forecasting of fog on a regional (on the order of 100 km) scale. To determine this, two fog events will be simulated using National Center for Atmospheric Research (NCAR) Eta

analysis data at 40km resolution to initialize the model. Finally, the third scientific objective to be addressed is what factors have the greatest contribution to the model's successes and failures. In determining such factors, researchers seeking to develop subsequent fog forecast products will have a better idea of what improvements will likely have the greatest impact on forecast accuracy.

Chapter 2 provides information on the RAMS@CSU model, both in general and as used in this study. The configuration of the real-time forecast model, and modifications made for this study, will be addressed. The model's nested-grid configuration will be presented. The initialization of the model will be discussed in detail, including the various data used and the generation of time-dependent lateral boundary conditions.

Chapter 3 will provide a discussion of the two fog events simulated in this study. Both surface and upper-air observations will be examined, and the mechanisms that led to the formation of fog will be explored.

Chapter 4 examines the numerical simulation of our two case studies. The results of each simulation will be presented and compared to observations. The scientific implications of the results will be discussed.

Chapter 5 will present several sensitivity studies. Results of a simulation initialized with data of decreased horizontal resolution will be presented and analyzed. Also examined will be simulations run with different degrees of vertical nesting in the third grid. Simulations initialized with different soil moisture values will be presented and discussed.

Chapter 6 will offer a summary of the study and an interpretation of the results presented in chapters 4 and 5, and will also suggest future research. Chapter 7 will provide a list of works cited in this study.

CHAPTER TWO: REAL-TIME FORECAST SYSTEM

2.1 GENERAL MODEL DESCRIPTION

The Regional Atmospheric Modeling Systems (RAMS), developed at Colorado State University (CSU), henceforth referred to as the RAMS@CSU model, has been running as a prototype real-time mesoscale forecast model since 1991. The RAMS model was developed through the merger of a non-hydrostatic cloud model (Tripoli and Cotton, 1982), a hydrostatic version of the cloud model (Tremback, 1990), and a sea breeze model (Mahrer and Pielke, 1977). A detailed description of the model can be found in Pielke *et al.* (1992) and Cotton *et al.* (2003).

For this study, the RAMS@CSU model version 4.3 was employed to simulate the atmosphere. The model's governing equations for momentum and mass-continuity are nonhydrostatic and Reynolds-averaged (Tripoli and Cotton, 1986). When calculating velocity and pressure, a leapfrog time-differencing is used for integration; for all other quantities, a forward time-differencing is used. Predicted variables in the RAMS model include the *u*, *v*, and *w* components of the wind, ice/liquid water equivalent potential temperatures, dry air density, total water mixing ratio, and mixing ratios of six of the seven

hydrometeors considered in RAMS (rain, snow, pristine ice, hail, aggregates, and graupel). Diagnosed from the predicted variables are pressure, potential temperature, vapor mixing ratio, and the cloud mixing ratio (cloud drops being the seventh hydrometeor in RAMS).

The RAMS@CSU model uses the staggered C grid (Mesinger and Arakawa, 1976). The horizontal grid is projected into an oblique-stereographic coordinate system, where the pole of the projection is specified by the user in order to minimize distortion of the projection in the area of interest. A terrain-following σ_z coordinate system (Gal-Chen and Somerville, 1975; Clark, 1977; Tripoli and Cotton, 1982) is used in the vertical grid structure. A two-way interactive nesting grid configuration is utilized, in which a smaller, higher-resolution horizontal grid is nested in a lower-resolution parent grid. A higher-resolution vertical grid can also be configured in a nested grid. The method used to implement a nested grid configuration is discussed in Clark and Farley (1984) and Clark and Hall (1991).

The Land-Ecosystem-Atmosphere Feedback model (LEAF2) (Walko *et al.*, 2000) is used for land-surface parameterization. The LEAF2 sub-model prognoses soil, vegetation, snow cover, and canopy air temperature and moisture fields based on vertical diffusion and exchange of thermal energy and moisture with the atmosphere. Soil data, including type, moisture, and temperature, are input by the user and will be described in Section 2.3.

Several turbulent closure and radiation schemes are available in the RAMS@CSU 4.3 model, with the user specifying which scheme should be utilized. For this study, vertical eddy mixing is parameterized using the second-moment turbulent closure scheme of Mellor and Yamada (1982), with horizontal mixing predicted by the deformation K closure scheme of Smagorinsky (1963). The radiation scheme used is a two-stream longwave/shortwave

model developed by Harrington (1997). This scheme is optimal for the simulation of radiation fog, as it accounts for interaction with liquid and ice hydrometeor size-spectra.

The RAMS@CSU real-time forecast model features a robust microphysical package. The current approach to cloud parameterizations was first described in the work of Verlinde *et al.* (1990), which showed that the collection efficiencies in the full stochastic collection equation are constant. Rather than using continuous accretion approximations, Walko *et al.* (1995) implemented this approach in the RAMS@CSU model for the prediction of hydrometeor mixing ratios, using look-up tables to enable fast and accurate solutions to the collection equations. This approach was later extended to both the mixing ratio and number concentration for the seven hydrometeors considered in the RAMS@CSU model (Meyers *et al.*, 1997).

The microphysical package of the RAMS@CSU model also give the user the option of specifying the number of cloud condensation nuclei, the drop concentration, or the mean drop radius for a hydrometeor, with the other values diagnosed based on the input value. For this study, the cloud drop concentration was diagnosed, with a value of 5 cm^{-1} chosen based on valley fog observations published by Pilié *et al.* (1975b).

2.2 GRID CONFIGURATION

The operational RAMS@CSU real-time model uses a three-grid, horizontally-nested configuration. The version of the RAMS@CSU model used for this study has a slightly modified grid configuration. Like the operational model, three nested grids are used in this

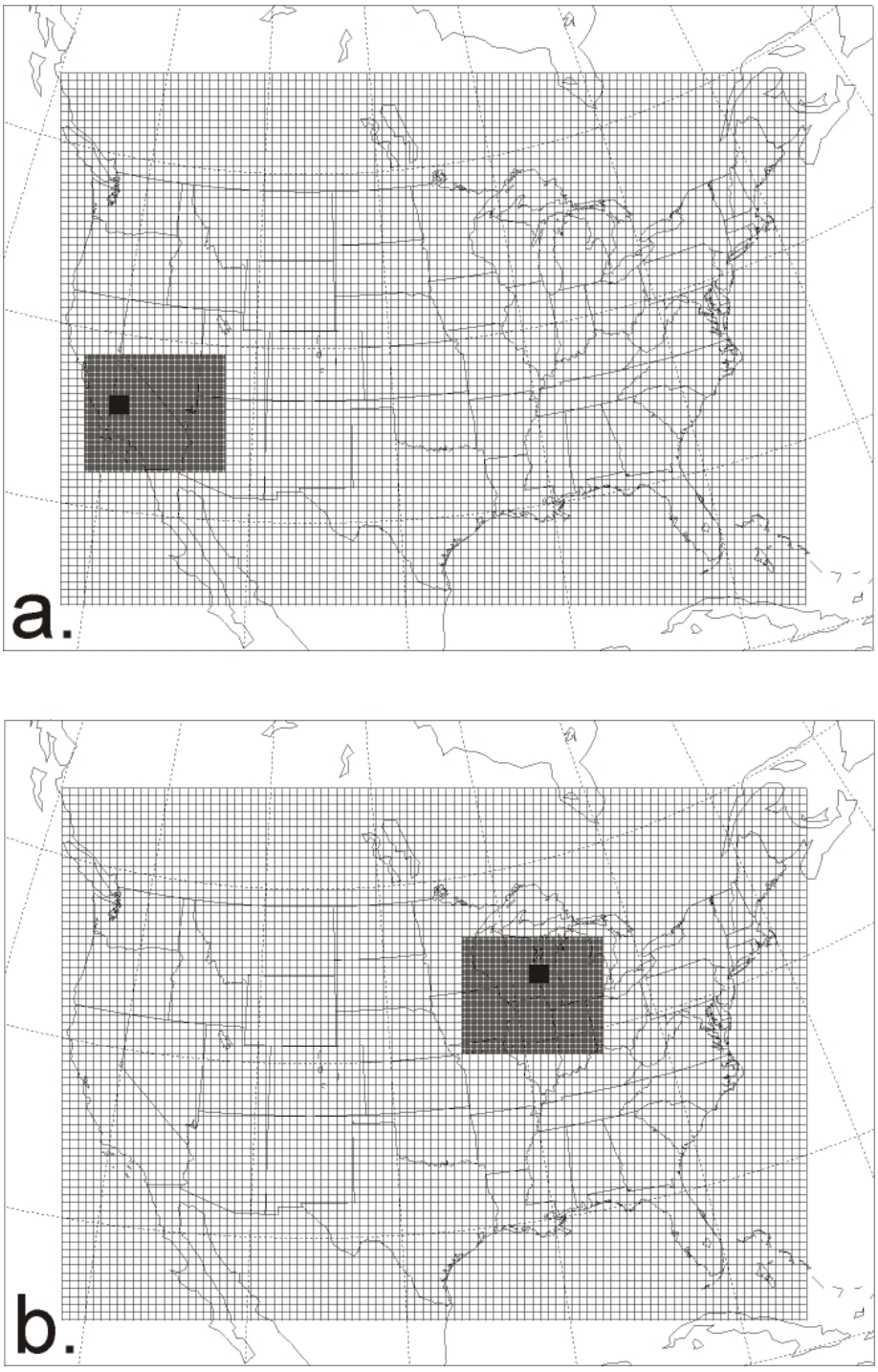

Figure 2.1 Three-grid configuration for the simulation of two cases found in this study. Configuration in (a.) is for the 21 January 2001 case near Angiola, CA. Configuration in (b.) is for the 11 October 2002 case near Sheboygan, WI.

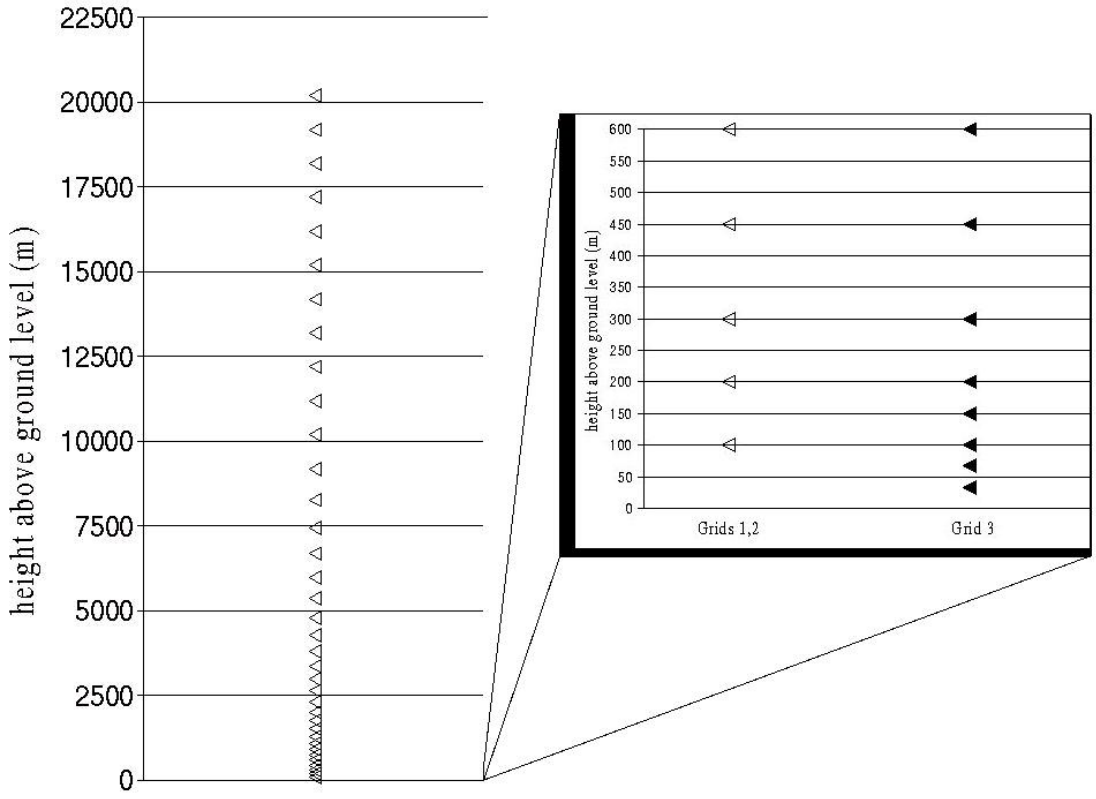

Figure 2.2 The 37 vertical levels for grids one and two are depicted by the white arrows in the left-hand column. The insert shows the lowest 600 m of the model, with the configuration for grids 1 and 2 illustrated by the white arrows on the left side of the insert, and the nested configuration for grid 3 illustrated by the black arrows on the right side of the insert.

study (Fig. 2.1). However, to accommodate the simulation of fog, additional vertical levels are nested in the third grid (Fig. 2.2).

The first grid covers the entire contiguous United States, spanning 4750 km west to east and 3400 km south to north. It features 96 × 69 grid points at 50-km resolution, with a timestep of 60 sec. The second grid spans 910 km west to east and 760 km south to north, with 92 × 77 grid points at a resolution of 10 km. The timestep of the second grid is 20 sec. The third grid, in which fog is simulated, spans 122 km in each direction, with 62 × 62 grid points at 2-km resolution and a timestep of 4 sec.

The configuration of the vertical levels for the first two grids is the same as that used in the operational RAMS@CSU model, which features 37 vertical levels as illustrated in the left-hand side of Figure 2.2. However, the third grid features two additional vertical levels nested within the first vertical level of the parent grids, and one additional vertical level nested within the second vertical level of the parent grid, as illustrated in the right-hand insert in Figure 2.2. This modification not only increases the model resolution for simulating fog, but it also moves the lowest level at which hydrometeors are produced from 50 m to 15.6 m AGL, which is consistent with the lowest level of other fog simulations (Teixeira, 1999; Bott and Trautmann, 2002). While only two cases are examined in this study, the grids can easily be moved by the user if other areas of concern are to be examined.

2.3 MODEL ALTERATIONS FOR THIS STUDY

The RAMS@CSU model was developed by the Colorado State University and the Mission Research Corporation, *ASTeR Division, to be a multi-purpose, numerical prediction model that can simulate the atmosphere from the microscale to the global scale (Cotton *et al.*, 2003). As such, there are many model specifications that must be specified by the user. Because this study is interested in examining the RAMS@CSU model's usefulness as a forecasting tool, the specifications currently used in the real-time forecast model were used in this study whenever possible. However, several modifications had to be made to the RAMS@CSU model to facilitate the simulation of fog.

One such alteration has already been described in the previous section: the modification of the three-grid structure. Two further alterations made for this study are the

use of Eta model Data Assimilation System (EDAS) 40-km data rather than 80-km data for model initialization (this topic is further addressed in Section 2.4), and the incorporation of EDAS 40-km soil moisture and soil temperature data rather than user-specified homogeneous fields. These changes were made considering the importance of accurate initialization and soil moisture data in simulating fog events (Musson-Genon, 1987). Another modification to the operational forecast model is the use of National Oceanic and Atmospheric Administration (NOAA) weekly 1° spatial resolution optimum interpolation (OI) sea surface temperature (SST) analysis data (Reynolds *et al.*, 2002), rather than thirty-year climatological values, for initializing the model's SST fields. This modification was made because both cases (as discussed in the next chapter) are near bodies of water, and Feit (1972) showed the significant role of SST's in fog formation near bodies of water.

2.4 INITIALIZATION

Two initializations are involved in running the RAMS@CSU model: the initialization of atmospheric fields and the initialization of surface fields. For the initialization of atmospheric fields, EDAS gridded analyses, as described by Rogers *et al.* (1996), are used. The data are derived from continually-cycling 3-hour forecasts produced by the Eta model. The Eta forecasts are adjusted every three hours to better conform to observational data through objective analysis. The RAMS@CSU model uses an isentropic analysis to interpolate the EDAS data into RAMS-ingestible data every three hours. While the EDAS data provide many atmospheric fields, the RAMS@CSU model uses only temperature, geopotential height, humidity, and wind component data. These values, provided for 26

pressure levels ranging from 1000 hPa to 50 hPa, are interpolated into RAMS for each of the three grids described in Section 2.2 (the EDAS soil data, mentioned in the previous section, is interpolated to the RAMS@CSU grid configuration off-line, prior to executing the model). For each grid, the portion of the Eta dataset which coincides with the RAMS grid is accessed and interpolated into a polar-stereographic/pressure coordinate dataset. The interpolation is then completed by linearly interpolating the dataset vertically to both the isentropic vertical coordinate and the terrain-following σ_z coordinate. While the operational RAMS@CSU real-time forecast model is initialized with EDAS 80-km data obtained from NCEP, this study uses EDAS 40-km data (specifically, 40.635 km in resolution) from the NCAR GEWEX (Global Energy and Water Cycle Experiment) Continental-Scale International Project (GCIP) archive for initialization.

For the initialization of surface fields, two main datasets are used. NOAA OI SST data (as described in the previous section), specific to the week of the simulation, are used to initialize the model's SST fields. The Olson Global Ecosystem (OGE) dataset (Olson *et al.*, 1985), with a spatial resolution of 0.5° is used to initialize the RAMS@CSU model's vegetation model. Both fields are linearly interpolated onto the RAMS@CSU polar-stereographic grid.

2.5 TIME-DEPENDENT LATERAL BOUNDARY CONDITIONS

In a model with a limited domain, such as the RAMS@CSU model as used in this study, external guidance is needed for the evolution of the model's boundaries. A process by which the RAMS lateral boundaries are "nudged" toward an external data analysis (also

known as Newtonian relaxation) has been developed by Davies (1976; Davies and Turner, 1977) and is used in the operational RAMS@CSU real-time model. The RAMS lateral boundary nudging scheme works by forcing the boundary values of the x- and y-components of horizontal winds (*u* and *v*, respectively), potential temperature (θ), relative humidity (r), and the Exner function (π) to externally specified values, using the model's internally-defined tendencies in the integration (Cram, 1990). This is done by adding an extra tendency term to each model prognostic equation which forces the predicted variable toward the value provided by the external guidance.

In the RAMS@CSU model, as used in real-time and in this study, Eta model forecasts (Mesinger *et al.*, 1999) provide the guidance necessary for nudging the lateral boundaries. The Eta forecasts cover much of North America and the adjacent oceans, and are generated at 32-km resolution with 45 vertical levels (Rogers *et al.*, 1996). The forecast datasets are available at 6-hour increments, from 0-hour to 48-hour. The 0-hour forecast is used for initialization (as described in the previous section), and lateral boundary conditions are updated every six hours, to coincide with the available EDAS datasets. The boundary conditions are linearly interpolated between 6-hour updates, and five horizontal nudging points are used in this study, consistent with the operational forecast model.

CHAPTER THREE: CASE STUDY OVERVIEW

3.1 OBSERVATIONS FOR 21 JANUARY 2001 FOG EVENT IN CENTRAL CALIFORNIA

In this study, two fog events are simulated. The first fog event occurred 21 January 2001 in the San Joaquin Valley of California. Patchy fog was observed from 12 UTC to 13 UTC, and a well-defined, homogeneous fog layer was observed from 14 UTC to 17 UTC. The twenty-four hour period starting at 00 UTC on 21 January is simulated. As stated in chapter one, radiation fogs are quite common to the central valleys of California, and many automobile accidents are attributed to these fogs. This particular case was chosen because data from the event were collected as part of the California Regional Particulate Air Quality Study (CRPAQS). The goal of CRPAQS was to study organic matter found in radiation fogs; an overview of the CRPAQS field campaign can be found in Herckes *et al.* (2002). Observations for CRPAQS were taken close to the small agricultural town of Angiola, CA (35.95º N, 119.54º W), and thus this location will be the focus of our first simulation. We will now examine the synoptic and mesoscale features that led to this fog event and present observations that will allow us to better understand the event.

3.1a UPPER-AIR OBSERVATIONS

Two important conditions necessary for the formation of fog are atmospheric stability and weak boundary-layer winds (Cotton and Anthes, 1989). Our main focus in examining these fields will be to determine whether the synoptic conditions will stabilize or destabilize the atmosphere over our area of concern, which can be visualized as the domain of the third grid of our simulation (centered on Angiola, CA for this case). At the 250-hPa constant-pressure level (Fig. 3.1), we see an amplified high-pressure ridge at 00 UTC, the hour at which the simulation is started. Likewise, at 500-hPa (Fig. 3.2), a high-pressure ridge is present with its axis to the east of our area of interest. Both of these observations suggest a

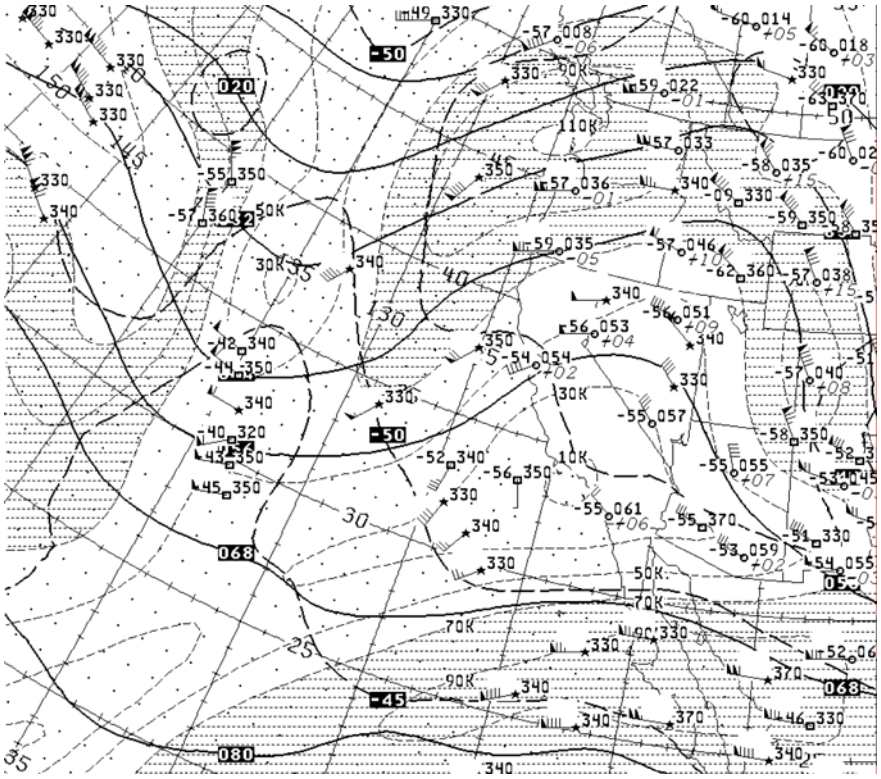

Figure 3.1 250-hPa geopotential height (solid) / temperature (thick dashed) / potential temperature (thin dashed) field, 00 UTC 21 January 2001, provided by NCEP.

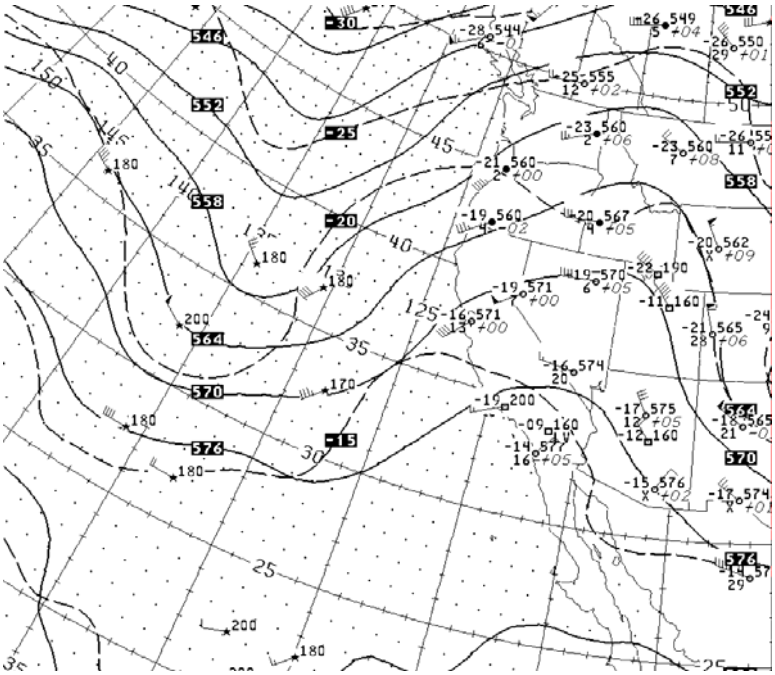

Figure 3.2 500-hPa geopotential height (solid) / temperature (dashed) field, 00 UTC 21 January 2001, provided by NCEP.

stationary, high-amplitude blocking pattern that will keep the atmosphere stable and suppress non-boundary-layer cloud formation (Bluestein, 1993). The 850-hPA geopotential height field (Fig. 3.3) further confirms the presence of an anticyclone aloft, with a height maximum located over Nevada. Overall, upper-air observations at the time of the model's initialization suggest that our area of concern will be under a high-pressure subsidence regime which should aid the formation of radiation fog by minimizing vertical mixing and suppressing cloud cover, thereby facilitating the long-wave radiative cooling that will generate fog.

3.1b SURFACE OBSERVATIONS

At 00 UTC, we observe a surface high-pressure system, centered over Idaho, dominating the weather over the entire western United States (Fig. 3.4a). A low-pressure system is observed in the eastern Pacific, off the California coast. However, the fact that the

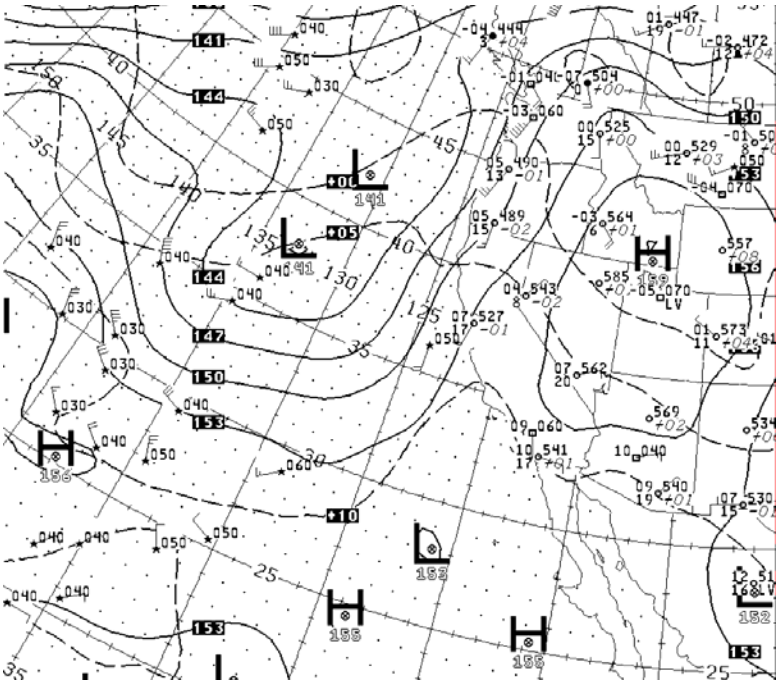

Figure 3.3 Same as Figure 3.2, but at 850-hPa.

system is already occluded, combined with the magnitude of the vertically-stacked anticyclone located over the continent, suggests that the low will not be strong enough to move the continental high and destabilize the region. A weak low is also shown in extreme southern California, though its proximity to the Pacific suggests that it is a shallow coastal front, and will likely dissipate within twelve hours (Bluestein, 1993).

Indeed, at 06 UTC, the surface analysis shows the coastal front weakening, and the low-pressure system over the Pacific remaining virtually stationary (Fig. 3.4b). It appears that the blocking pattern identified in the upper-air observations will keep the atmosphere stable for at least 24 hours, which spans the temporal domain of our simulation. At 12 UTC (Fig. 3.4c), we see very little change in the synoptic features over California, and by 00 UTC on 22 January (Fig. 3.4d) our synoptic conditions are still almost identical to

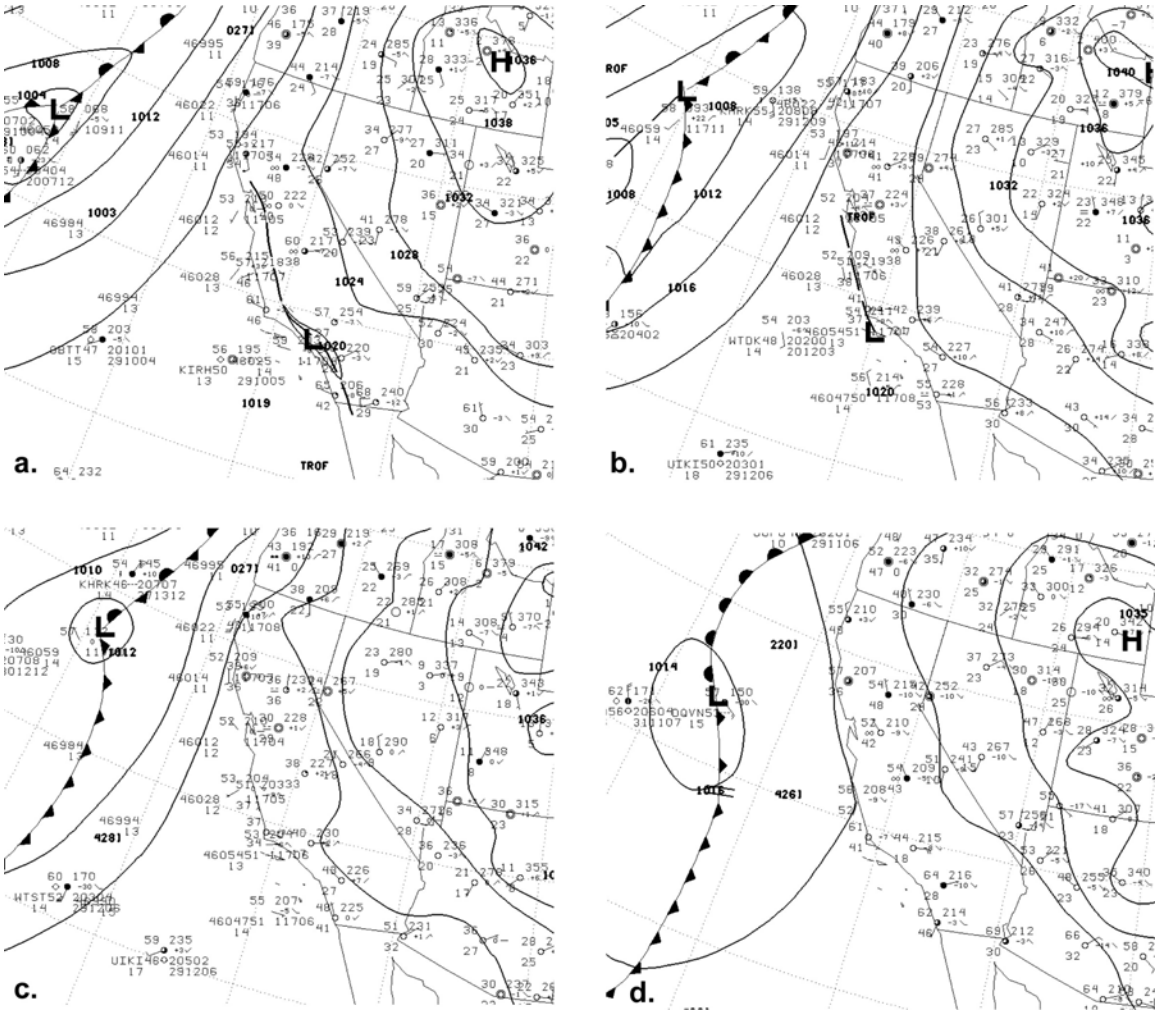

Figure 3.4 Surface analyses, 00 UTC (a.), 06 UTC (b.), 12 UTC (c.) 21 January, and 00 UTC 22 January (d.) 2001, provided by NCEP.

those twelve hours prior. The atmospheric stability and weak winds necessary for fog are present throughout the time of concern.

At this point, we will examine the mesoscale features of this event and how these features led to fog formation. The CRPAQS data only provide meteorological observations starting at 12 UTC, so observations from three nearby Automated Surface Observing System (ASOS) sites will be examined. Bakersfield, CA (KBFL: 35.43º N, 119.05°W) is located approximately 80 km southeast of Angiola. Hanford, CA (KHJO: 36.32° N, 119.63° W)

is located approximately 40 km north of Angiola. Porterville, CA (KPTV: 36.03° N, 119.07° W) is located approximately 40 km northeast of Angiola. The location of each of these sites relative to Angiola can be seen in Figure 3.5. Observations from these locations, as well as CRPAQS data, when available, can be seen in Table 3.1.

The dewpoint values throughout 21 January clearly show that there was no influx of moisture; radiative cooling was the dominant contributor to fog formation. Following sunset

	KBFL	elev:	150m		KPTV	elev:	135m	
Time	Temp	Dewpt	Winds	Cloud	Temp	Dewpt	Winds	Cloud
00 UTC	n/a	n/a	3.6	haze	17.0	2.0	3.1	clear
01	18.0	4.0	2.6	clear	11.0	4.0	2.1	clear
02	n/a	n/a	6.1	clear	11.0	4.0	0	clear
03	n/a	n/a	7.2	clear	8.0	3.0	0	clear
04	n/a	n/a	4.1	clear	7.0	2.0	3.1	clear
05	n/a	n/a	5.7	clear	6.0	2.0	2.1	clear
06	n/a	n/a	3.6	clear	4.0	1.0	1.6	clear
07	12.0	3.0	2.1	haze	3.0	1.0	3.1	clear
08	8.0	2.0	1.6	haze	3.0	0.0	3.1	clear
09	6.0	0.0	1.6	clear	4.0	0.0	2.6	clear
10	5.0	0.0	1.6	clear	3.0	-1.0	2.6	clear
11	6.0	2.0	0	haze	1.0	-2.0	2.6	clear
12	11.0	0.0	4.1	clear	2.0	-1.0	3.6	clear
13	5.0	1.0	2.6	clear	1.0	-1.0	1.6	clear
14	2.2	0.6	2.1	mist	1.0	-2.0	1.6	clear
15	4.4	0.0	2.1	clear	3.0	-2.0	2.1	clear
16	7.0	1.0	3.6	haze	2.0	-2.0	2.6	clear
17	12.0	1.0	5.7	clear	5.0	0.0	3.1	clear
18	12.0	2.0	3.1	haze	9.0	1.0	3.1	clear
19	16.0	1.0	2.1	clear	13.0	-1.0	0	clear
20	17.2	1.7	3.1	clear	n/a	n/a	n/a	n/a
21	n/a	n/a	n/a	n/a	n/a	n/a	n/a	n/a
22	n/a	n/a	n/a	n/a	n/a	n/a	n/a	n/a
23	n/a	n/a	n/a	n/a	n/a	n/a	n/a	n/a
00	n/a	n/a	n/a	n/a	n/a	n/a	n/a	n/a

Table 3.1 ASOS observations for 21 January 2001. Temperatures and dewpoints are in degrees Celsius; wind speeds are in meters per second. KBFL is Bakersfield, KPTV is Porterville, and KHJO is Hanford. Angiola data is from the CRPAQS field campaign. Continued on next page.

(01:12 UTC), a steady radiative cooling is observed at each station until around 14:00 UTC,

with sunrise occurring at 15:05 UTC. While mesonet data are unavailable, the 15:00 UTC surface analysis (Fig. 3.6) shows an observation of northwest winds at the north end of the San Joaquin Valley and an observation of southeast winds at the south end, suggesting the development of a valley drainage flow. Note also in Table 3.1 that a decrease in dewpoint is observed at KHJO and KPTV. Both of these observations are consistent with the model of radiative valley fog developed by Pilié *et al.* (1975a). In the

	KHJO	elev:	74m		Angiola	elev:	0m	
Time	Temp	Dewpt	Winds	Cloud	Temp	Dewpt	Winds	Cloud
00 UTC	15.6	5.6	3.1	clear				
01	15	6.1	0	haze				
02	10.6	6.1	0	haze				
03	10.6	5	2.1	haze				
04	10	5.6	3.6	haze				
05	8.3	5.0	1.6	haze				
06	7.8	4.4	2.1	haze				
07	7.2	4.4	0	haze				
08	3.9	2.8	1.6	clear				
09	4.4	3.3	1.6	clear				
10	4.4	3.3	2.6	clear				
11	3.3	2.8	0	clear				
12	2.2	1.7	0	clear	n/a	n/a	n/a	fog
13	1.7	1.1	2.1	overcast	n/a	n/a	n/a	clear
14	0.6	0.6	0	clear	2.7	2.0	2.1	fog
15	1.1	0.6	3.1	scattered	2.6	2.0	1.2	fog
16	2.2	1.7	1.6	scattered	3.0	2.5	2.4	fog
17	4.4	3.9	2.1	clear	5.1	4.5	0.8	fog
18	7.2	5.0	1.6	clear	n/a	n/a	n/a	clear
19	10	7.2	1.6	clear				
20	n/a	n/a	n/a	n/a				
21	n/a	n/a	n/a	n/a				
22	n/a	n/a	n/a	n/a				
23	n/a	n/a	n/a	n/a				
00	n/a	n/a	n/a	n/a				

Table 3.1 (continued)

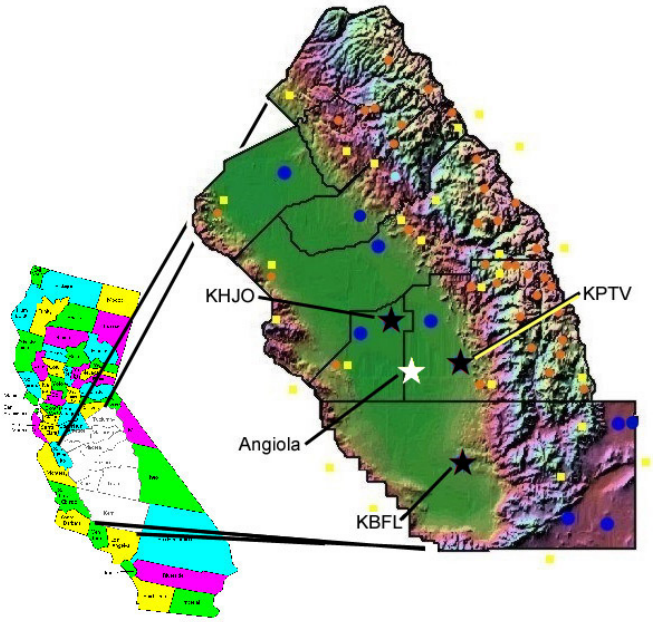

Figure 3.5 Map of observations used in the 21 January case study. Black stars represent ASOS sites (labeled with their four-letter identifiers) and the white star represents Angiola, the site of the CRPAQS field study.

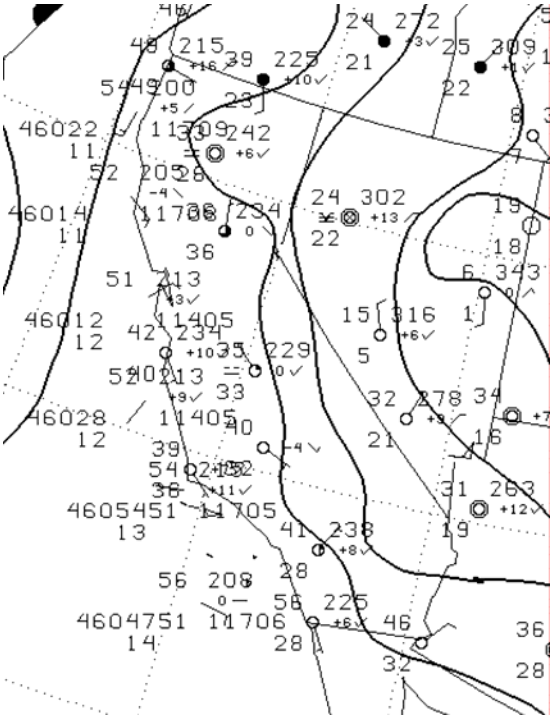

Figure 3.6 Surface analysis, 15 UTC 21 January 2001, provided by NCEP.

model, radiative cooling leads to a downslope flow of cool, dense air into the valley. Dew deposition at the cool surface reduces surface dewpoints and generates a dewpoint inversion. Convergence of downslope winds forces the cooler air upward, leading to saturation at mid-levels (50-200m AGL). The fog at mid-levels descends to the surface, due to continued cooling and turbulent mixing, in one-half to one hour. One observation that does not fit this model is the presence of overcast conditions at KHJO at 13 UTC. This observation will be examined in the next subsection, with the introduction of satellite observations.

The fog observed at Angiola persists for two hours after sunrise. The persistence of radiative fog after sunrise is believed to result from the evaporation of dew at the surface (Pilié *et al.,* 1975b). This evaporation also explains the observed increase in dewpoints at Angiola and KHJO after 15:00 UTC. Once all the surface dew evaporated, the surface heating destabilized the lower boundary layer, thereby dissipating the fog through vertical mixing.

3.1c SATELLITE IMAGERY

This study is interested in providing a spatial fog forecast. As such, spatial observations of our two fog events are of great interest. Due to the lack of mesonet data, the most effective means of observing the two-dimensional evolution of each event is through satellite observations. For this study, Geostationary Operational Environmental Satellite (GOES) I-M-series data are used. For nocturnal observations, the 3.9μm albedo product is used, with the 0.65μm albedo product used after sunrise (Kidder *et al.*, 2000). While

observed clouds may not always be fog, cross-referencing the GOES imagery with available ASOS surface data allows us to accurately identify fog.

In the 3.9μm albedo product, fog and other low clouds are visible as bright white. Upper-air cold clouds create a "negative albedo," and as such appear black. At 11:15 UTC (Fig. 3.7a), a small patch of low cloud appears to be forming to the northwest of Angiola, but no low clouds are visible over Angiola. High clouds are also visible northwest of Angiola. These high clouds likely explain the observation of overcast and scattered conditions between 13 and 16 UTC at KHJO, northwest of Angiola. At 12:15 UTC (Fig. 3.7b), when patchy fog was observed at Angiola, no low clouds are detected by the 3.9μm albedo product, suggesting the fog was localized. At 13:15 UTC (Fig. 3.7c), when clear skies were again reported at Angiola, a small patch of fog appears to be developing just south of Angiola; a line of fog may also be developing along the 120° line of longitude northwest of Angiola, though high clouds obscure our observation. By 14:15 UTC (Fig. 3.7d), low clouds are clearly developed to the northwest of Angiola. Though high clouds obscure the observation of low clouds over Angiola, the surface observation of fog at this time suggests that the fog is developing from north to south, as hypothesized in the previous subsection. At 15:15 UTC (Fig. 3.7e), fog can clearly be identified stretching north from Angiola. Unfortunately, at this point the sun is rising, and subsequent 0.65μm albedo product images are too obscured by high clouds to offer further observations of the fog event. However, the nocturnal 3.9μm albedo images have captured the development of the fog and give us a general idea of the fog's spatial distribution, which will be useful in verifying our model results.

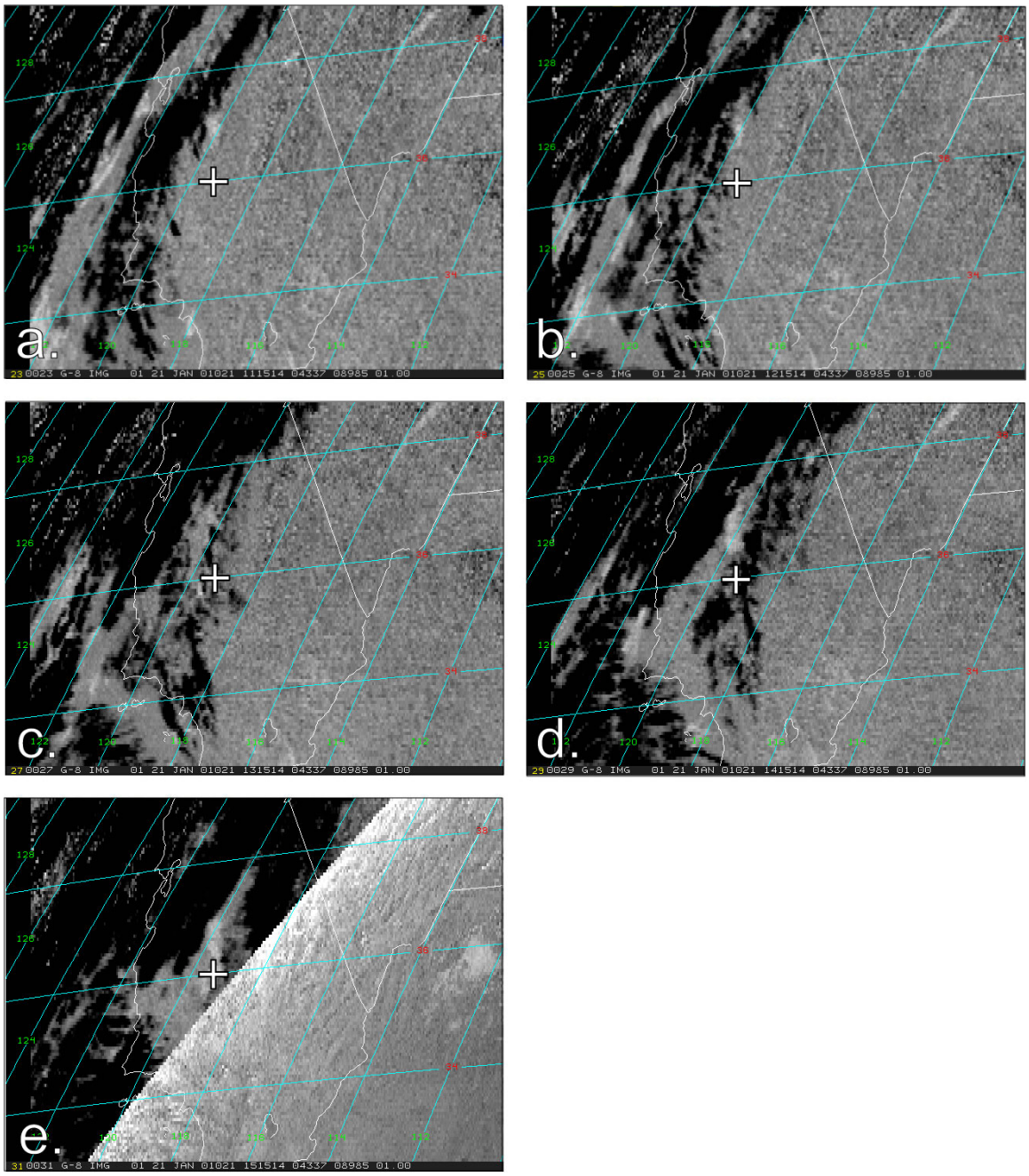

Figure 3.7 GOES-8 imagery, 3.9μm albedo products, for 11:15 UTC (a.), 12:15 UTC (b.), 13:15 UTC (c.), 14:15 UTC (d.), and 15:15 UTC (e.), 21 January 2001. Low clouds, including fog, are displayed as bright white, while high clouds are black. The white line bisecting panel (e.) represents the switch from the 3.9μm albedo product (left side of image) to the 0.65μm albedo product (right side of image) as the sun rose. Angiola, CA is marked with a white cross on all images. Images prepared by Stan Kidder/CIRA.

3.2 OBSERVATIONS FOR 11 OCTOBER 2002 FOG EVENT IN EASTERN WISCONSIN

Dense fog is common along Interstate-43, which runs along the western coast of Lake Michigan, between Milwaukee, WI and Green Bay, WI. The Wisconsin Department of Transportation estimated that fog, smog, and smoke contributed to over 1,000 crashes in 2001 alone (Johnson, 2002). On the morning of 11 October 2002, dense fog on the interstate led to a 38-car accident in Sheboygan County, which took the lives of ten motorists. While, unlike our first case study, there was no field project taking detailed meteorological observations during the fog, there is an ASOS located in Sheboygan, WI (KSBM: 43.77°N, 87.85° W). Fog was observed from 00 UTC to 15 UTC on 11 October at KSBM. Our second simulation is initialized at 18 UTC on 10 October and run for 24 hours. We will now examine the synoptic and mesoscale features that led to this second fog event, and present observations that will allow us to better understand the event.

3.2a UPPER-AIR OBSERVATIONS

Compared to the 21 January California event, upper-air observations suggest the atmosphere over Wisconsin on 11 October was less stable. At the 250-hPa constant-pressure level (Fig. 3.8), one can see that Wisconsin is under the entrance region of the polar jet at 00 UTC 11 October. However, by 12 UTC, the jet has propagated eastward and the flow has become much more zonal, suggesting increased stability as the day proceeded. Similarly, at 500-hPa (Fig. 3.9), we see the development of split flow over the Great Lakes from 00 UTC

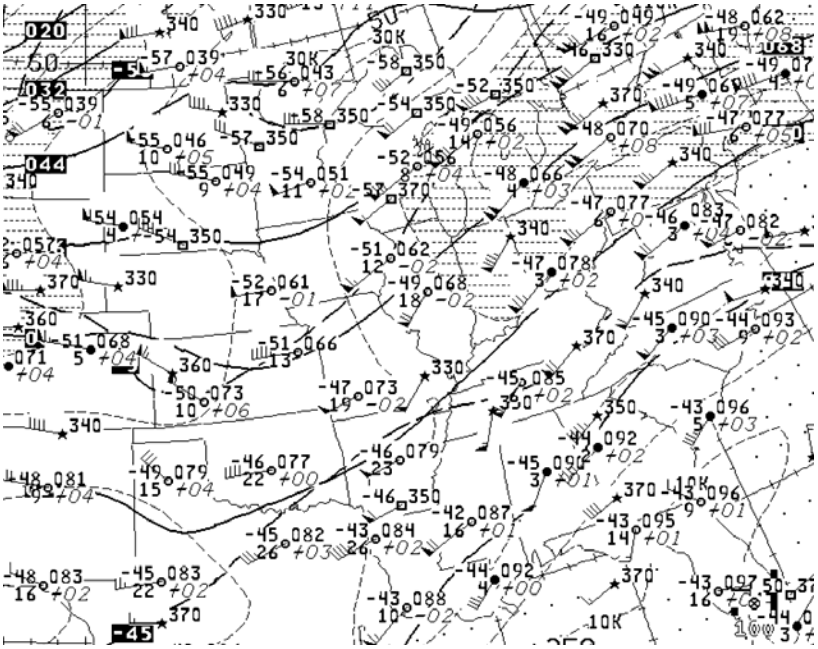

Figure 3.8 250-hPa geopotential height (solid) / temperature (thick dashed) / potential temperature (thin dashed) field, 00 UTC 11 October 2002, provided by NCEP.

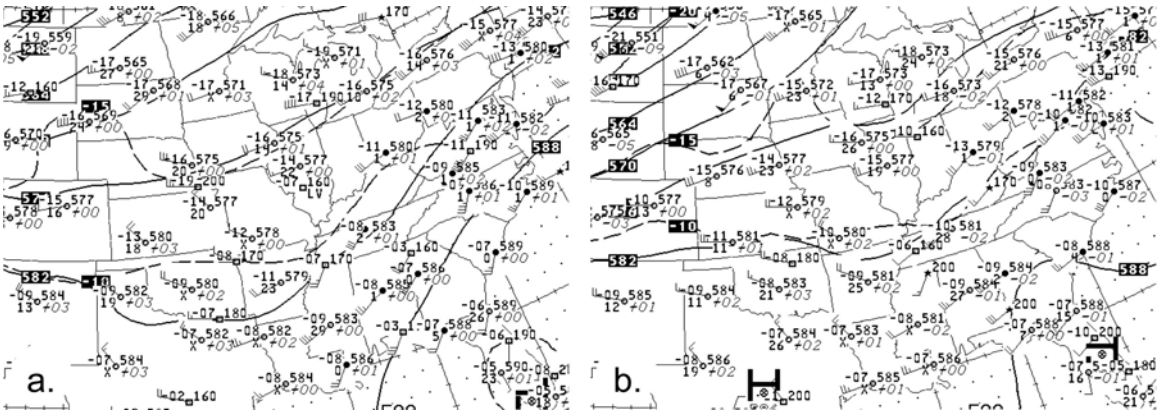

Figure 3.9 500-hPa geopotential height (solid) / temperature (dashed) fields, for 00 UTC (a.) and 12 UTC (b.) 11 October 2002, provided by NCEP.

to 12 UTC, further suggesting increasing stability on the north side of the split flow (Bluestein, 1993). At 850-hPa (Fig. 3.10), 00 UTC observations indicate that Wisconsin is in transitional phase between a high-pressure system that has moved over New England and a low-pressure system that is approaching from the west. However, the low does not reach our area of concern until 12 October. Unlike the 21 January fog event in California, the upper-air observations for the Wisconsin event do not suggest strong stability and subsidence; however, they do suggest that the atmosphere became more stable with time. The transitional nature of the upper-air flow is weak enough so as to not dominate the mesoscale and microscale features which will lead to the formation of fog.

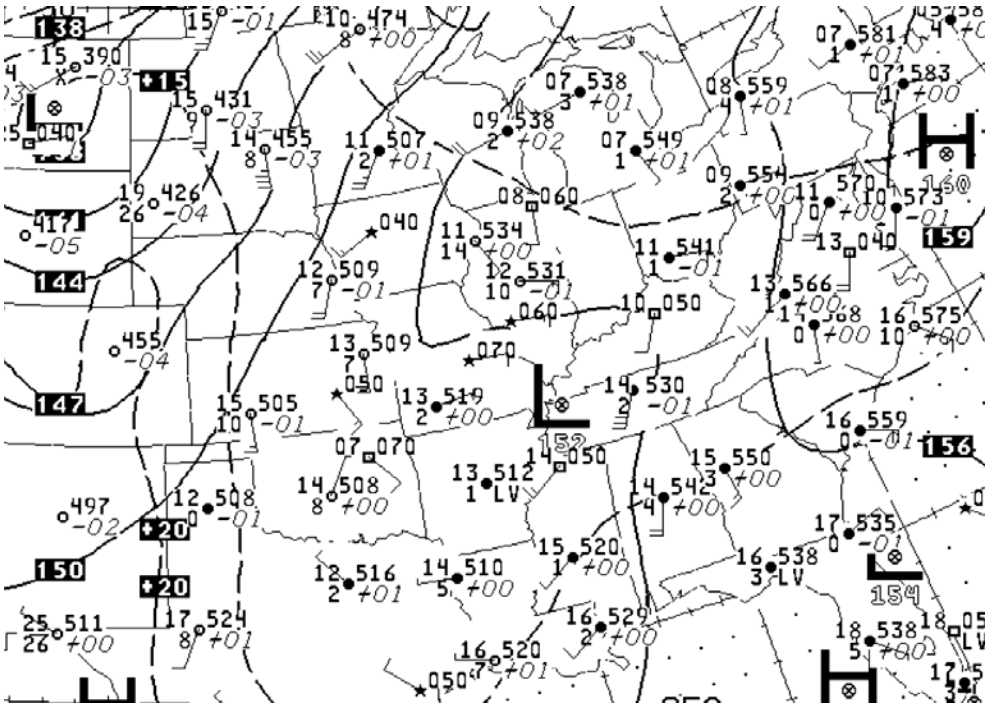

Figure 3.10 850-hPa geopotential height (solid) / temperature (dashed) field, 00 UTC 11 October 2002, provided by NCEP.

3.2b SURFACE OBSERVATIONS

Six hours prior to the start of our simulation, at 12 UTC on 10 October (Fig. 3.11a), a low-pressure system is centered over northern Minnesota, with heavy rain being observed in the warm sector of the system. However, as the upper-level support weakens, so too does the surface cyclone. At 00 UTC (Fig. 3.11b), all that is left of the cyclone is a stationary front. By 03 UTC (Fig. 3.11c), most of the stationary front is no longer identifiable, and reports of fog can be seen all across the northern Great Lakes. At 12 UTC (Fig. 3.11d), widespread reports of fog persist across northern and eastern Wisconsin. At 18 UTC (Fig. 3.11e), winds across Wisconsin shift from east-southeast to south, and fog is no longer observed.

With this background we will now observe the mesoscale and microscale features that led to this fog event. Hourly observations from KSBM can be found in Table 3.2. Unlike the 21 January event, the precipitation which preceded this event has left a relatively humid atmosphere. With sundown at 23:18 UTC, the atmosphere quickly radiatively cooled to its dewpoint. This combined with the lack of wind led to a quick fog formation.

After sundown, a steady decrease in dewpoint is observed. As in the 21 January event, this can be traced to surface dew deposition, and the subsequent increase in dewpoint after sunrise is partly the result of the dew's evaporation. The evaporation of ground moisture allows for the atmosphere to maintain saturation for several hours after the 11:58 UTC sunrise. However, by 16 UTC, ground moisture has been evaporated, and an increased wind mixes the lower boundary layer, thus dissipating the fog.

	KSBM			
Time	Temp	Dewpt	Winds	Cloud
18 UTC 10/10	n/a	n/a	n/a	n/a
19	n/a	n/a	n/a	n/a
20	n/a	n/a	n/a	n/a
21	n/a	n/a	n/a	n/a
22	n/a	n/a	n/a	n/a
23	13.3	11.1	2.1	clear
00 UTC 10/11	11.7	10.6	2.6	mist
01	8.9	8.9	0	fog
02	7.8	7.8	0	fog
03	7.8	7.8	0	fog
04	7.2	7.2	0	fog
05	7.2	7.2	0	fog
06	7.2	7.2	0	fog
07	6.7	6.7	0	fog
08	6.1	6.1	0	fog
09	6.1	6.1	0	mist
10	6.1	6.1	0	fog
11	5.6	5.6	0	fog
12	5.6	5.6	0	fog
13	7.2	6.7	0	fog
14	10.0	10.0	0	fog
15	13.9	13.3	3.6	mist
16	17.2	11.1	3.6	clear
17	19.4	9.4	4.6	clear
18	19.4	10.0	5.7	clear

Table 3.2 ASOS observations for 10-11 October 2002, from KSBM (Sheboygan, WI). Temperatures and dewpoints are in degrees Celsius; wind speeds are in meters per second.

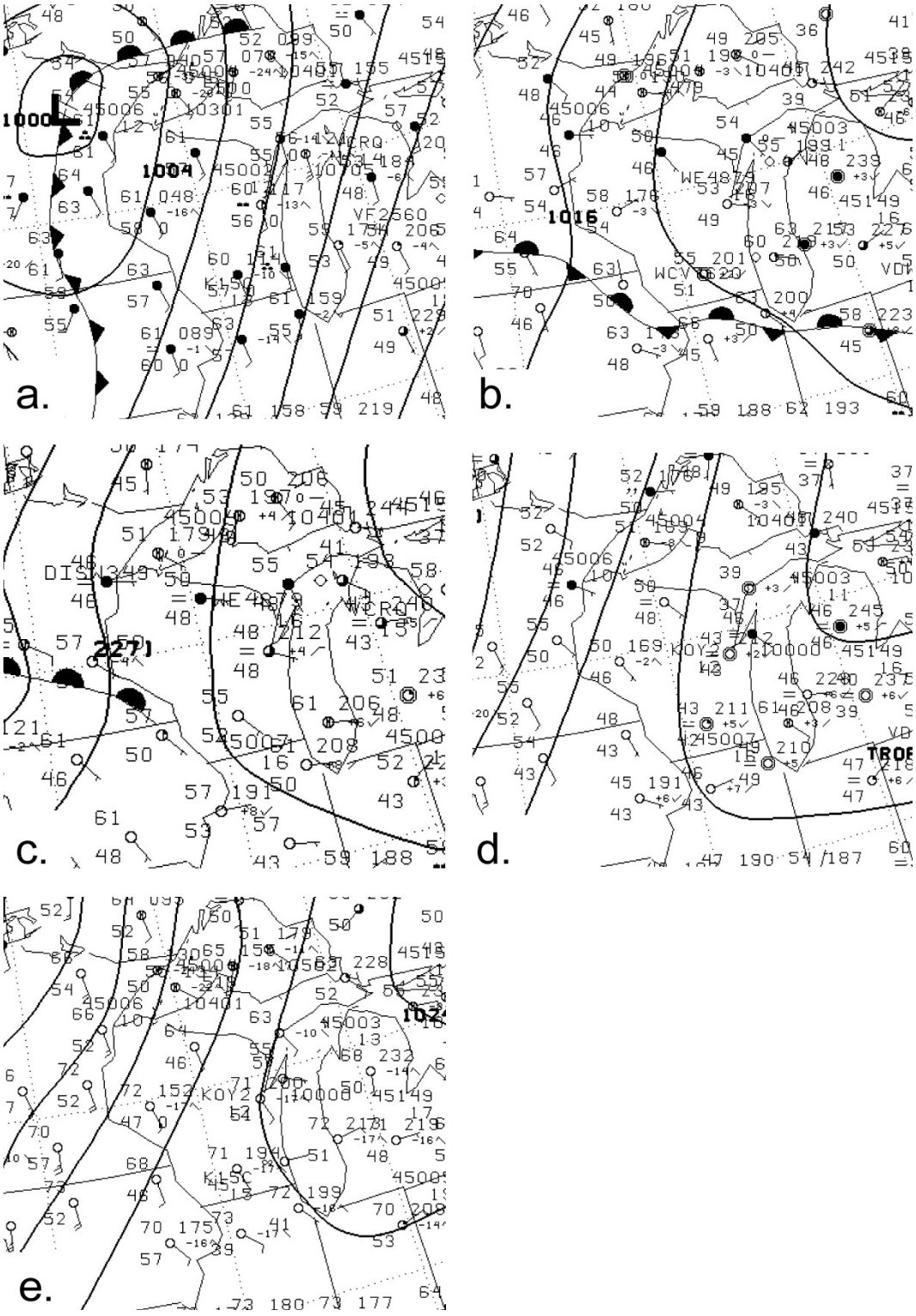

Figure 3.11 Surface analyses, 18 UTC 10 October (a.), 00 UTC (b.), 03 UTC (c.), 12 UTC (d.), and 18 UTC 11 October 2002 (e.), provided by NCEP.

3.2c SATELLITE IMAGERY

Once again, GOES data will be used to provide spatial observations of our fog event. At 00:15 UTC on 11 October, widespread fog can be seen over northern Wisconsin (Fig. 3.12a), though none is evident near Sheboygan. At 01:15 UTC (Fig. 3.12b), an isolated patch of condensate is observed stretching from Sheboygan eastward into Lake Michigan. As fog is observed by the Sheboygan ASOS at this time, it is likely that the visible patch of condensate is fog. At 02:15 UTC (Fig. 3.12c), this patch appears to thicken. By 07:15 UTC (Fig. 3.12d), several changes are observed. The widespread fog over northern Wisconsin begins to dissipate. The fog extending over Lake Michigan from Sheboygan appears to have dissipated. And from Sheboygan northward, a patch of fog seems to be forming along the coast of Lake Michigan.

The observation of fog along the Lake Michigan coast, but not further inland, suggests that the atmosphere near the coast is being modified by the lake. The three means by which the lake could modify the atmosphere and produce fog would be to advect cooler air, advect moisture, or decrease winds. As the lake temperature that day was approximately 15°C near the Sheboygan coast, it is unlikely the daytime sea breeze contributed to the cooling of air near the lake. With ASOS data unavailable prior to 23 UTC on 10 October, we will now turn to data provided by the National Data Buoy Center (NDBC) Coastal-Marine Automated Network (C-MAN) to examine the lake's effect on atmospheric moisture near Sheboygan. The NDBC has a C-MAN station located in Sheboygan on the Lake Michigan coast (station SGNW3; 43.75° N, 87.69° W). In Figure 3.13, we see that winds are onshore roughly from 15 UTC on 10 October until 01 UTC on 11 October. In Figure 3.14, an increase of over three degrees is observed in the dewpoint from 16 UTC to 23 UTC. By

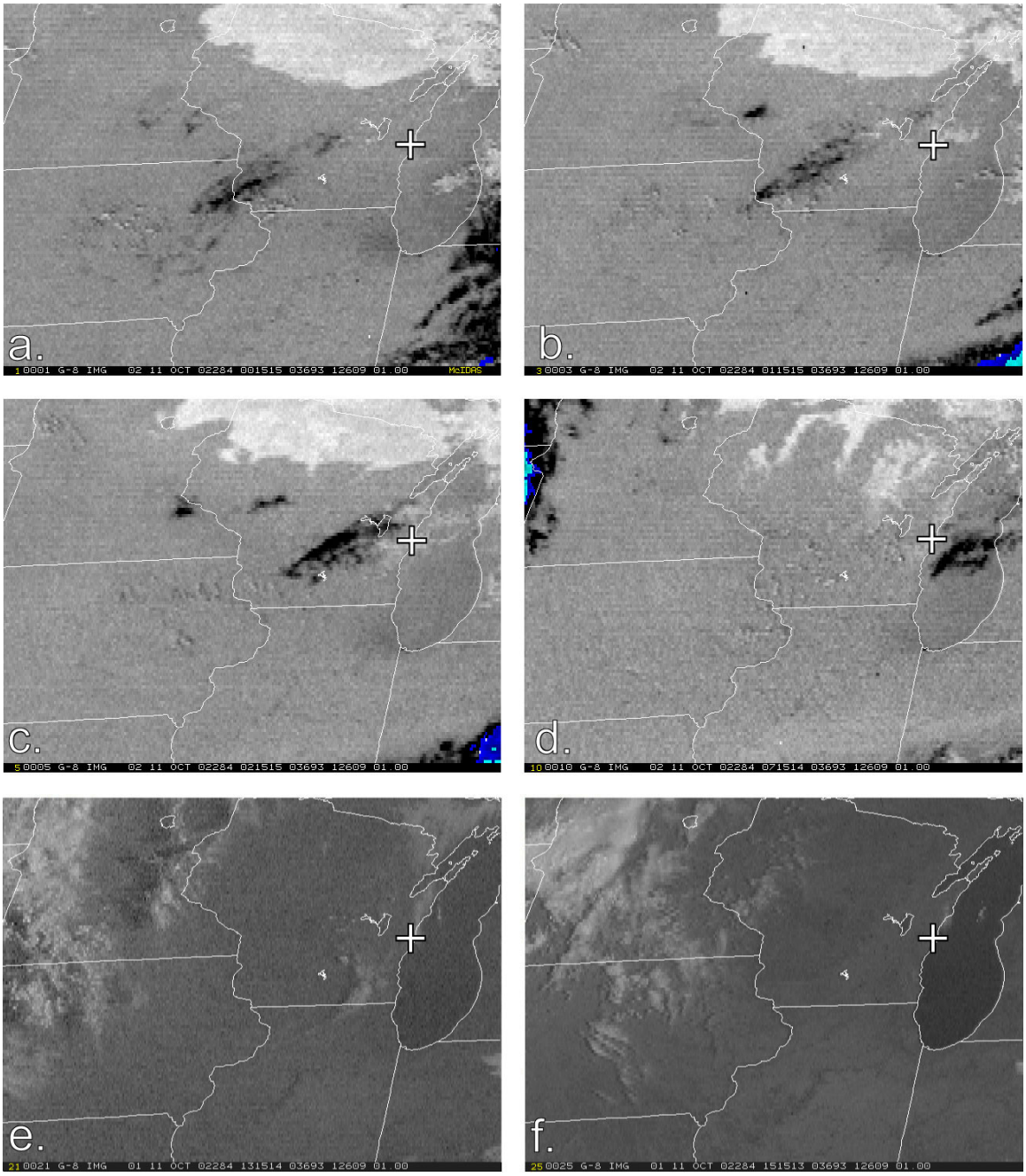

Figure 3.12 GOES-8 imagery for 00:15 UTC (a.), 01:15 UTC (b.), 02:15 UTC (c.), 07:15 UTC (d.), 13:15 UTC (e.), and 16:15 UTC (f.), 11 October 2002. Images (a.)-(d.) are 3.9μm albedo products for the nighttime observation of low clouds, and images (e.)-(f.) are 0.65μm albedo products for visible observation of low clouds. Low clouds are displayed as white and high clouds as black in the 3. 9μm albedo product. Sheboygan, WI is marked with a white cross on all images. Images prepared by Stan Kidder/CIRA.

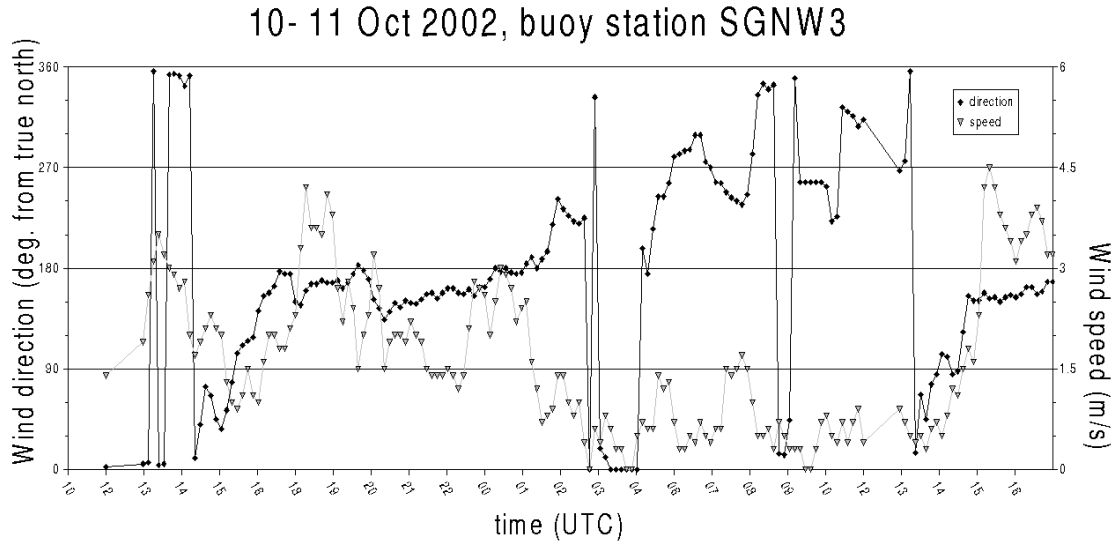

Figure 3.13 Wind speed (m/s; right axis) and direction (degrees from true north; left axis) observations for 10-11 October 2002, recorded by NDBC C-MAN buoy station SGNW3, located in Lake Michigan, on the coast of Sheboygan, WI (43.75°N, 87.69°W).

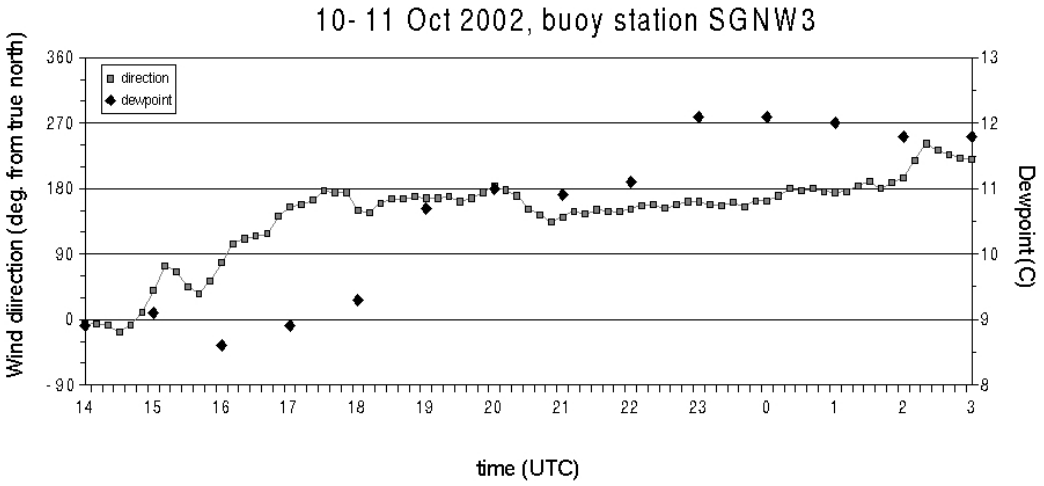

Figure 3.14 Dewpoint (degrees C; right axis) and wind direction (degrees from true north; left axis) observations for 10-11 October 2002, recorded by NDBC C-MAN buoy station SGNW3, located in Lake Michigan, on the coast of Sheboygan, WI (43.75°N, 87.69°W).

comparison, the ASOS observations at Juneau, WI, located 80 km inland, only record a one-degree increase over the same time period. It seems that this influx of lake moisture helped increase dewpoints near the coast, thus requiring less radiative cooling to produce fog near Lake Michigan than would be necessary further inland.

While the influx of lake moisture may have aided fog formation near the coast, another mechanism is necessary to explain why fog only occurred near the coast prior to sunrise. One may note in Figure 3.11b that calm winds are observed on the shore of Lake Michigan at a station near Milwaukee, while a 2.6 m s^{-1} wind is observed due east of that station, in the middle of the lake. The synoptic circulation produces a east-southeast flow over most of eastern Wisconsin, yet Sheboygan reports calm winds throughout the duration of the fog event. This is likely due to the development of a land breeze which cancels out the mean flow. With significant radiative cooling over land and a relatively warm lake, it is common for an off-shore land breeze to develop, resulting from the pressure gradient that develops between the cooler, denser air over land and the warmer, less dense air over the lake. However, the easterly synoptic wind cancels out the land breeze, and the result is no wind near the lake while winds are observed further inland. As Chapter 1 reported that a 2 m s^{-1} wind is sufficient for mixing the lower boundary layer and preventing fog formation, this process explains the formation of fog along the coast while clear skies are observed further inland.

An hour after sunrise, at 13:15 UTC (Fig. 3.12e), the fog along the coast is less visible, though surface observations suggest it is still present. Also observed by satellite is a patch of fog advecting over south-central Wisconsin, resulting from the solar-induced

evaporation of surface moisture over low-lying agricultural lands. By 16:15 UTC (Fig. 3.12f), the fog is no longer visible by satellite, and surface observations confirm the fog has dissipated.

CHAPTER FOUR: MODEL RESULTS AND ANALYSIS

4.1 MODEL RESULTS OF 21 JANUARY FOG SIMULATION

As previously stated, the fog event of 21 January 2001 was simulated, using the RAMS@CSU model, from 00 UTC 21 January to 00 UTC 22 January. Analysis files were output every model hour. The simulation took approximately 12 hours using a cluster of eight dual-processor personal computers. Please note that model results will be assumed to be from the lowest level of the simulation's third grid unless specified.

As fog is nothing more than a cloud at the ground level, the presence of fog will be determined by examining the cloud mixing ratio predicted by the model at the lowest level of grid three, which is 15.6m AGL. Hourly predicted values of cloud mixing ratio for the lowest level of grid three, along with wind fields, from 07 UTC until the end of the simulation can be seen in Figure 4.1. A non-zero cloud mixing ratio was not observed over Angiola, CA until 11 UTC. Predicted values of cloud mixing ratio at Angiola, CA are compared with observed mixing ratios from the CRPAQS study from 14 to 17 UTC (the time period for which liquid water content data are available) in Figure 4.2.

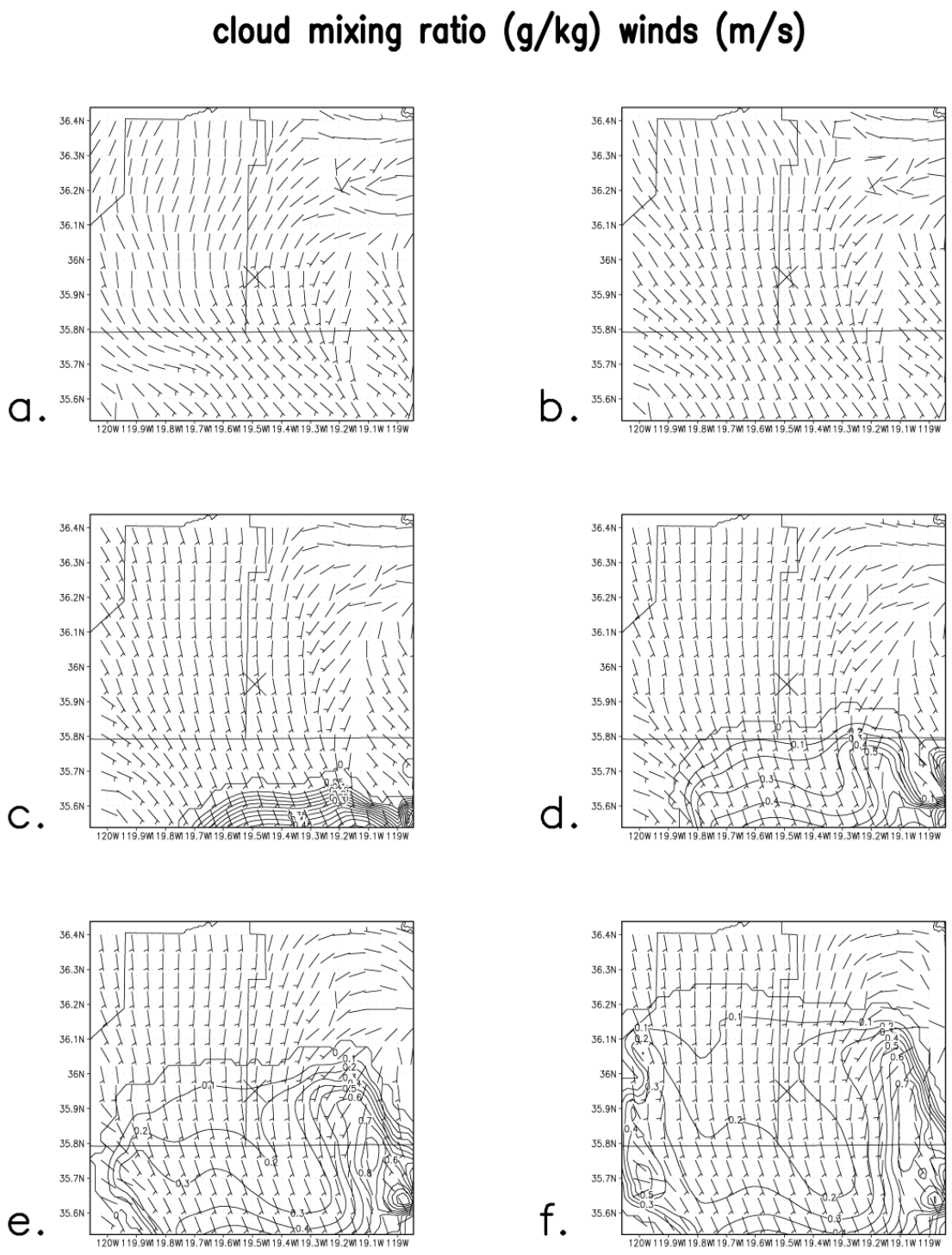

Figure 4.1 Model results for 07 UTC (a.), 08 UTC (b.), 09 UTC (c.), 10 UTC (d.), 11 UTC (e.), and 12 UTC (f.), from the 21 January 2001 simulation. Cloud mixing ratio (g kg^{-1}) is contoured with wind barbs (m s^{-1}) overlayed. County borders are included, and Angiola marked with an "x." Figure is continued on next two pages.

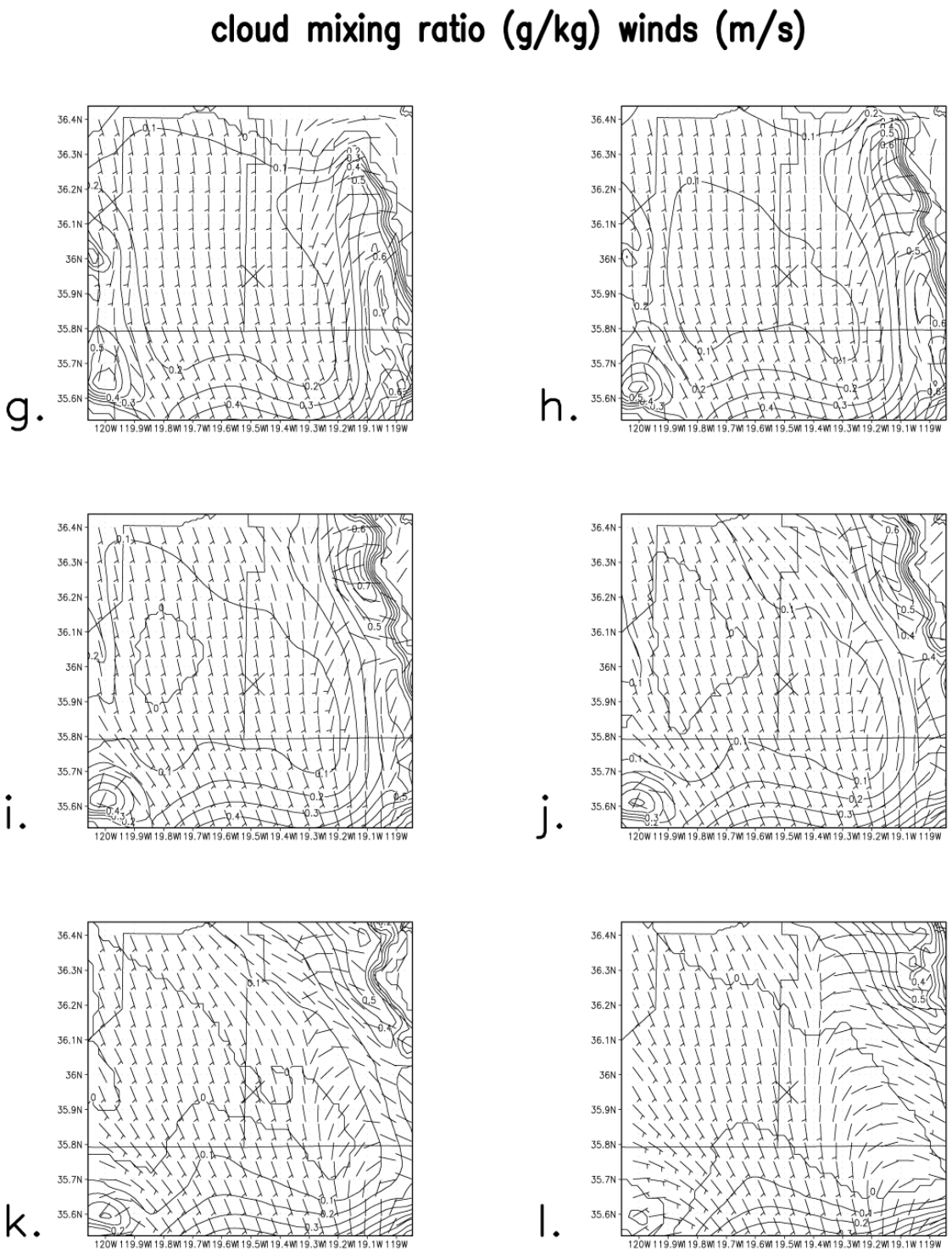

Figure 4.1 (continued) Model results for 13 UTC (g.), 14 UTC (h.), 15 UTC (i.), 16 UTC (j.), 17 UTC (k.), and 18 UTC (l.). Figure is continued on next page.

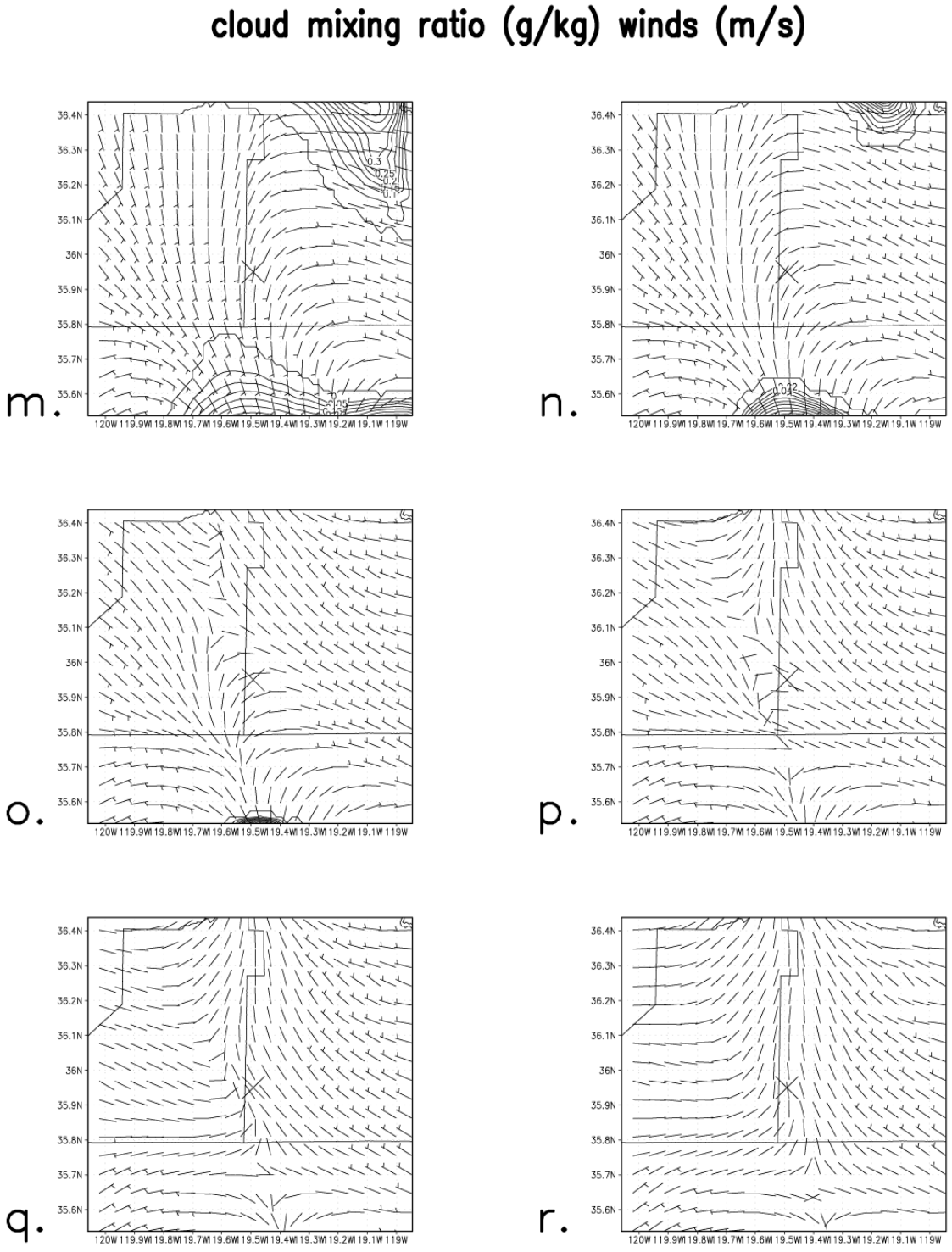

Figure 4.1 (continued) Model results for 19 UTC (m.), 20 UTC (n.), 21 UTC (o.), 22 UTC (p.), and 23 UTC (q.) 21 January, and 00 UTC 22 January 2001 (r.).

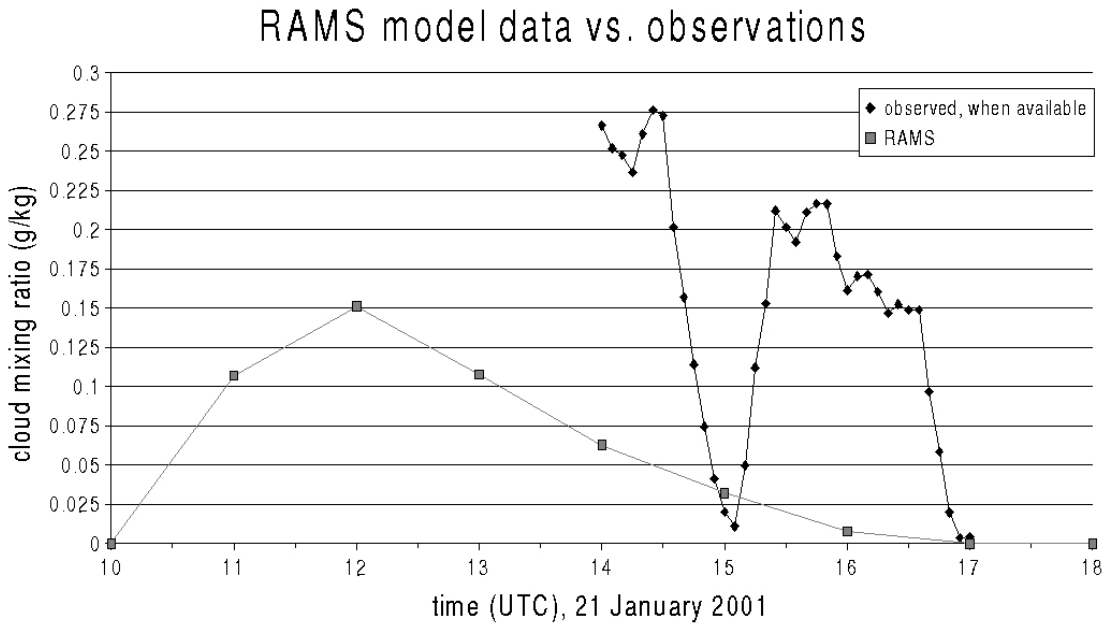

Figure 4.2 Model results (diamonds) and observations (squares) of cloud mixing ratio (g kg^{-1}) at Angiola, CA, from 10 to 18 UTC, 21 January 2001. While cloud mixing ratio observations are not available prior to 14 UTC, patchy fog was observed at 12 UTC.

When comparing the results of the simulation with observations presented in Chapter 3, the model appears to have captured the main features of the fog event rather accurately. However, three significant errors are observed. The first error involves the temporal accuracy of the fog simulation over Angiola. According to CRPAQS observations, patchy fog is first observed at 12 UTC, with clear conditions reported at 13 UTC. A homogeneous fog layer develops at 14 UTC, at which point cloud mixing ratios begin to be measured, and the fog dissipates at 17 UTC. Our simulation has fog first appearing over Angiola at 11 UTC (Fig. 4.1c), and remaining until 16 UTC. The second error is with regards the mixing ratios observed in the fog. The maximum observed mixing ratio at the Angiola site was 0.276 g kg^{-1}, which is within the bounds of fog mixing ratios presented by Seinfeld and Pandis (1998), as mentioned in Chapter 1.

However, one can see in Figure 4.2 that the model only produces a maximum mixing ratio of 0.15 g kg^{-1}. The third error noted concerns the presence of fog near the edge of the valley. Along the southern and eastern boundaries of the valley, which coincide with the southern and eastern boundaries of grid three, mixing ratios of up to 0.8 g kg^{-1} are simulated in the early stages of the fog's formation (Fig. 4.1e). At first glance, these three errors would lead one to question whether the real-time forecast model has a microphysical package capable of providing an accurate, three-dimensional fog forecast. In the next section, evidence will be presented which suggests that the model indeed handled the microphysics of the fog event quite well.

4.2 ANALYSIS OF RESULTS OF 21 JANUARY FOG SIMULATION

A model of radiative valley fog published by Pilié *et al.* (1975a, 1975b), henceforth referred to as the Pilié model, was presented in Section 3.1. Comparisons to observations from 21 January suggest that this theoretical model accurately represents the fog event observed over Angiola, CA. The simulation of the 21 January event will be examined to see if significant characteristics identified by the Pilié model can be found in the numerical simulation's results. As an understanding of the local topography is essential to applying the Pilié model to our simulation, the topography used by the model for the second and third grids is depicted in Figure 4.3.

The first characteristic observed in the Pilié model is the development of a valley drainage flow. Observations at the north and south ends of the San Joaquin Valley

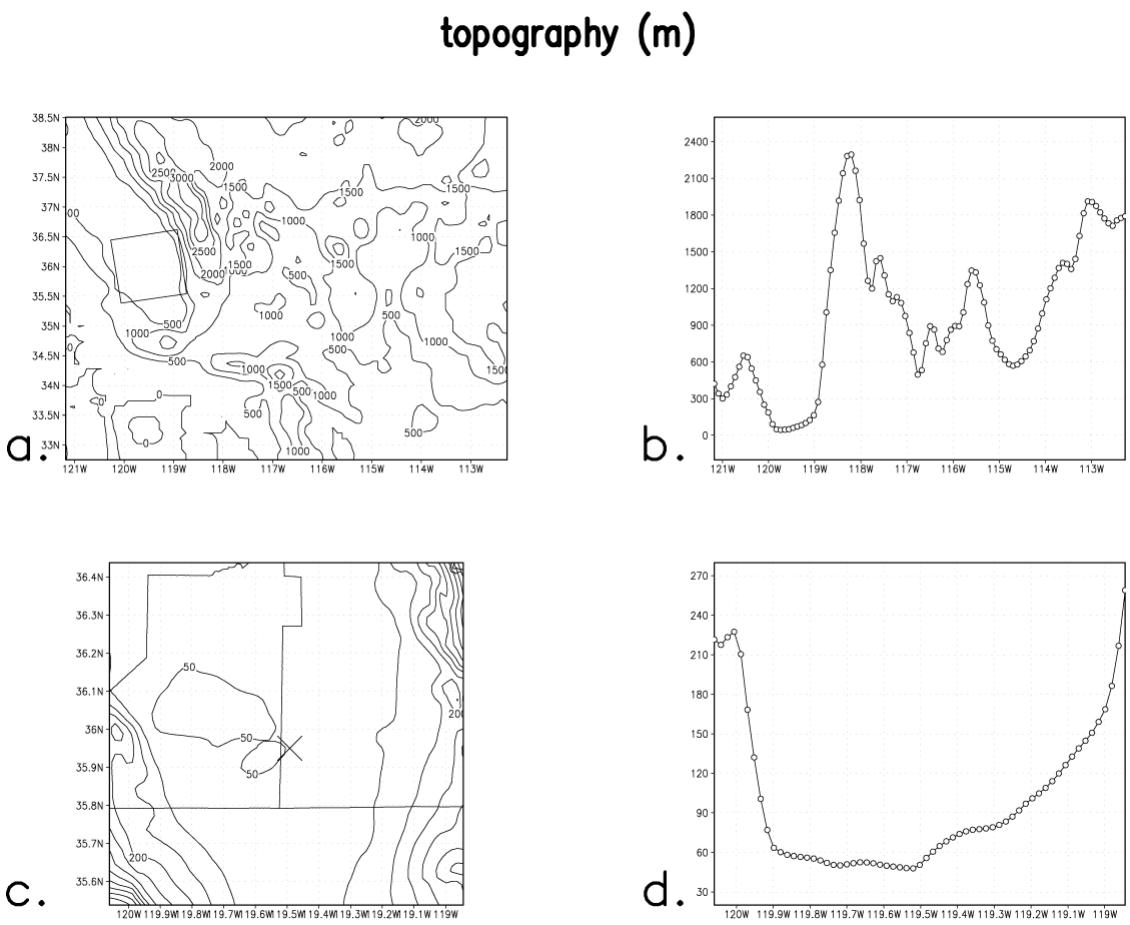

Figure 4.3 Topography (m AGL) used in the 21 January simulation. Panel (a.) depicts a planar view of the topography of grid 2, with the topography of an east-west cross-section through Angiola shown in panel (b.). Panels (c.) and (d.) are the same as (a.) and (b.), only for grid three. The box in (a.) represents the domain of grid three, and the "x" in panel (c.) marks Angiola, CA.

indicated a down-valley flow toward the center of the valley. Similarly, results from the third grid of the model simulation show a south-southeast wind which flows from the south end of the valley toward the center (Fig. 4.1). While the second and third grids do not cover the north end of the valley, the lowest level of the first grid (50m AGL) shows the development of a northeasterly drainage flow near Red Bluff, CA (Fig. 4.4), which is located on the north end of the valley with mountains running southeast to northwest.

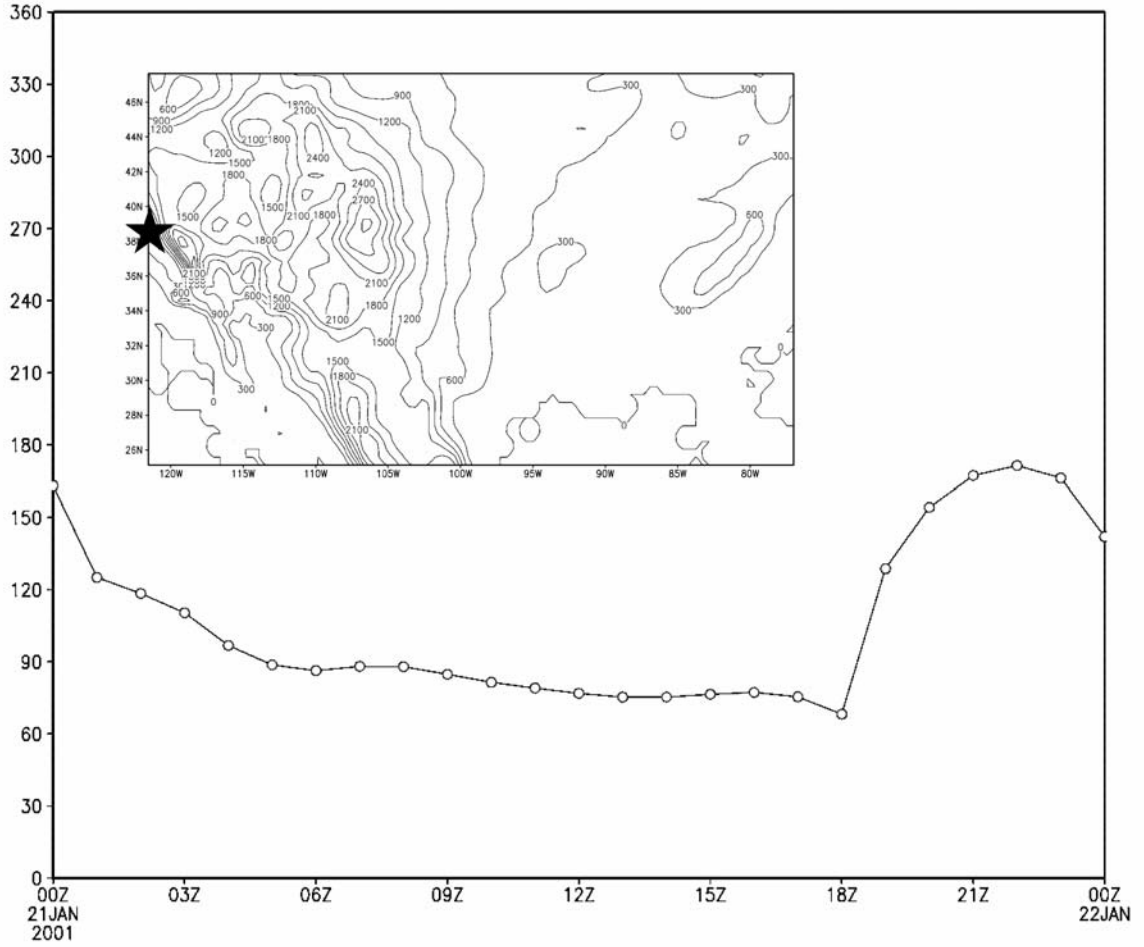

Figure 4.4 Wind direction (degrees from true north), as simulated in the lowest level of grid one (50m AGL), from 00 UTC 21 January to 00 UTC 22 January 2002, near Red Bluff, CA. The location of the wind observation is marked by the star in the inserted panel, in which the topography of grid one is contoured every 300m AGL.

What is somewhat curious is that weak upslope winds are observed at the eastern boundary of the valley, rather than the expected downslope drainage flow. Unfortunately, no surface observations of wind direction are available at the east or west boundaries of the valley. However, one can conclude that, with observed winds into the valley at the north and south ends, and a stable atmosphere suppressing significant vertical motion, a weak upslope wind developed by conservation of mass. Regardless of

the mechanism for this wind, the circulation simulated by the model is consistent with observations during that time.

The second phenomenon offered by the Pilié model is the development of a dewpoint inversion. In Figure 4.5, east-west dewpoint cross-sections through Angiola, CA show the development of a dewpoint inversion from 08 to 11 UTC. The presence of a dewpoint inversion indicates that the model is accurately simulating the microphysics involved in the fog's formation. Particularly, the process of dew deposition at the surface (the primary mechanism by which the dewpoint inversion develops) seems to be handled well by the model. An examination of dewpoints over Angiola at the model's lowest level (Fig. 4.6) confirms that dew deposition is being accurately simulated by the model, as Pilié *et al.* (1975a) wrote that one should observe a decrease in dewpoint after fog formation that can be attributed to dew deposition.

One aspect of the Pilié model not handled properly by the model is the evaporation of dew after sunrise, which increases the dewpoint and allows fog to persist several hours after sunrise. One notes in Figure 4.6 that the dewpoint does not increase immediately after 15 UTC, as observed in Table 3.1. It is this lack of dew evaporation that explains the fact that the model dissipates the fog two hours earlier than observed.

While the timing of the formation and dissipation of fog is off by two hours, the vertical structure of the fog is consistent with the Pilié model. The Pilié model suggests that fog initially forms around 100 to 150m AGL. At 11 UTC (Fig. 4.7a), an east-west cross-section of cloud mixing ratio through Angiola, CA shows highest values just above 100m AGL. As the previous hour's analysis shows a cloud mixing ratio of zero

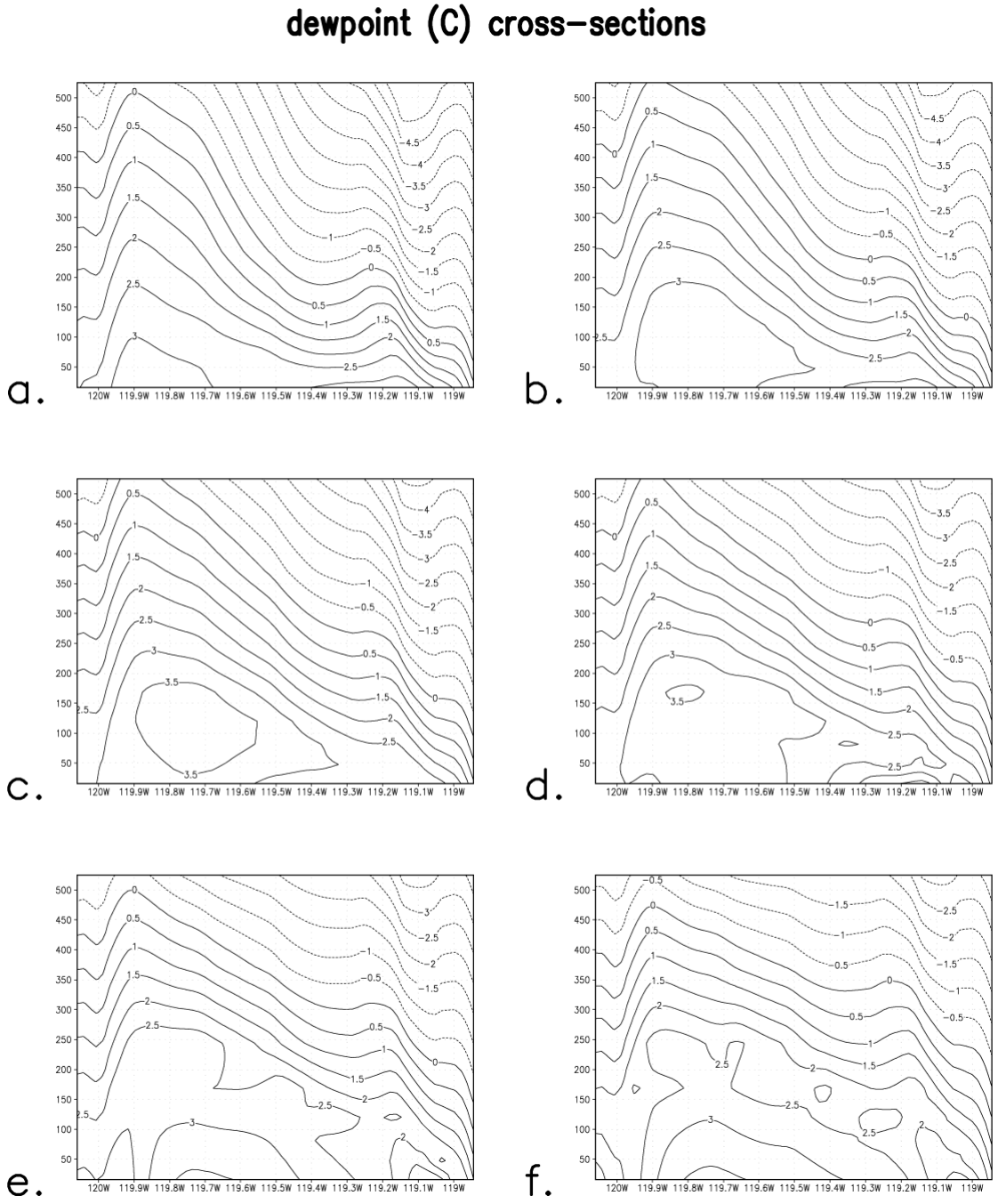

Figure 4.5 East-west cross-sections of dewpoint values (degrees C) from 0 to 500m AGL, through Angiola, CA, from the 21 January simulation. Times depicted are 08 UTC (a.), 09 UTC (b.), 10 UTC (c.), 11 UTC (d.), 12 UTC (e.), and 13 UTC (f.).

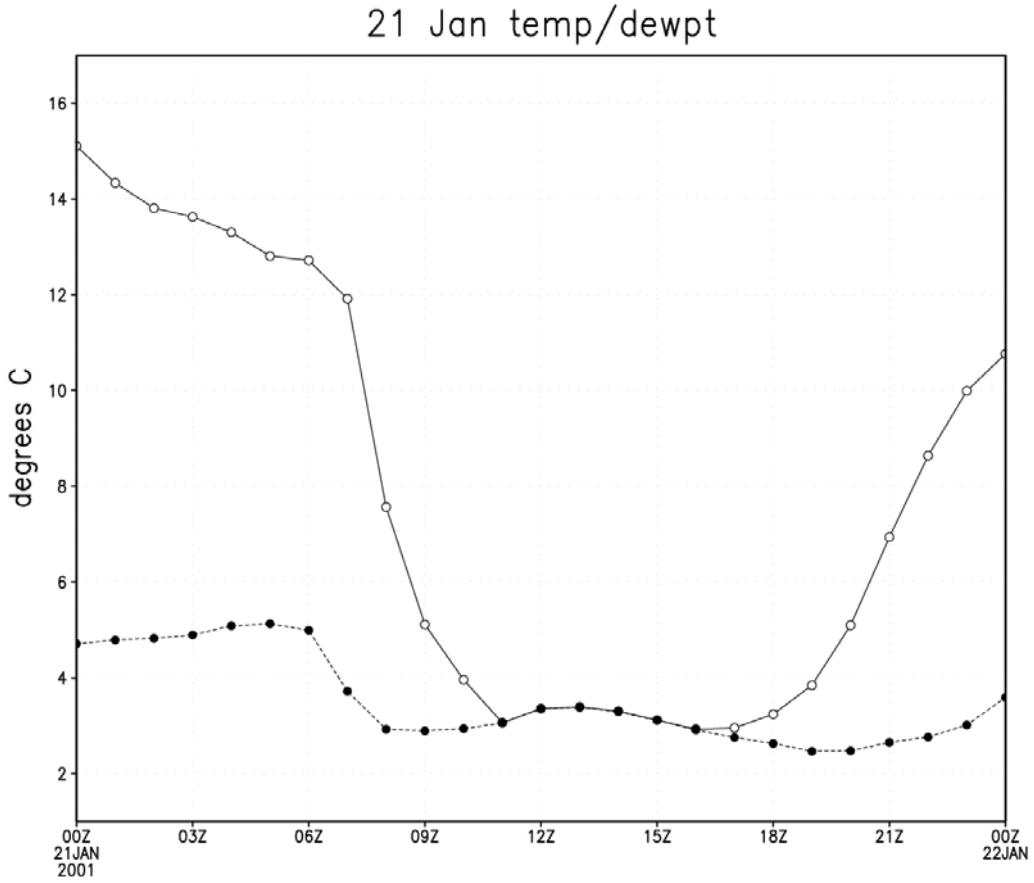

Figure 4.6 Temperature (solid) and dewpoint (dashed) values (degrees C) at Angiola, CA, from the lowest level of the 21 January simulation. Values span from 00 UTC 21 January to 00 UTC 22 January.

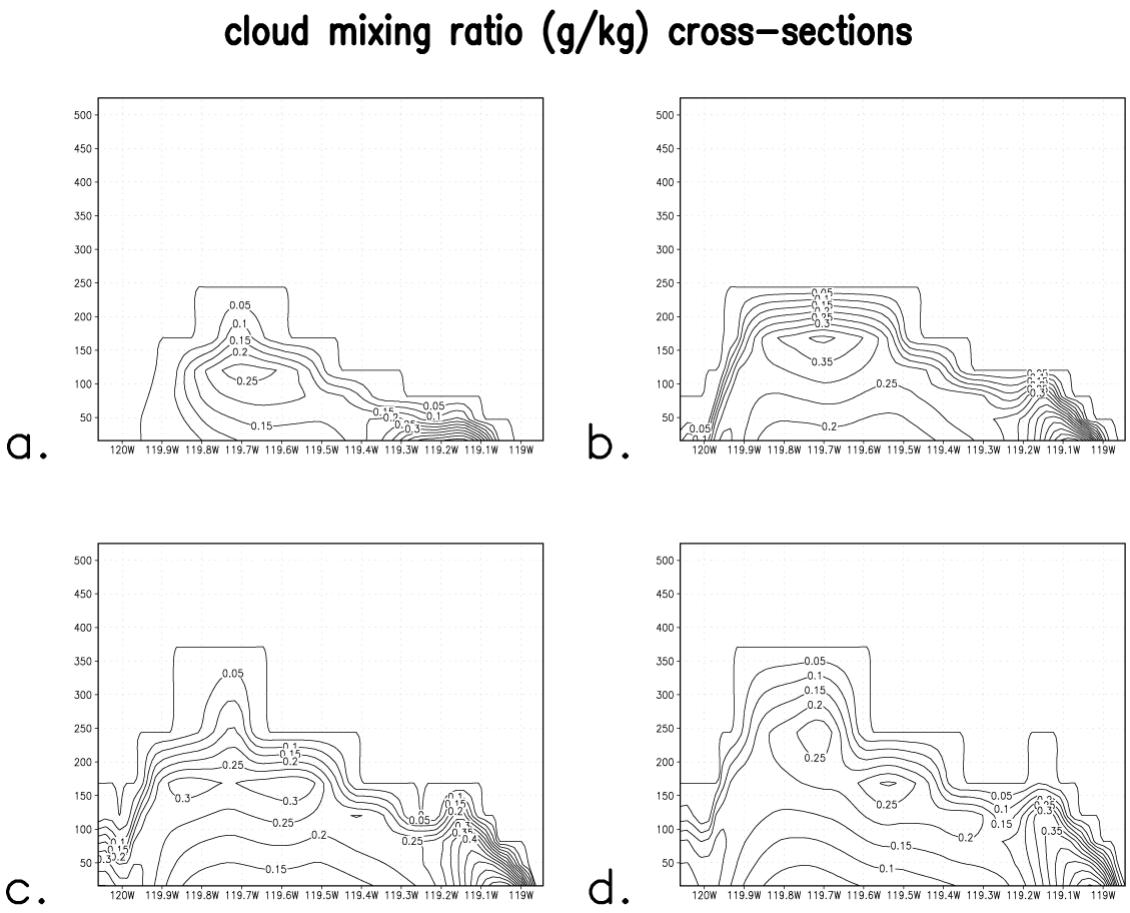

Figure 4.7 East-west cross-sections of cloud mixing ratios (g kg^{-1}) from 0 to 500m AGL, through Angiola, CA, from the 21 January simulation. Depicted are the first four hours of fog, 11 UTC (a.), 12 UTC (b.), 13 UTC (c.), and 14 UTC (d.).

throughout the domain, one can conclude that the fog initially developed at the level of highest mixing ratios and subsequently mixed down. The Pilié model also suggests that the fog first dissipates at the lowest levels (once dew evaporation can no longer maintain saturation at the surface), and subsequently lifts. In Figure 4.8, such a process is observed, with no fog present at the surface at 19 UTC (Fig. 4.8d) while mixing ratios over 0.15 g kg^{-1} were observed near 250m AGL. When examining the cross-sections,

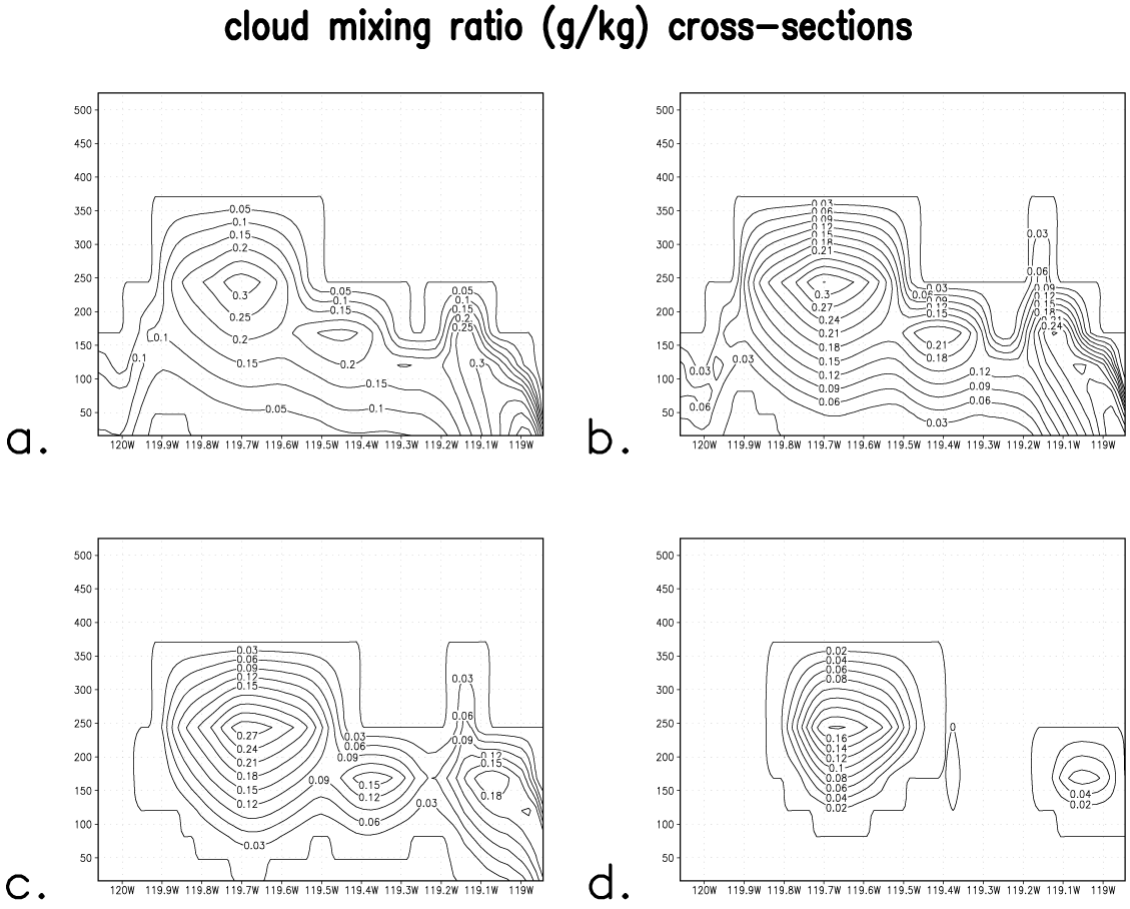

Figure 4.8 Same as figure 4.7, but for the last four hours in which fog was simulated, 16 UTC (a.), 17 UTC (b.), 18 UTC (c.), and 19 UTC (d.).

one should consider the local topography (Fig. 4.3d), which explains the somewhat anomalous observations on the eastern portion of the cross-sections.

While the model appears to have simulated the microphysical characteristics of the case well, as seen in comparing the micrometeorology of the simulation with observations, the errors identified in the beginning of this chapter must still be addressed. The first error (slight inaccuracies in the timing of the simulation) has already been partly explained by our previous discussion of dew evaporation. The model's inability to

evaporate enough ground moisture led to the premature dissipation of the fog due to lack of surface-level moisture. The lack of evaporation could also be the result of initial soil moisture values that are too low or errors in the soil type itself, as the model is initialized with a homogeneous soil type which is not applicable for the entire valley. As far as the formation of fog is concerned, its early formation is likely due to slight inaccuracies in the model's radiative cooling. Also contributing to premature cooling may be the σ_z coordinate system used by the RAMS@CSU model. The coordinate system has been shown to have problems calculating horizontal diffusions, and one such variable particularly susceptible to such a problem is temperature diffusion. Zängl (2002) showed that the σ_z coordinate system tends to cool the air in valleys, which would lead to the simulation of fog earlier than observed.

The second error to be addressed is the unusually high cloud mixing ratios near areas of significantly steep topography. Again, the σ_z coordinate system used by the model gives us reason for concern. In operational use, the coordinate system has had difficulty handling boundary-layer processes in areas of steep terrain. Such problems are often observed in areas of ascent, such as the eastern boundary of grid three, as discussed earlier in this section. Pielke (2001) identified enhanced cooling in areas of ascent in the σ_z coordinate system, and such cooling would contribute to decreased saturation mixing ratios and, subsequently, higher liquid water contents. A second process specific to the σ_z coordinate system also contributes to increased mixing ratios. Like temperature diffusion, the σ_z coordinate system also has problems with the horizontal diffusion of water vapor mixing ratios. Calculating the diffusion of water vapor mixing ratios along

the sigma surface has been shown to dry the air in valleys and moisten the atmosphere above mountains (Zängl, 2002). Such a process is consistent with our model results, both above the mountains and at the edges of the valley. This process also accounts for our third error, that of mixing ratios nearly 50% lower than those observed over Angiola. Also contributing to the low mixing ratios in the valley is the fact that the higher simulated mixing ratios along the southern boundary of the valley led to small amounts of precipitation, thereby reducing the available moisture upwind of the fog event.

4.3 MODEL RESULTS OF 11 OCTOBER FOG SIMULATION

The fog event of 11 October 2002 was simulated, using the RAMS@CSU model, from 18 UTC 10 October to 18 UTC 11 October. Analysis files were output every model hour. The simulation took approximately 12 hours using a cluster of eight dual-processor personal computers. Please note that, as in the previous sections of this chapter, model results will be assumed to be from the lowest level of the simulation's third grid unless specified.

Again, the presence of fog will be determined by examining the cloud mixing ratio predicted by the model at the lowest level of grid three, which is 15.6m AGL. Hourly predicted values of cloud mixing ratio for the lowest level of grid three, along with wind fields, from 01 UTC 11 October until the end of the simulation can be seen in Figure 4.9. A non-zero cloud mixing ratio was not observed in grid three until 05 UTC, with a non-zero cloud mixing ratio first simulated over Sheboygan, WI at 12 UTC. The

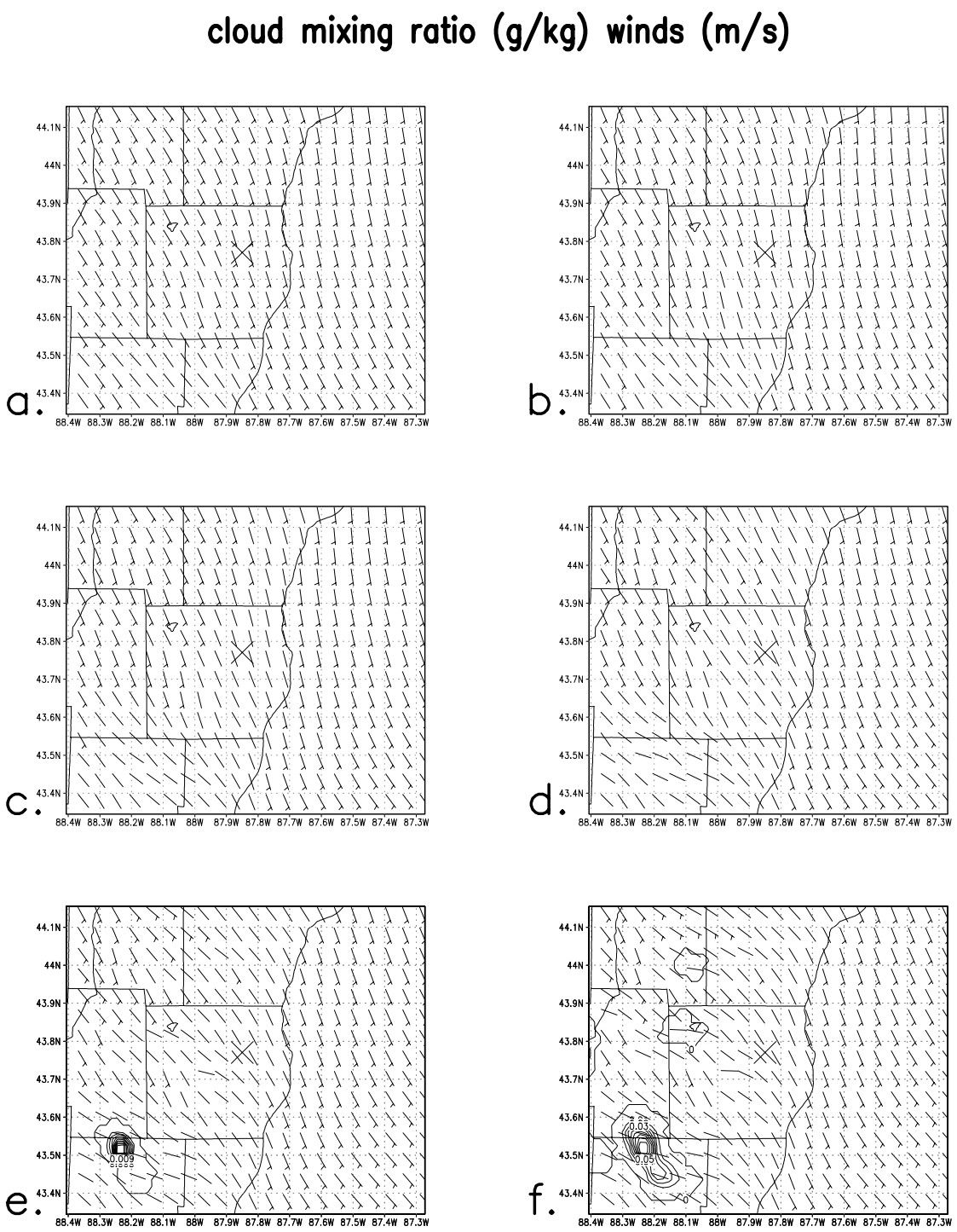

Figure 4.9 Model results for 01 UTC (a.), 02 UTC (b.), 03 UTC (c.), 04 UTC (d.), 05 UTC (e.), and 06 UTC (f.), from the 11 October 2002 simulation. Cloud mixing ratio (g kg^{-1}) is contoured with wind barbs (m s^{-1}) overlayed. County borders are included, with Sheboygan, WI marked with an "x." Figure is continued on the next two pages.

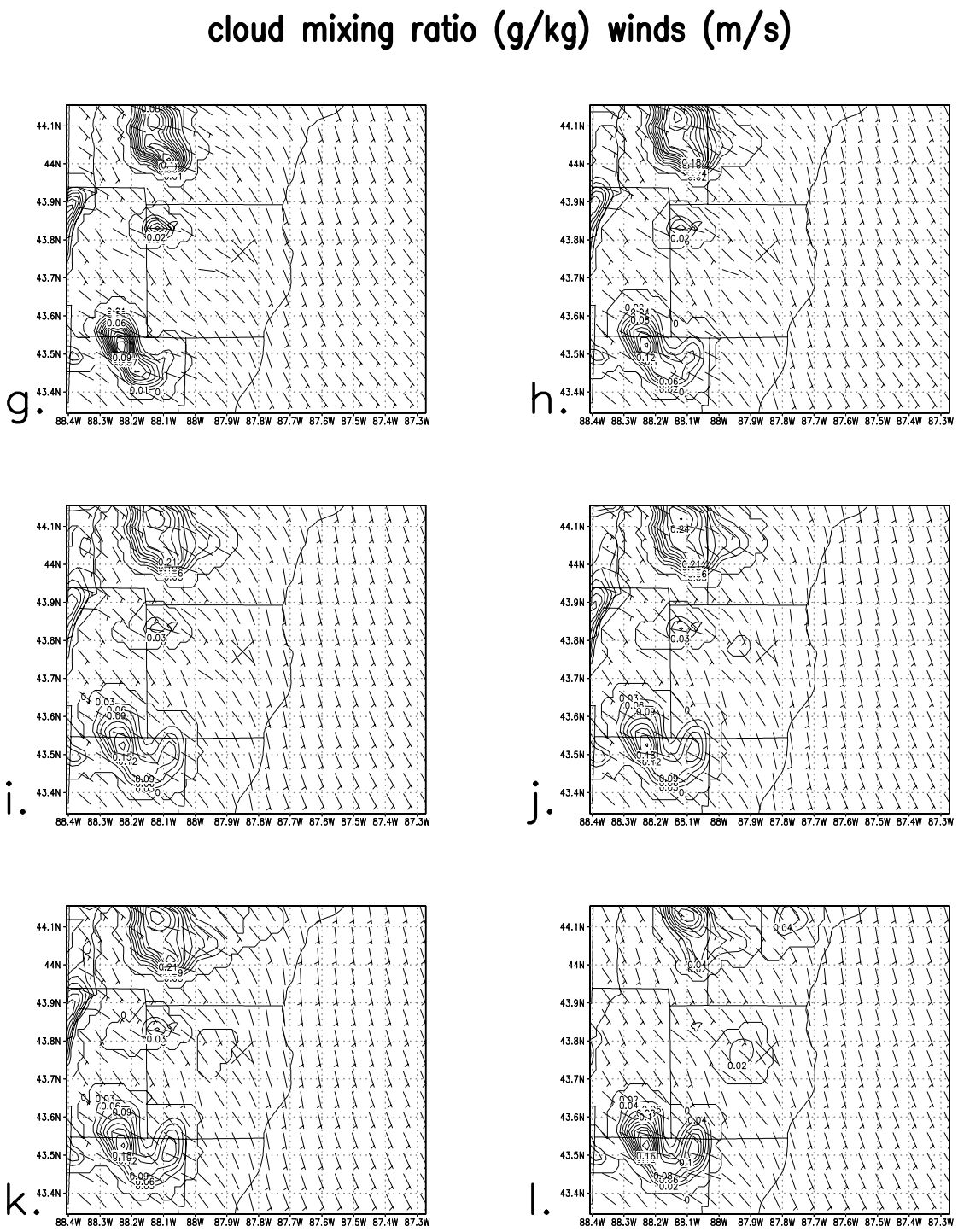

Figure 4.9 (continued) Model results for 07 UTC (g.), 08 UTC (h.), 09 UTC (i.), 10 UTC (j.), 11 UTC (k.), and 12 UTC (l.). Figure is continued on the next page.

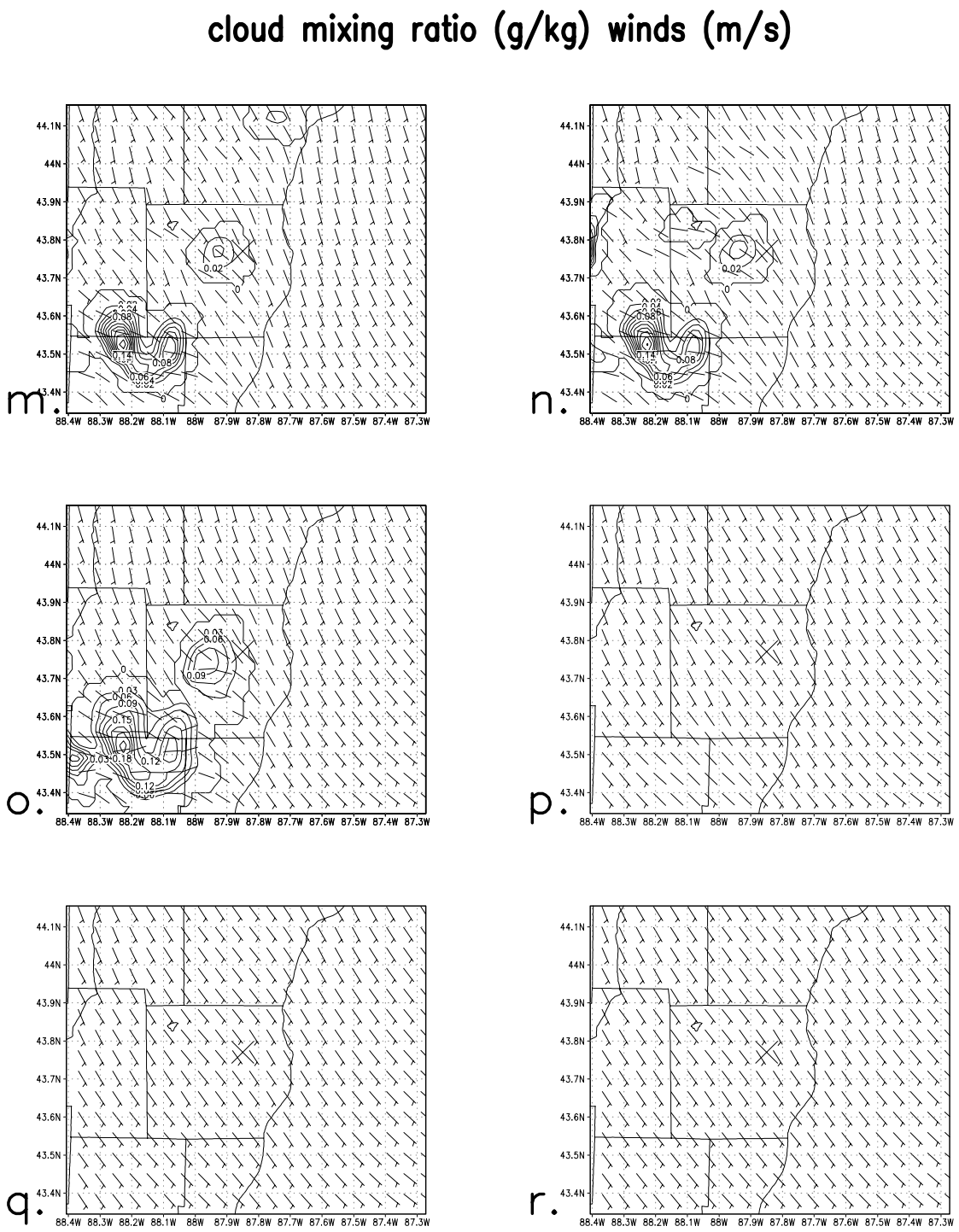

Figure 4.9 (continued) Model results for 13 UTC (m.), 14 UTC (n.), 15 UTC (o.), 16 UTC (p.), 17 UTC (q.), and 18 UTC (r.).

simulated fog dissipates at 16 UTC. As the satellite imagery presented in Chapter 3 suggests that a rather uniform cloud bank should be found over the inland domain of grid three, the first discrepancy noticed between observations and the simulation results is the patchy nature of the simulated fog. The simulated fog over Sheboygan only lasts for three hours and never reaches a mixing ratio greater than 0.0025 g kg^{-1}, while the simulated fog over Kewaskum, WI (43.53°N, 88.25°W, located approx. 50 km southwest of Sheboygan) persists from 05 UTC until 15 UTC, with mixing ratios approaching 0.25 g kg^{-1} (a mixing ratio time series for Kewaskum, WI, along with a map showing Kewaskum's location in grid three, can be found in Figure 4.10). These results lead one to question why such a discrepancy occurs in our simulation. In our analysis, this question will be answered, and again the microphysical package used in the RAMS@CSU model will be shown to be quite capable of simulating fog.

4.4 ANALYSIS OF MODEL RESULTS OF 11 OCTOBER FOG SIMULATION

If one examines the results at Kewaskum, WI, the model appears to have handled the fog event rather well. The onset of fog was four hours late, but the dissipation was simulated the same hour as observed. On the other hand, the results at Sheboygan, WI suggest the model missed the event altogether. In order to understand the results of the simulation, one must first address this discrepancy. In Figure 4.11, temperatures, dewpoints, and mean wind speeds are shown for both Kewaskum and Sheboygan. A similar trend in each value is found for both locations. However, two important

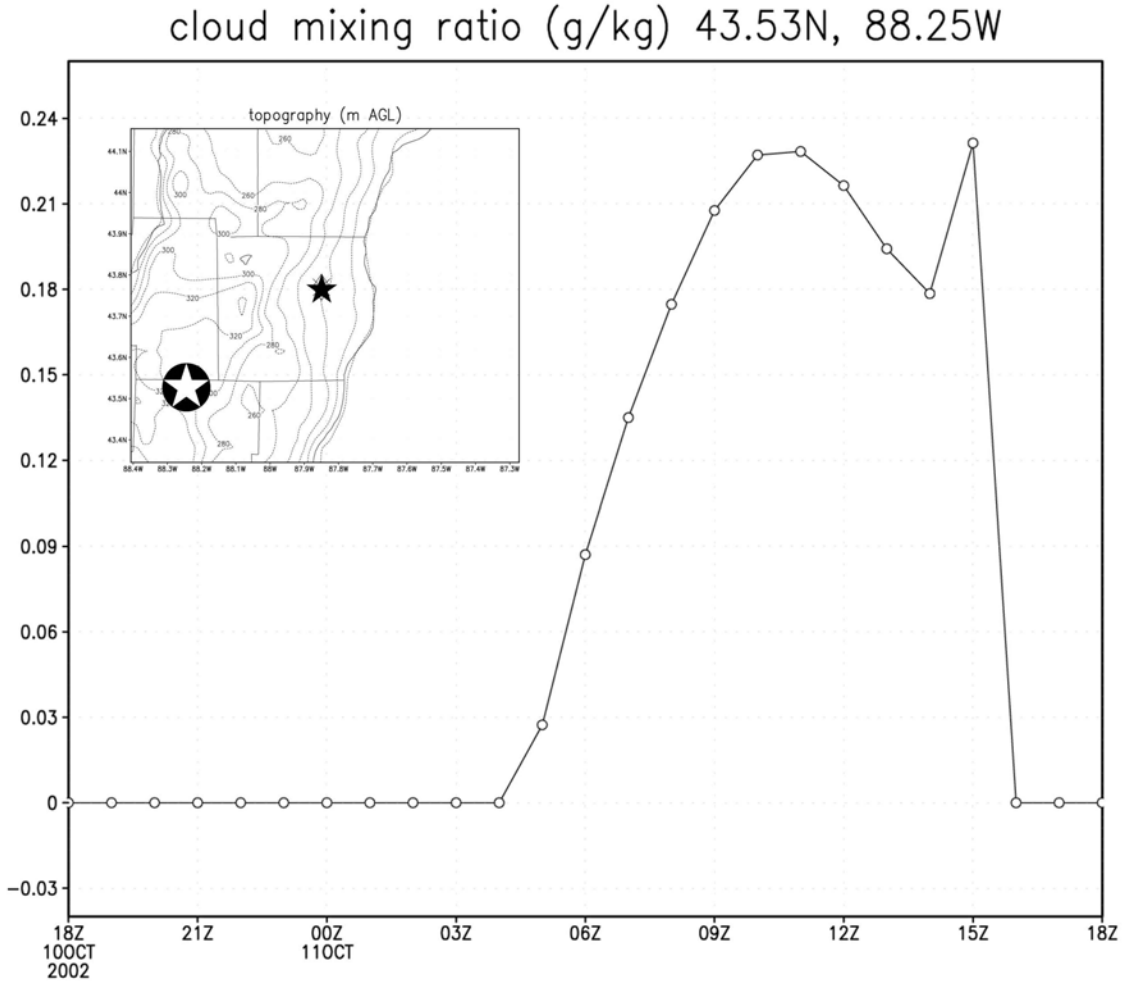

Figure 4.10 Model results of cloud mixing ratio (g kg^{-1}) over Kewaskum, WI from 18 UTC 10 October to 18 UTC 11 October 2002. Kewaskum is marked with the encircled white star on the inset topographical map; Sheboygan, WI is marked with the black star.

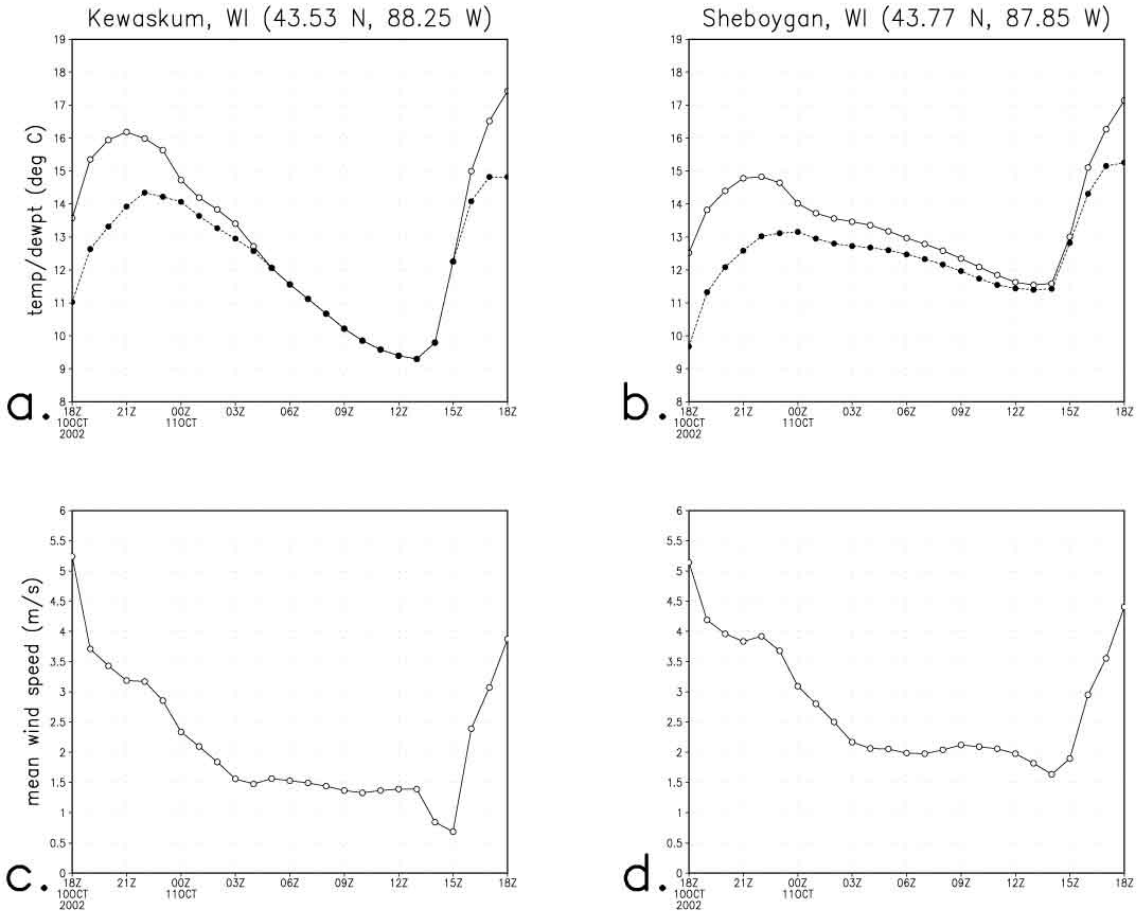

Figure 4.11 Model results of temperatures (solid) and dewpoints (dashed) (degrees C) over Kewaskum, WI (a.) and Sheboygan, WI (b.), as well as mean wind speeds (m s^{-1}) for Kewaskum (c.) and Sheboygan (d.), are depicted.

distinctions are found. First, saturation is reached by 05 UTC at Kewaskum while saturation is never achieved at Sheboygan. The second distinction explains the first, and that can be found in the wind field. From 03 UTC to 13 UTC, the winds at Kewaskum remain steady at 1.5 m s^{-1}. One might recall that, in Chapter 1, a wind speed of 2 m s^{-1} is referenced as the minimum speed at which sufficient mixing is induced to dissipate fog. Over the same time period, wind speeds of 2 m s^{-1} are simulated at Sheboygan. It appears that the 2 m s^{-1} wind speed over Sheboygan was strong enough to mix the

boundary layer such that saturation was never achieved, while the 1.5 m s^{-1} wind speed over Kewaskum was insufficient, and allowed for saturation and the subsequent formation of fog. Note that Table 3.2 showed that no winds at all were observed throughout the duration of the fog event.

If varying wind speeds account for the discrepancy in the fog simulation over grid three, then the next question one must answer is why there is a discrepancy in wind speed. One may recall that, in the previous chapter, land breeze dynamics are identified as canceling out the mean easterly winds near the coast. It appears that, in our simulation, this mechanism did not develop adequately over parts of the domain. One explanation for this observation is that the model inaccurately simulated radiative cooling after sundown (in Figure 4.11b, one can see a temperature of 13.7°C simulated by the model at 01 UTC, when observations report a temperature of 8.9°C). Inadequate cooling over land weakens the pressure gradient between the land and the water, and thus reduces the strength of the land breeze. Note that weaker easterly winds are reported at Kewaskum, where stronger cooling is simulated. It is also possible that the model simply simulated stronger synoptic winds than observed near the lake, and that the winds mixed down warmer air from the low-level inversion. Unfortunately, sounding data are not available for the area, and as such the model's vertical profile cannot be compared to observations to verify this theory.

With stronger cooling over Kewaskum, the model appears to have more accurately simulated the fog event at that location than it did over Sheboygan. As such, we will examine the fog simulated over Kewaskum to determine how well the

microphysics of the model handled this fog event. In Figure 4.12, we examine east-west cross-sections of dewpoints through Kewaskum. As in the 21 January case, we see a slight dewpoint inversion prior to the fog's formation (Fig. 4.12b). Unlike the 21 January case, the dewpoint inversion only reaches up to the first 50m AGL. This is because the flow is unidirectional, unlike the convergent valley flow seen in the previous case. The lack of convergence prevents the cool, dry air from being forced upward and deepening the inversion, as described in the Pilié model. However, the presence of a dewpoint inversion, along with the steady decrease in dewpoint found in Figure 4.11a, suggests the model has once again sufficiently handled dew deposition.

In Figure 4.13, simulated cloud mixing ratios during the fog's formation are depicted. Here an important distinction from the previous simulation can be found. Unlike the 21 January simulation, the highest mixing ratio values are found at the surface, suggesting that the fog formed at the surface, rather than aloft. This too can be attributed to the lack of a convergent flow. While a slight dewpoint inversion is present, the strongest radiative cooling still takes place at the surface, and thus the fog forms from the surface upward. Note that the fog top extends only to the top of the dewpoint inversion. The results suggest that the model has again accurately simulated the microphysical properties involved in fog's formation and dissipation.

One error not observed in this simulation is the timing of the fog's dissipation. Unlike the 21 January fog event over Angiola, CA, the mode simulated the fog's dissipation the same hour as observed. At first glance, this seems to suggest that the model accurately handled the evaporation of dew in this case, while failing to accurately

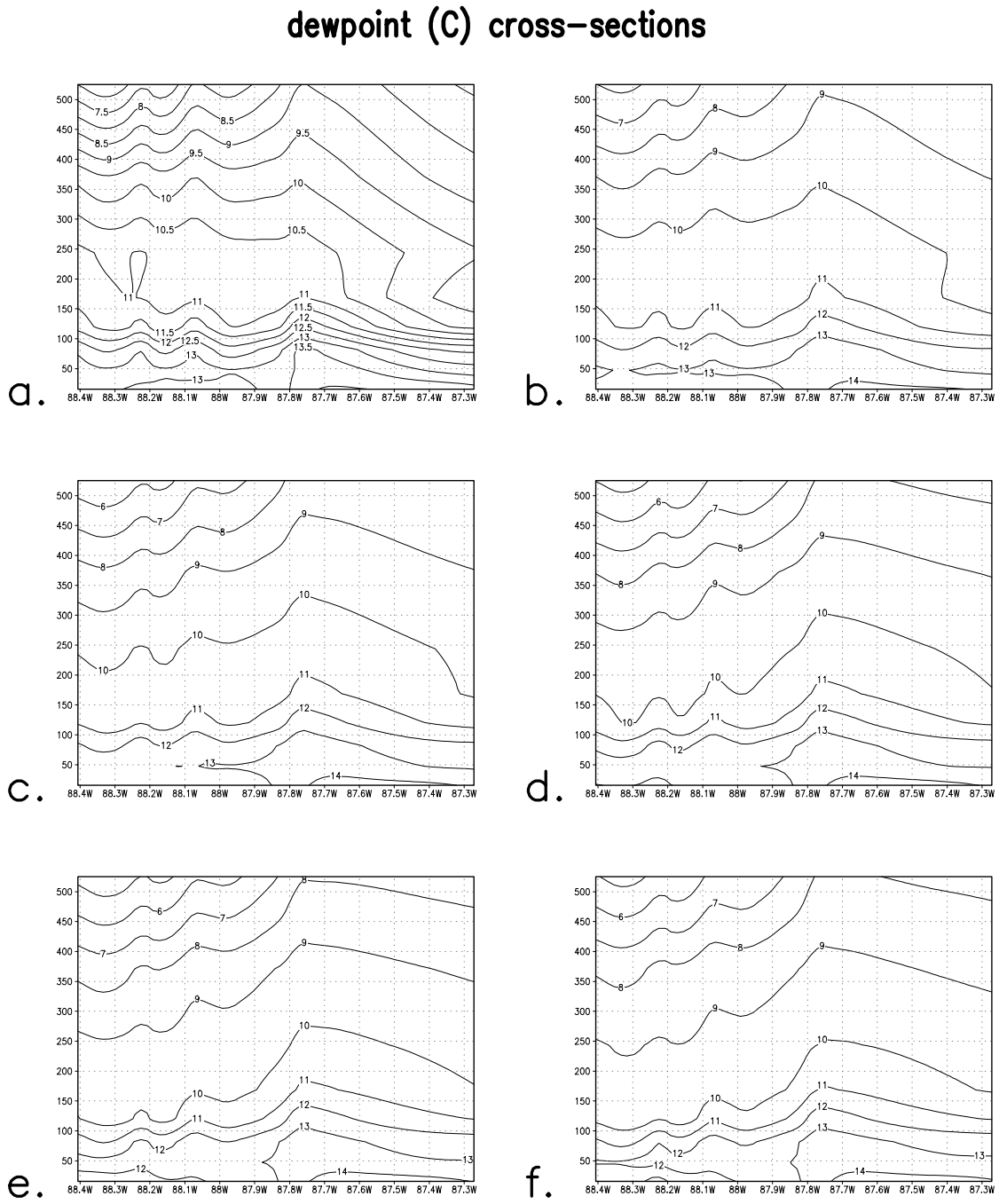

Figure 4.12 East-west cross-sections of dewpoint values (degrees C) from 0 to 500m AGL, through Kewaskum, WI, from the 11 October 2002 simulation. Times depicted are 03 UTC (a.), 04 UTC (b.), 05 UTC (c.), 06 UTC (d.), 07 UTC (e.), and 08 UTC (f.).

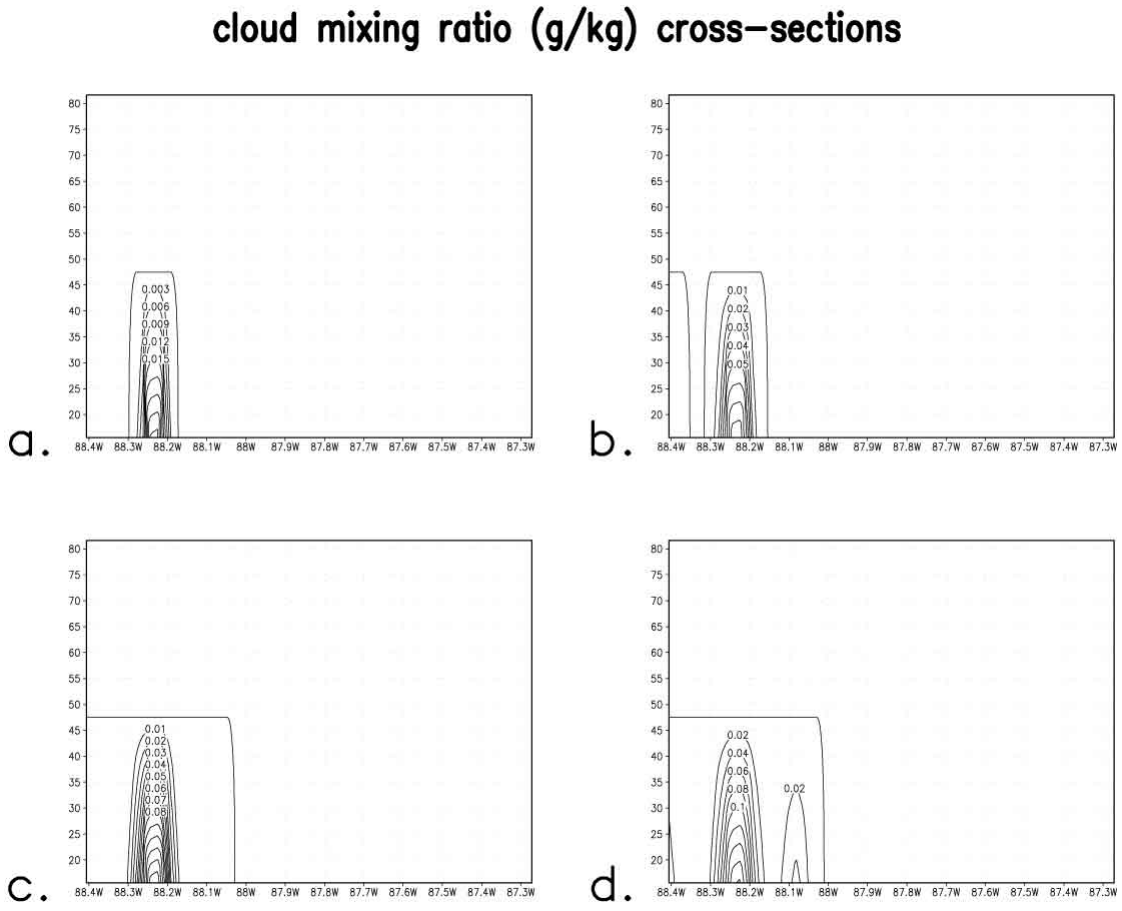

Figure 4.13 East-west cross-sections of cloud mixing ratios (g kg^{-1}) through Kewaskum, WI, from 0 to 500m AGL, from the 11 October 2002 simulation. Depicted are the first four hours of fog, 05 UTC (a.), 06 UTC (b.), 07 UTC (c.), and 08 UTC (d.).

simulate the evaporation of dew in the 21 January case. However, it is more likely that the discrepancy in the two simulations is explained by moisture found in the soil itself. The LEAF-2 vegetation model maintains a separate reservoir for holding moisture deposited on surface vegetation. The capacity of this reservoir is 0.22 kg of water per square meter of vegetation surface. Once this reservoir is full, further moisture deposition is run off onto the soil. Unlike the 21 January case, the 11 October case was

preceded by significant precipitation which left the ground rather moist. The increased dewpoints after sunrise, and the subsequent persistence of fog for two more hours, is more likely explained by the evaporation of ground moisture than by that of dew.

The 11 October fog event over Sheboygan, WI was clearly not simulated with the accuracy that the 21 January fog event over Angiola, CA was. However, the model's shortcomings did not lie in the microphysics. The lack of fog, or its delayed formation, can clearly be traced to errors in the wind field. This underscores the necessity of a model to accurately predict basic meteorological fields in order to yield an accurate fog forecast. However, all other aspects of the fog event appear to have been simulated with remarkable accuracy. When wind fields permitted, fog not only formed in our simulation, but it formed with a vertical structure consistent with published studies. The simulation also dissipated the fog at the same hour as observed. While the results leave much room for improvement, the model product would still prove useful to a forecaster, despite the model's inability to accurately simulate the land-lake interaction.

CHAPTER FIVE: SENSITIVITY STUDIES

5.1 OVERVIEW OF SENSITIVITY STUDIES

In this chapter, the model's sensitivity to changes in the horizontal resolution of initialization data, the number of nested vertical levels in the lower boundary layer, and changes in soil data will be examined by running several additional simulations with slight modifications to our original simulations. Doing so provides several benefits to scientists interested in developing numerical fog forecasts. First, examining model results under varying initial conditions allows a forecaster to identify the model's vulnerabilities, and to better determine the certainty of a forecast. Second, certain modifications to the model code decrease the computational efficiency of the model. Sensitivity studies allow one to achieve a balance between computational efficiency and model accuracy. Third, we have already seen that the numerical simulation of fog is highly dependent on an accurate simulation of the mesoscale and synoptic features accompanying the event. Sensitivity studies can give those interested in simulating fog with other mesoscale models an idea of the degree of accuracy required of a model if one wishes to produce an accurate simulation. While many different variables have an effect

on the simulation of fog, the author of this study has chosen to examine three variables for which a modeler has several options from which to choose.

5.2 VARIATIONS IN HORIZONTAL RESOLUTION OF INITIALIZATION DATA

As long as scientists have been interested in numerically modeling the atmosphere, there has been a desire for higher resolution initialization data. Often the modeler has no choice in the matter. The military application of an accurate fog forecast has already been discussed, but areas of interest such as the Middle East are virtually devoid of data. Within a vertical level, initialization data with a horizontal resolution of 40 km, as used in this study, provide between nine and sixteen initialization data points for the third grid of our model, which is comprised of 3844 grid points. If initialization data with a horizontal resolution of 80 km are used, the number of initialization data points in a vertical level is reduced to between one and four. Because the 21 January 2001 simulation over Angiola, CA represents a more accurate simulation, the simulation will now be repeated just as presented in Chapter 4, only with EDAS gridded analyses of 80-km horizontal resolution used for initialization. The 80-km EDAS gridded analyses are in the same format as the 40-km EDAS data, and are produced in the same manner, as described in Chapter 2.

The model initialized with 80-km EDAS data failed to simulate fog over any point on the third grid. Clearly this suggests that a horizontal resolution of 80 km is simply too coarse for initializing the simulation of a fine-scale event such as fog.

However, it is important to identify exactly why the 80-km initialization failed to simulate fog. In Figure 5.1, we see temperatures and dewpoints simulated over Angiola, CA, for both the simulation initialized with 80-km data and the simulation initialized with 40-km data. In the 80-km run, the initial temperature over Angiola was three degrees higher than the initial temperature in the 40-km run, and the initial dewpoint was two degrees lower. This difference was enough to keep saturation from occurring, and thus fog was never formed. In Figure 5.2, we see that the wind fields were quite similar in both runs. However, the nature of fog is such that temperature, dewpoint, and wind fields all have to be simulated accurately if the model is to simulate the fog itself. The use of 80-km initialization data simply allows for a larger error in the initialization fields than is allowed for an accurate fog simulation. This is particularly true of localized fog events, such as valley fogs. While higher-resolution initialization data were unavailable for this study, one would suspect even better results when the model is initialized with data

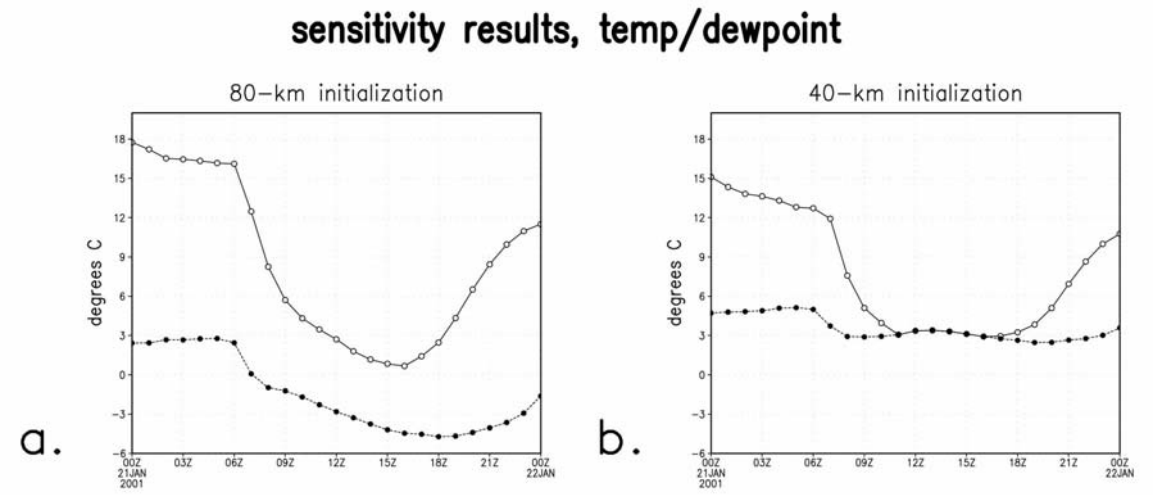

Figure 5.1 Model temperatures (solid) and dewpoints (dashed) (degrees C) over Angiola, CA, from a simulation of the 21 January fog event initialized with 80-km EDAS data (a.), in which fog was not simulated, and the control simulation initialized with 40-km data (b.), in which fog was simulated.

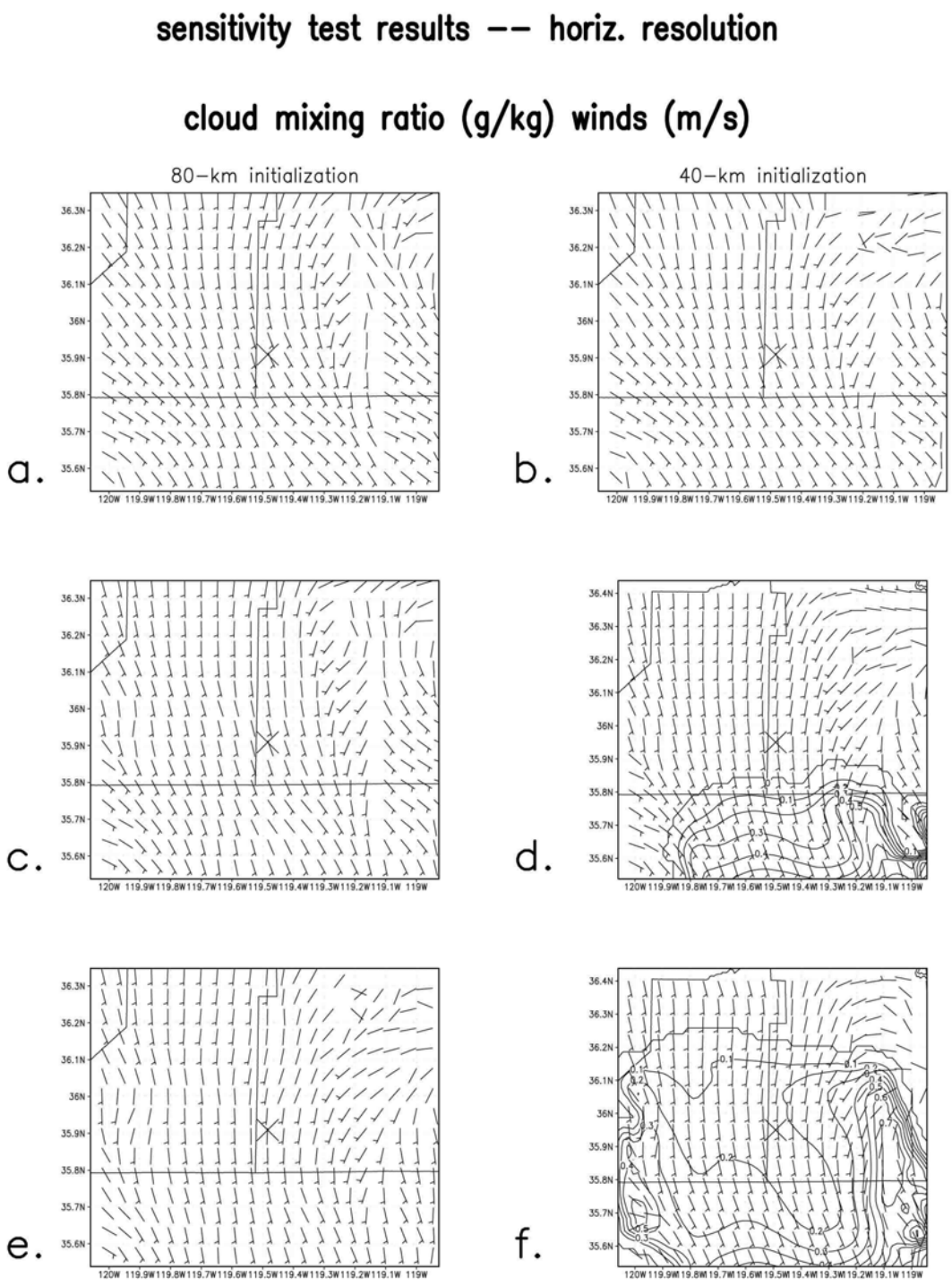

Figure 5.2 The left-hand side of the figure shows results of cloud mixing ratio (g kg^{-1}) and wind speed (m s^{-1}) from the simulation of the 21 January fog event initialized with 80-km EDAS data, for 08 UTC (a.), 10 UTC (c.), and 12 UTC (e.). The right-hand side of the figure is the same, but for the control simulation initialized with 40-km EDAS data, for 08 UTC (b.), 10 UTC (d.), and 12 UTC (f.).

exceeding 40 km in resolution. However, it seems that 40-km initialization data will generally provide an initialization adequate enough to simulate fog, while 80-km initialization data may produce too large an error to simulate fogs on a horizontal scale of 100 km or less.

5.3 VARIATIONS IN THE NESTING OF VERTICAL GRID LEVELS

One significant modification made to the operational RAMS@CSU mesoscale forecast model for this study was the addition of nested vertical levels in the lower boundary layer in the model's third grid. The purpose of this modification was two-fold. First, additional vertical levels allow for a lowest vertical level of 15.6m AGL instead of 50m AGL. As some fog never reaches above 50m AGL, this is quite important for an accurate fog forecast. Second, additional vertical levels allows the model to better resolve boundary-layer processes that are essential to the simulation of fog. However, adding additional vertical levels to the model's third grid reduces the computational efficiency of the model, which can make real-time forecasting unfeasible without state-of-the-art computer resources. Again, because the case represented a more accurate simulation, the 21 January fog event over Angiola, CA will be used for our sensitivity simulations. Our first simulation, hereby referred to as NestNull, will be run without any vertical nesting in the third grid. Our second simulation, hereby referred to as NestTen, will be run with ten additional vertical levels nested into the third grid. These results will

be compared to our control run, with three additional vertical levels as described in Chapter 2. A comparison of the vertical levels in the lower boundary layer used for each test run, as well as the control run, can be found in Figure 5.3.

The resulting values for cloud mixing ratio 50m AGL at Angiola, CA, for each of our sensitivity runs and the control run, can be found in Figure 5.4. While there is a slight discrepancy between the control run and the NestTen run, the significant discrepancy is found in the NestNull run. Clearly the addition of nested vertical levels in the third grid of our model contributes substantially to the accuracy of our simulation. However, the mechanism by which additional vertical levels reduce the cloud mixing ratio of our simulated fog is not initially clear. In order to identify this mechanism, we

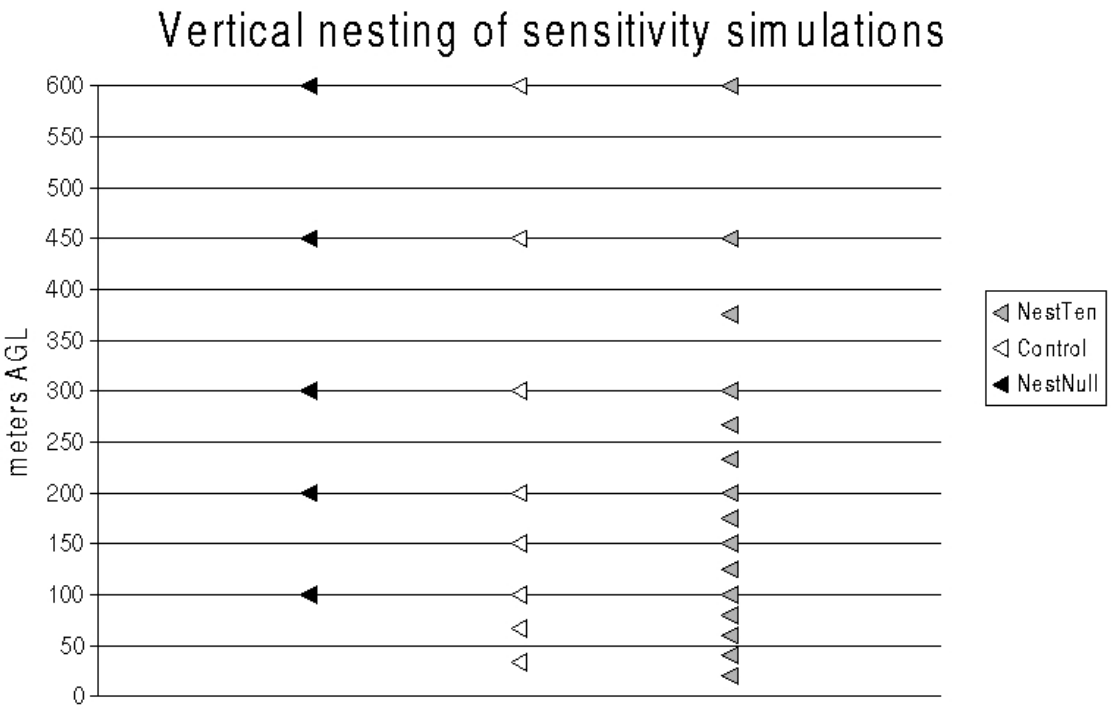

Figure 5.3 Vertical levels in the lower boundary layer used by the model for each sensitivity run and for the control run.

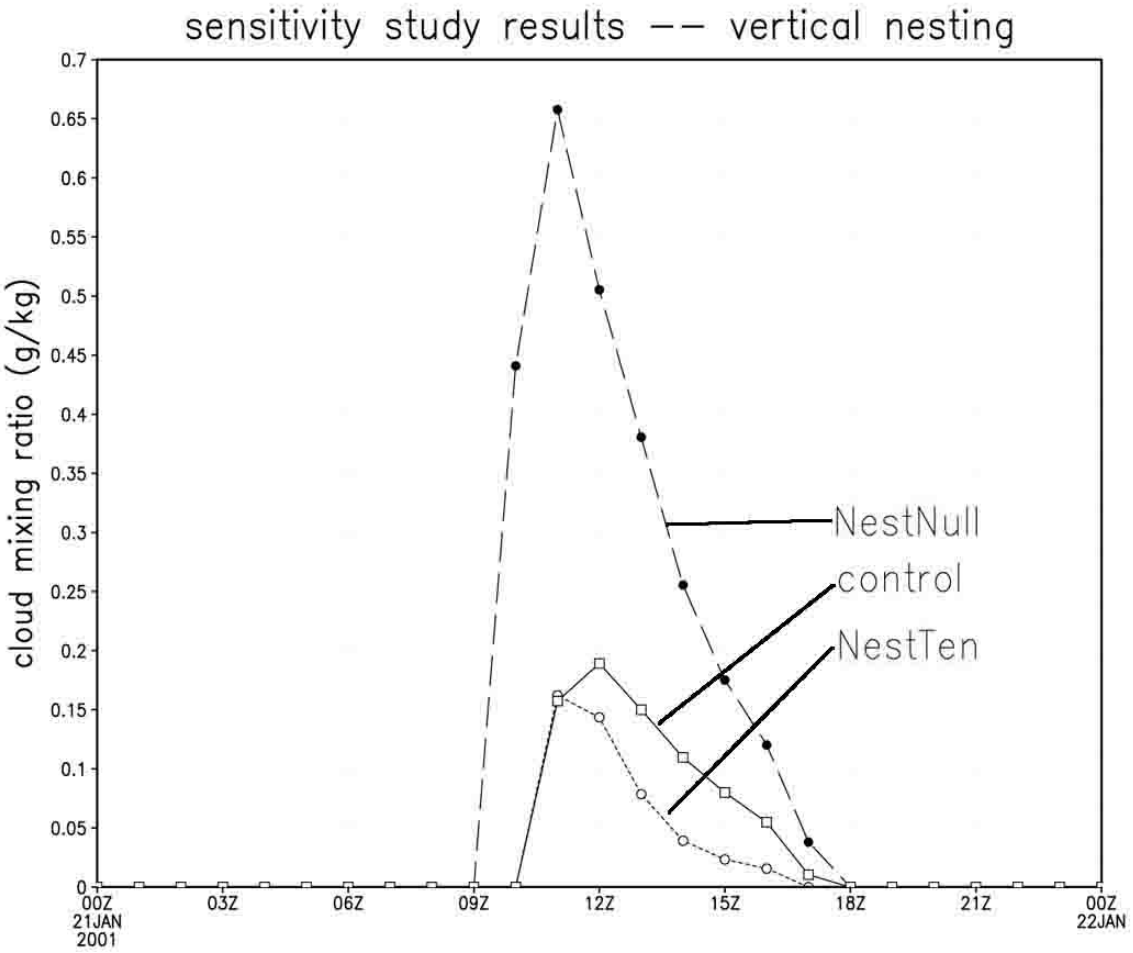

Figure 5.4 Model results of cloud mixing ratio (g kg^{-1}) over Angiola, CA at 50m AGL for two sensitivity simulations and the control run. Results from the NestTen simulation, with ten nested vertical levels, are represented by the short-dashed line. Results from the NestNull simulation, with no nested vertical levels, are represented by the long-dashed line. The control simulation is represented by the solid line.

must first examine the spatial characteristics of our simulated fog for each run. In Figure 5.5, the cloud mixing ratio at 50m AGL over the third grid is shown at 09 UTC and 10 UTC for each of our simulations. Very little difference is noted between the control run and the NestTen run. However, we again note a large discrepancy between the runs with nested vertical levels and the NestNull run. If one examines the fog at the southern boundary of the third grid, there is little difference between any of the three runs.

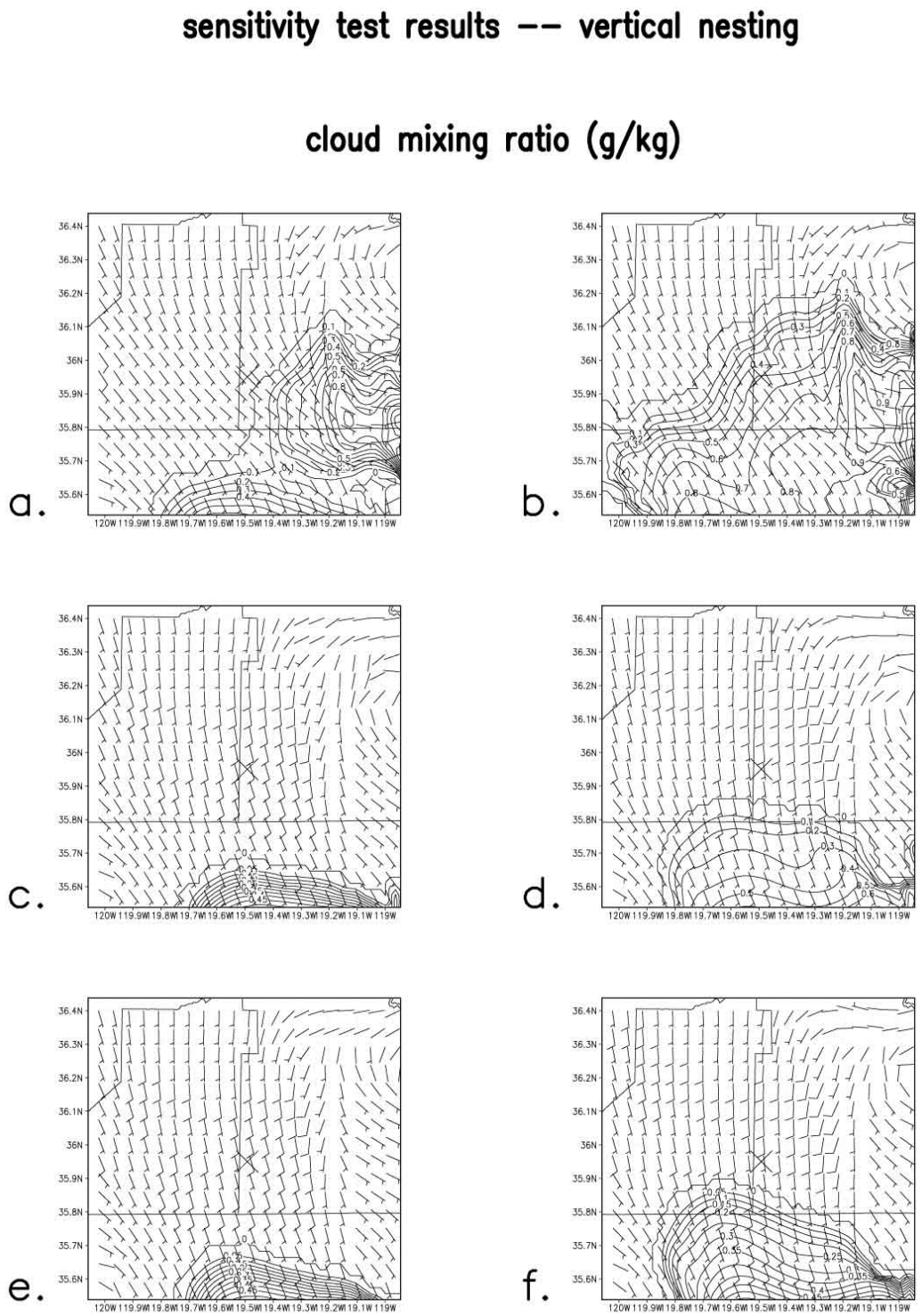

Figure 5.5 Model results of cloud mixing ratio (g kg^{-1}) and mean wind speed (m s^{-1}) for grid three at 50m AGL. Panels (a.) and (b.) are from 09 and 10 UTC from the NestNull simulation, (c.) and (d.) are from 09 and 10 UTC from the control run, and (e.) and (f.) are from 09 and 10 UTC from the NestTen simulation.

However, in the NestNull run, a second patch of fog with mixing ratios twice those suggested by Seinfeld and Pandis (1998) develops in the southeast portion of the third grid. It is this patch of fog that is responsible for mixing ratios significantly higher than observed over Angiola in the NestNull run.

This conclusion leads one to subsequently ask why this patch of fog forms, and why its mixing ratio values are so high. The answer to this question can be found by examining upward vertical velocities produced in each simulation (Fig. 5.6). One can see that the NestNull simulation produced upward vertical velocities nearly an order of magnitude greater than those produced by the NestTen run along the eastern boundary of the valley. While the exact mechanism of this error is unknown, the simulation's insufficient vertical resolution likely prevented the model from accurately simulating the circulation in the lower boundary layer. One may recall that, in the previous chapter, it was noted that the σ_z coordinate system tends to simulate higher-than-observed liquid water contents in areas of ascent. These results are consistent with such an evaluation. It appears that vertical levels of resolution greater than 50m are necessary in the lower boundary layer for the model to accurately simulate vertical winds near the surface. Fortunately, it appears that three additional levels are adequate for simulating fog, even in complex terrain. Further nesting of vertical levels offer no noticeable improvement in the fog simulation.

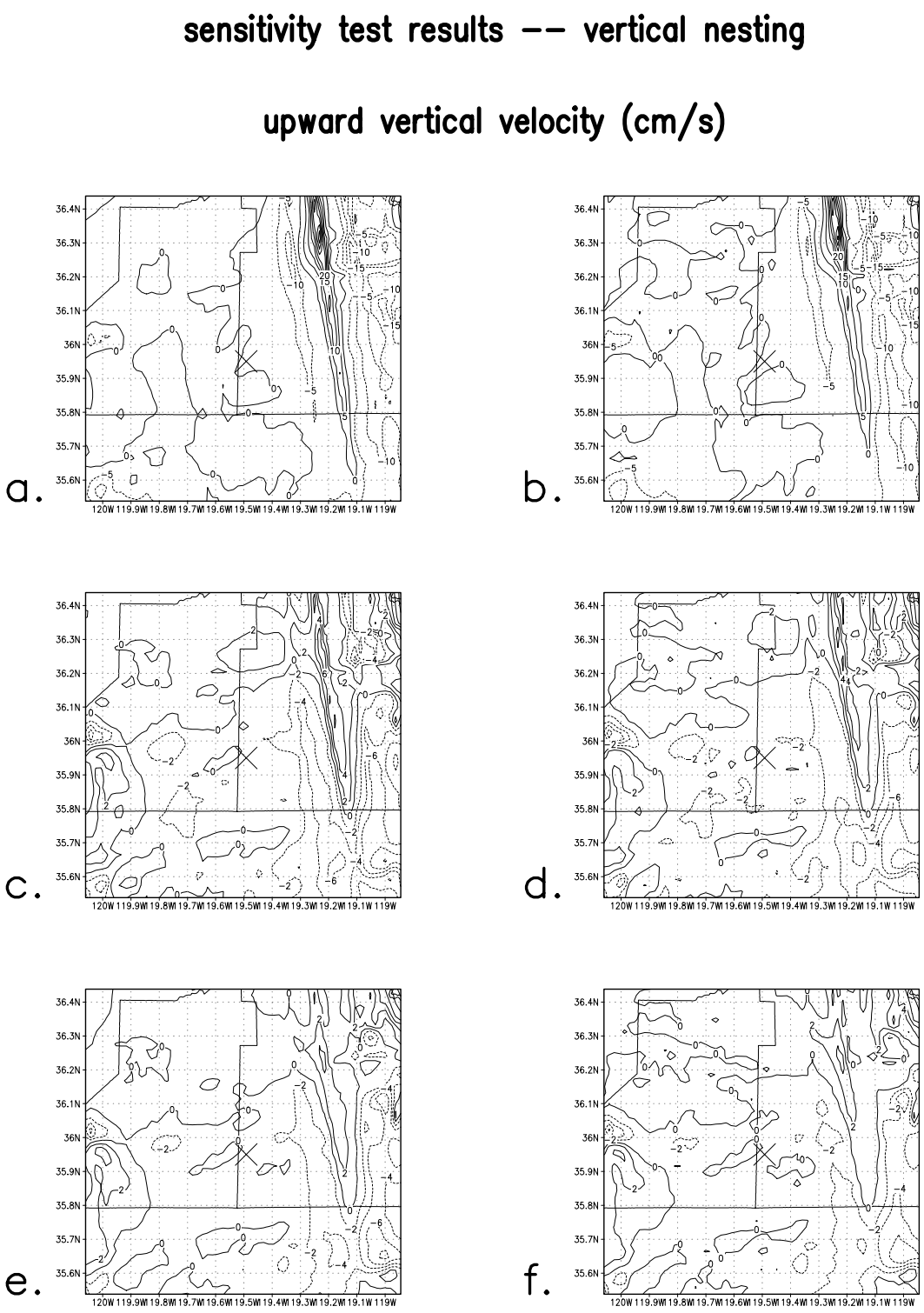

Figure 5.6 Same as Figure 5.5, but contours are of upward vertical velocities (m s^{-1}).

5.4 VARIATIONS IN SOIL MOISTURE

Another modification made to the RAMS@CSU real-time mesoscale forecast model was the ingestion of soil moisture and temperature data. Because moisture sources and sinks that are often ignored in mesoscale models become first-order sources and fog. However, many mesoscale models use homogeneous values for soil moisture, particularly when operating in real-time. As such, the model's sensitivity to soil moisture will be examined in three sensitivity simulations. The first sensitivity run, hereby referred to as SoilDry, uses a homogeneous volumetric soil moisture value of 0.10 $m^3 m^{-3}$. The second sensitivity run, hereby referred to as SoilWet, is initialized with a homogeneous volumetric soil moisture value of 0.45 $m^3 m^{-3}$. The third run, hereby referred to as SoilSplit, is run with a volumetric soil moisture value of 0.10 $m^3 m^{-3}$ on the southern half of the grid three domain and a value of 0.45 $m^3 m^{-3}$ on the northern half of the grid three domain; a sinusoidal gradient of 10-km width provides continuity between the two regions. Volumetric soil moisture values for grid three along the 88° W line of longitude, for each of the sensitivity runs and the control run, can be found in Figure 5.7.

The results of each sensitivity simulation, as well as the control run, for 09 UTC are shown in Figure 5.8. One immediately notices that two distinct patches of fog develop. The patch to the south, near Kewaskum, WI, has already been identified in Chapter 4. Another patch of fog develops in the northwest quadrant of grid three. This patch, simulated in all three sensitivity runs as well as the control run, is near Chilton, WI, and will henceforth be referred to as the Chilton patch. As one might expect, the

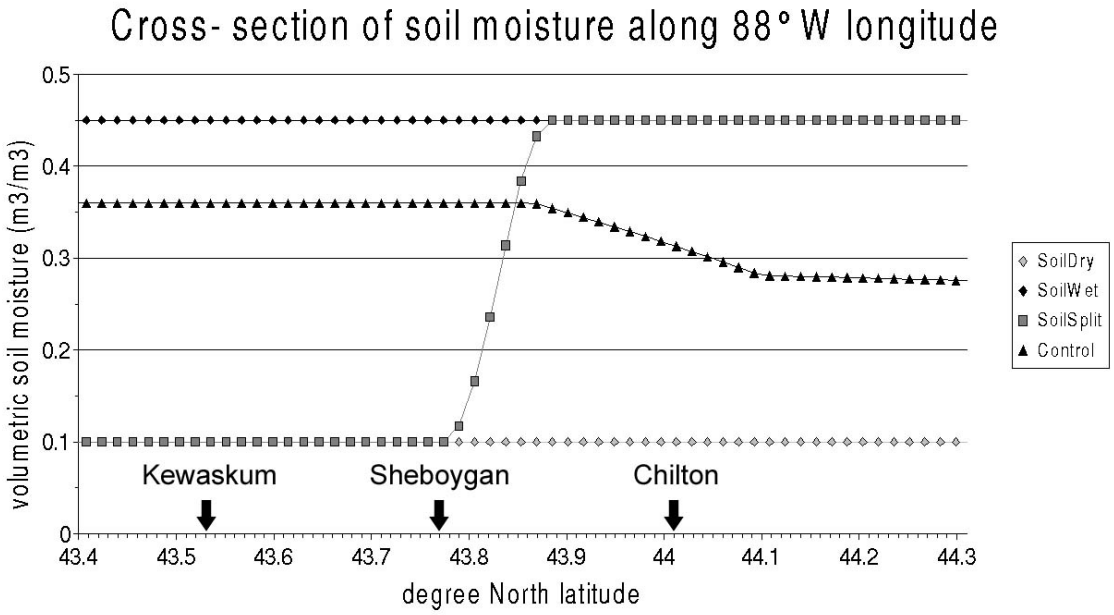

Figure 5.7 Volumetric soil moisture values ($m^3\ m^{-3}$) along the 88°W line of longitude, from 43.4°N latitude to 44.3°N latitude, for each soil sensitivity simulation, as well as the control run which used EDAS 40-km soil data.

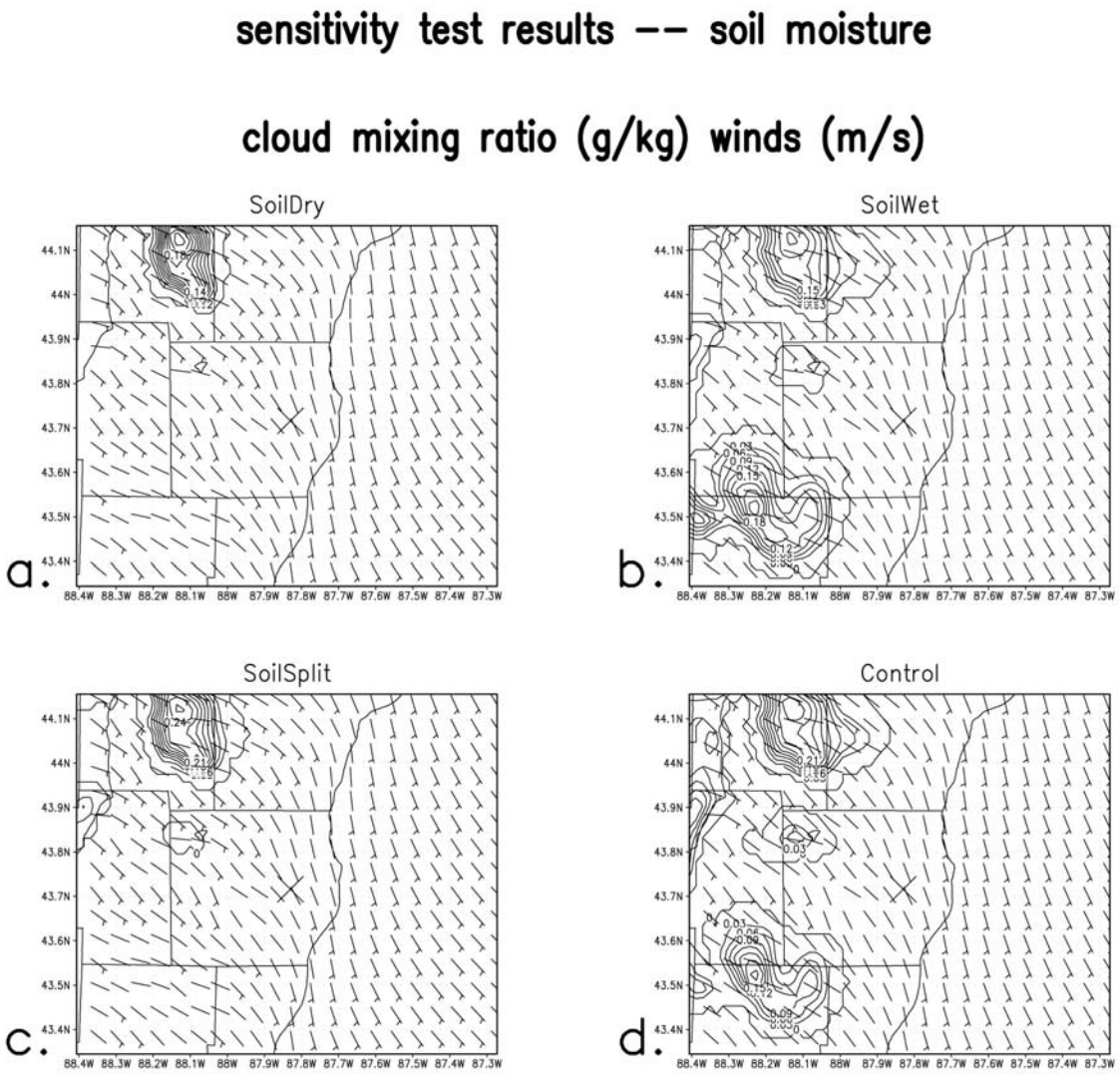

Figure 5.8 Model results of cloud mixing ratio (g kg^{-1}) and mean wind speed (m s^{-1}) at 09 UTC for each of the three sensitivity runs and the control run. Panel (a.) is the SoilDry run, (b.) is the SoilWet run, (c.) is the SoilSplit run (with the upper half of the domain wet and the lower half dry), and (d.) is the control run (using EDAS soil moisture values).

Kewaskum patch only develops in the SoilWet run and the control run, as these are the two runs in which the southern half of the domain contains moist soil. The Chilton patch also develops in the three runs where its soil is relatively moist. However, the Chilton patch likewise develops in the run with dry soil throughout the domain. If we look six hours later (Fig. 5.9), the Chilton patch is still observed in all three sensitivity simulations. In the control run, however, the Chilton patch has dissipated. On the whole, it seems that the SoilDry and SoilSplit runs have produced one result (the development of the Chilton patch but not the Kewaskum patch), while the SoilWet and control runs have produced another (the development of both the Chilton and Kewaskum patches).

In order to better understand these model results, cloud mixing ratio, temperature, and dewpoint values over Chilton and Kewaskum, for the duration of each simulation, are illustrated in Figure 5.10. One notices that, over Chilton, no obvious distinction exists between the meteorological values produced by each run. However, the results over Kewaskum can clearly be divided into two groups: the values for the SoilWet and control runs are almost identical, as are the results for the SoilDry and SoilSplit runs. The results over Kewaskum suggest that the simulation of fog can be quite sensitive to soil moisture values. Specifically, Figures 5.10e and 5.10f show that soil moisture has a significant effect on surface dewpoints. However, in the results over Chilton, we see that soil moisture, despite its effect on dewpoint, does not always suppress the fog. The soil near Chilton was relatively moist in each run except the SoilDry run, yet fog formed even in the SoilDry simulation. Figure 5.10e shows that, while the soil conditions clearly

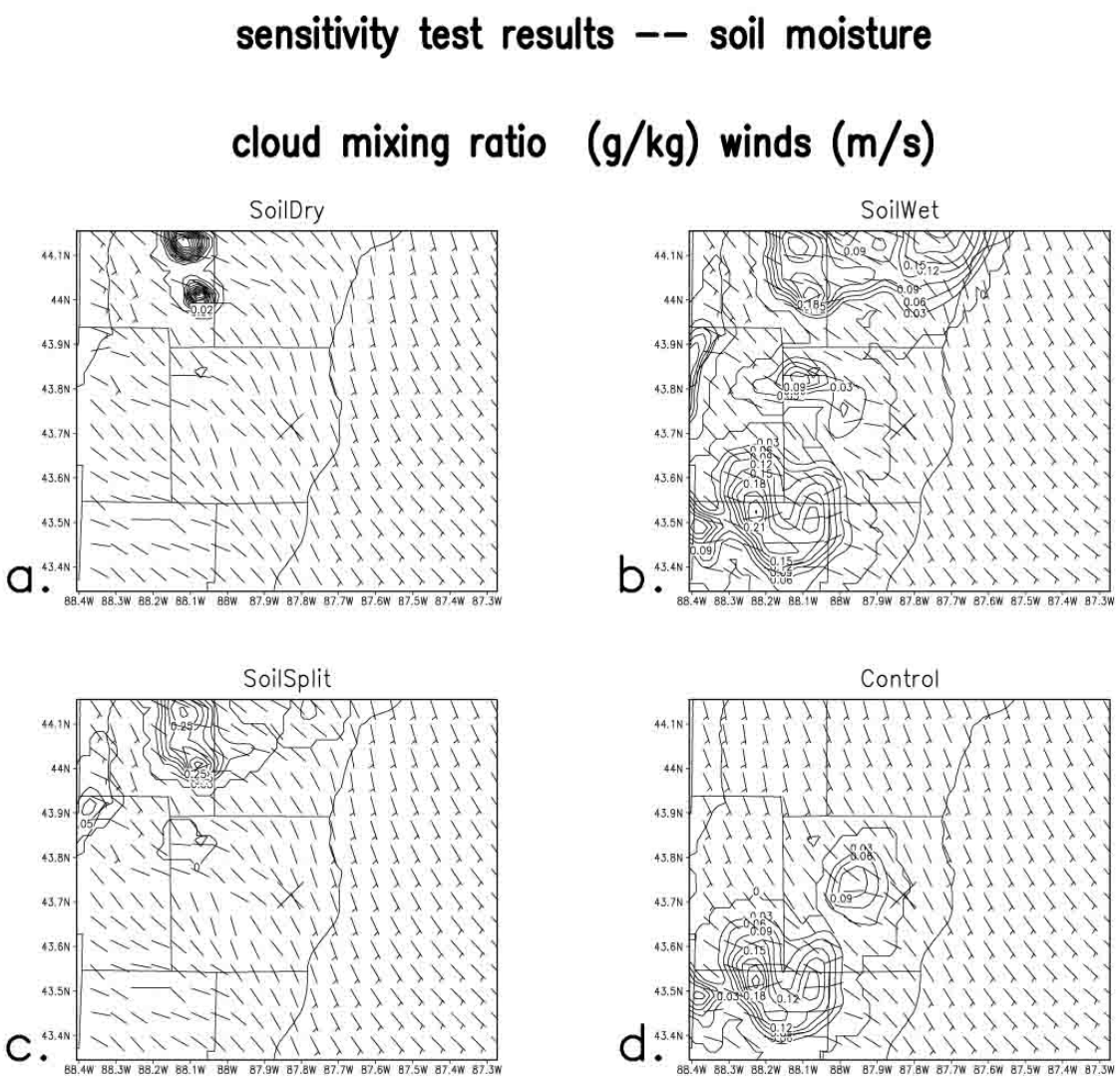

Figure 5.9 Same as Figure 5.8, but at 15 UTC.

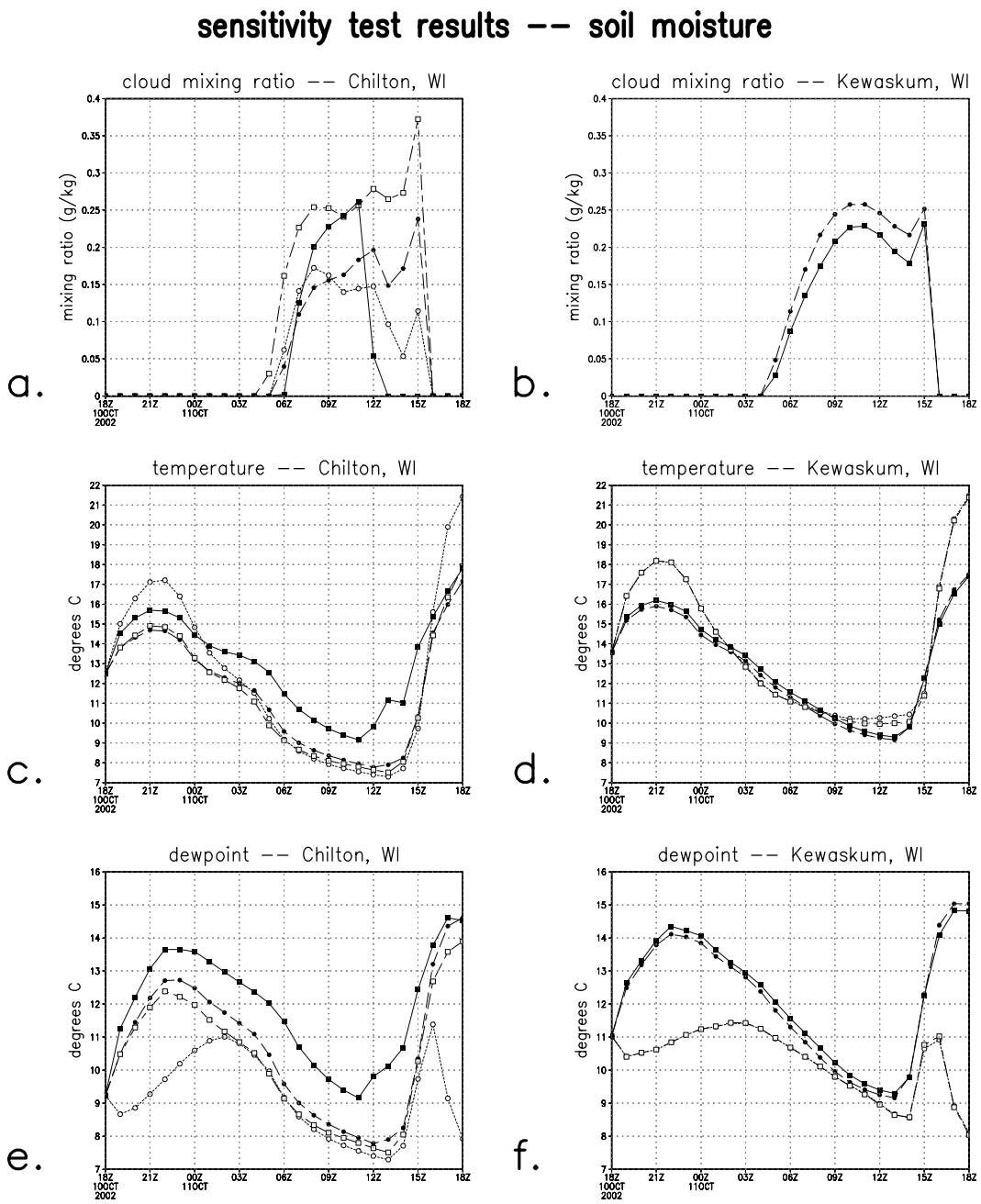

Figure 5.10 The left-hand side of this figure represents cloud mixing ratio (g kg^{-1}) (a.), temperature (degrees C) (c.), and dewpoint (degrees C) (e.) values simulated over Chilton, WI, in each soil sensitivity run and the control run. The right-hand side represents cloud mixing ratio (b.), temperature (d.), and dewpoint (f.) values simulated over Kewaskum, WI, for each soil sensitivity run and the control run. SoilDry simulation values are represented by a short-dashed line with white circles. SoilWet simulation values are represented by a long-dashed line with black circles. SoilSplit simulation values are represented by a short-long-dashed line with white squares. The control simulation is represented by a solid line with black squares.

lowered dewpoints when compared to the other runs, saturation was still met by 06 UTC. It appears the explanation for this observation is that dew deposition lowered dewpoint values in the other three runs, while dewpoints in the SoilDry rose due to advection of moist air from Lake Michigan. At 02 UTC, the dewpoint in the SoilDry run reached a level where deposition processes began, and after that point the dewpoint profile was quite similar to the other three runs. It seems merely coincidental that dew deposition in the SoilDry run began when the dewpoint was near the same value as the other three runs. Over Kewaskum (Fig. 5.10f), we see a similar pattern in the dewpoint from the SoilDry run and the SoilSplit run (recalling that the two runs have the same soil characteristics at Kewaskum). However, in the Kewaskum case, the dewpoints in the SoilDry and SoilSplit runs are still two degrees lower than the other runs when dew deposition begins. As such, the dewpoint never reaches a level adequate for saturation, and fog does not form. In the end, the Kewaskum patch was much more sensitive to the soil moisture than the Chilton patch was. The SoilDry run had two unique occurrences that allowed fog to form at Chilton. First, as previously mentioned, dew deposition did not begin until it reached the same dewpoint as simulated in the other runs. Second, there was moisture advection to increase the dewpoint in the first place. It seems likely that the majority of fog simulations would not have the benefit of both these occurrences, and as such most simulations will be quite sensitive to soil moisture, as was the case over Kewaskum.

One other curious observation is made from our sensitivity study. The cloud mixing ratios in Figure 5.10 show similar behavior for each case in which fog is

simulated except for the control simulation over Chilton. The control run over Chilton is the only time we see a significant change in a fog's formation or dissipation. As the soil moisture content at Chilton for the control is between that of the SoilDry run and SoilWet run, such a result is unexpected. The mechanism for the early dissipation can be found in the wind speeds simulated over Chilton (Fig. 5.11). The fog's premature dissipation in the control run is actually the result of an increased wind field, rather than a lack of adequate soil moisture. One notes that, again in Figure 5.11, it seems that 2 m s^{-1} is the threshold between fog and no fog. It is important to recognize that this result suggests that variations in soil moisture may have secondary effects on variables such as horizontal winds that can significantly alter the fog simulation. On the whole, the sensitivity study suggests that representative soil moisture values should be integrated into the third grid of the model for improved accuracy in the numerical simulation of fog.

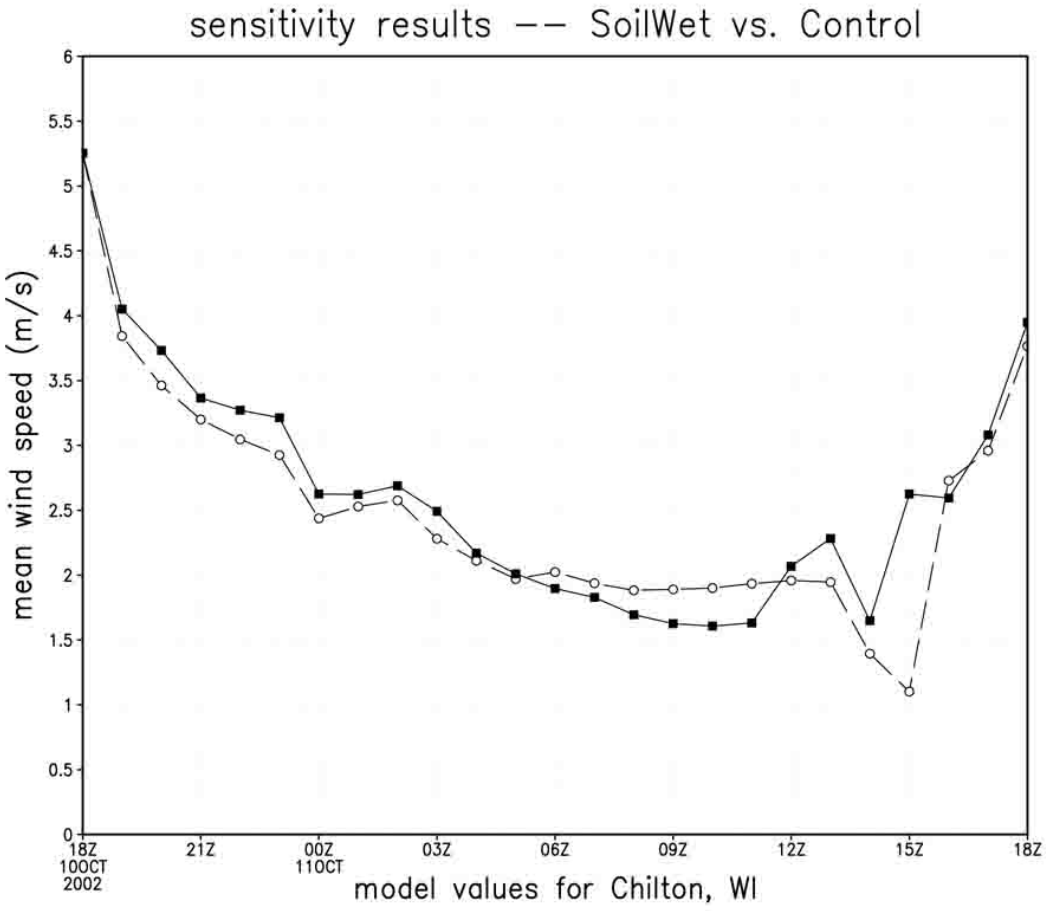

Figure 5.11 Model results of mean wind speed values (m s^{-1}) over Chilton, WI for the SoilWet sensitivity simulation (long dashed with white circles) and the control simulation (solid with black squares).

CHAPTER SIX: CONCLUSIONS

6.1 SUMMARY AND CONCLUSIONS

In this study, the RAMS@CSU mesoscale forecast model was used to simulate two fog events. The model was run with three nested grids, the smallest being of 2-km horizontal resolution, with nested vertical levels allowing for 16-m vertical resolution in the lower boundary layer of grid three. Atmospheric fields in the model were initialized with EDAS 40-km data, and surface fields were initialized with EDAS soil data and NOAA OI sea surface temperature data.

Two fog events were simulated. The first event was a valley fog observed 21 January 2001 over Angiola, CA, located on the southern end of the San Joaquin Valley. This fog event occurred under a strong subsidence regime, and was representative of the valley fog model presented by Pilié *et al.* (1975a, 1975b). Liquid water content observations were taken by the CRPAQS field campaign, which made this case particularly attractive. The second fog event chosen was 11 October 2002 over Sheboygan, WI. Unlike the 21 January event, this particular fog event occurred in a transitional weather pattern, with a low-pressure system having died out earlier that day,

and a stationary front present to the south. The fog resulted from radiative cooling after sundown, with the development of a land breeze near the coast of Lake Michigan negating the easterly synoptic winds and leading to still conditions that facilitated the fog's development.

Each of our two cases were simulated for twenty-four hours, and the results were examined both in terms of cloud mixing ratios simulated at the lowest level, and in terms of the microphysical processes which led to the fog's development. In the 21 January event, the model simulated fog an hour prior to the first observed fog, and dissipated fog an hour earlier than observed. The maximum liquid water content of the fog was approximately twice that simulated by the model. Closer inspection of the model's results revealed that the model simulated nearly all of the processes involved in the development of a valley fog. A valley drainage flow, a dewpoint inversion in the lowest 150m AGL, the deposition of dew, the fog's development near 150m AGL, and the fog's dissipation from the surface up, all consistent with the theoretical model developed by Pilié *et al.* (1975a, 1975b), are found in the model's results. Errors in liquid water content are explained by known transformation errors in the σ_z coordinate system. The fog's premature formation is the result of the model simulating stronger cooling than observed, and its premature dissipation is due to model's inability to accurately evaporate ground moisture after sunrise. Overall, the model accurately simulated the fog event.

In the 11 October fog event, the model failed to simulate significant fog over Sheboygan, WI. However, fog was simulated over much of the third grid. If one examines cloud mixing ratios over nearby Kewaskum, WI (which, according to satellite

observations, was under the same fog patch as Sheboygan), the model appears to have simulated the fog event rather well. While the model's onset of fog was four hours late, the dissipation was simulated the same hour as observed. The discrepancy between the forecast over Sheboygan and the forecast over Kewaskum can be explained by the simulated wind fields. Cotton and Anthes (1989) suggest that winds greater than 2 m s^{-1} generate enough turbulent mixing to inhibit saturation and fog development, while winds weaker than 2 m s^{-1} facilitate the development of fog. The winds over Sheboygan stay just above this threshold, while the winds at Kewaskum dip to 1.5 m s^{-1} in our simulation. This error is likely due to slight inaccuracies in the model's simulation of the land-lake interaction which stilled the easterly synoptic winds in observations. Other meteorological results from the simulation, including the vertical structure of dewpoints and cloud mixing ratio, suggest that microphysical processes involved in the fog event have been accurately simulated. As such, it is reasonable to conclude that, had the winds been accurately simulated, fog would have been simulated as observed. Despite this error, the fog product would still prove quite useful to a forecaster, and the time of the fog's dissipation was accurately simulated.

Additional simulations were completed to test the model's sensitivity to changes in the horizontal resolution of initialization data, the number of additional vertical levels nested into the third grid, and soil moisture values. The use of EDAS 80-km initialization data, rather than EDAS 40-km data, was found to contribute to poorer synoptic forecasts, particularly temperatures and dewpoints, and thus decrease the accuracy of fog forecasts. While additional nested vertical levels were found to offer

little improvement from the standard simulation run with three nested levels, a simulation run without any nested vertical levels was found to produce erroneous fog in areas of upward vertical motion. This can be attributed to the model's inability to accurately simulate winds in the lowest 100m AGL when no vertical level exist below 100m. This error is magnified by the fact that saturation mixing ratios are decreased in areas of upward vertical motion in the σ_z coordinate system, and thus the erroneous fog simulated also contained liquid water contents much higher than that proposed by Seinfeld and Pandis (1998) as the maximum observed in fog. The third set of sensitivity simulations revealed that soil moisture values have a significant effect on surface dewpoints, and can thus affect whether or not saturation occurs. The simulations also showed that soil moisture values can have secondary effects on local circulations, and can affect the development of fog through such mechanisms as well.

The results of our two simulations, as well as the sensitivity studies, suggest three main conclusions regarding the numerical simulation of fog. First, our simulations confirm the conclusions of Brown (1980), that thermal cooling, turbulent transport, and the deposition of moisture on the soil are necessary for the simulation of fog, and Ballard *et al.* (1991), that accurate initialization and high vertical resolution near the surface are also necessary for the simulation of fog. With the development of vegetation models, the assessment of Brown (1980) should be modified to include the deposition of moisture on vegetation as well as soil. Our results also suggest that the evaporation of ground moisture after sunrise is necessary for an accurate simulation of the dissipation of fog. Overall, our model simulations have been shown to handle the aforementioned processes

adequately, and when model errors in the forecasting of fog were identified, they were generally the result of inaccuracies in the model's simulation of these processes. Specifically, errors in thermal cooling often resulted in the premature or delayed onset of fog, errors in turbulent transport (associated with erroneous wind fields) led to delayed fog or no fog at all, and errors in moisture deposition led to the premature dissipation of fog. One can logically conclude that, as the numerical modeling community improves on our current abilities to simulate these processes, our ability to numerically forecast fog will improve as well.

The second conclusion reached in this study is that the RAMS@CSU model, as modified for this study, is capable of simulating the microphysical processes necessary to accurately simulate fog. The modifications made to the real-time model, particularly the addition of nested vertical levels in the boundary layer of the third grid, have been shown to be necessary if one is to accurate simulate fog. While errors, as described in the previous paragraph, occasionally contributed to inaccuracies in the formation of fog, our simulations were shown to recreate fine-scale features, such as dewpoint inversions and initial formation aloft, that are suggested by observations and previous studies. While Teixeira (1999) has previously published the simulation of fog on a continental scale, this is the first published study in which a mesoscale model is employed to simulate fog at such a fine resolution and with such detailed results. What's more, such a simulation could be run in real-time. This is of the utmost importance because it suggests that, when synoptic-scale and mesoscale features are properly simulated, the model will not only

forecast fog, but it will provide valuable information about the horizontal and vertical structure of the fog.

The numerical simulations presented in this study also underscore the need for an accurate synoptic forecast. Small errors in the temperature, dewpoint, or wind fields can easily prevent the model from accurately simulating fog. As such, it is recommended that a modeler initialize the model as accurately as possible to ensure an accurate synoptic forecast. This can be achieved by initializing the model with the highest-resolution data available, both for the atmosphere and the surface. Observational or model-derived data are always preferred to climatological data or homogeneous fields for soil moisture, soil temperatures, sea surface temperatures, and vegetation type. A postulate to this conclusion is that problematic areas for the model's synoptic forecast (e.g. lee of the Rockies) will likewise be problematic areas for the fog forecast. Again, as initialization data increase in resolution and accuracy, and as mesoscale models improve in their overall forecasting abilities, our ability to simulate fog will improve.

In conclusion, the RAMS@CSU mesoscale forecast model has shown itself to be capable of simulating fog. Discrepancies between the simulations and observations generally resulted from errors in the model's temperature, dewpoint, or wind forecasts. As mesoscale models, and the quality of their initialization data, improve, so too will the accuracy of fog simulations. Even with today's modeling technology, significant features of fog development, including the deposition of dew and the lifting of fog after sunrise, are identified in the model results. This suggests that, when the synoptic and mesoscale features of a fog event are accurately simulated, fog will indeed be produced by a model

with advanced microphysics and sufficient vertical levels near the surface. Indeed, even with errors in the fog's timing and spatial distribution, both simulations presented in this study would serve as useful tools to forecasters.

6.2 FUTURE WORK

While the author feels this study is an important first step toward the development of a real-time fog forecast product, future work is required before such a product could become operational. First and foremost, higher resolution initialization data would yield a more accurate synoptic and mesoscale simulation, thereby increasing the accuracy of a fog product. While unavailable for this study, such data are used operationally in products such as the NCEP Rapid Update Cycle (RUC) model. Further improvements to the fog forecast could be made by improving the surface initialization of the model. The EDAS 40-km soil moisture and temperature data used in this study are model-derived, and verification data near the cases presented in this study were unavailable. Furthermore, the offline interpolation method used to convert the data from the Eta projection to the RAMS projection sometimes led to errors near coastlines. An accurate real-time fog forecast product would require the online interpolation of accurate, high-resolution soil data. Likewise, daily SST data would be preferred to the weekly averaged SST data used in this study. Finally, the use of a homogeneous soil type was cited in Chapter 4 as a possible source of error in the evaporation of dew after sunrise. The implementation of a soil-type dataset for North America, similar to the Zobler dataset as

distributed by Webb *et al.* (1993), could improve the moisture exchange between the surface and the boundary layer, and subsequently improve fog forecasts.

While many suggested improvements pertain to the data used to initialize the model, the RAMS@CSU model itself also has room for improvement. The σ_z coordinate system has been discussed previously in this study as a source of error, particularly in areas of complex terrain. Modifications such as those published by Zängl (2002) have been suggested as means of improving the computation of horizontal diffusion in a σ coordinate system. Such an improvement would certainly improve the quality of a fog forecast product. Another improvement involves the simulation of cloud drops in the model. For this study, the drop concentration was specified in the model. Another model option allows for the number of cloud condensation nuclei (CCN) to be specified, but the activation of CCN is a function of upward vertical velocities. As such, in stable cases such as fog, the activation of CCN is not accurately simulated. While the lack of CCN initialization data makes it unlikely a real-time product would utilize this option, subsequent numerical studies might find such an option useful. Thus it is recommended that the activation of CCN be reformulated to account for radiative cooling as well as the adiabatic cooling that results from upward motion. Also, operational forecasters may find a real-time fog product more useful if the output were in terms of visibility rather than cloud mixing ratio. An empirical relationship between liquid water content and observed visibility is derived in Kunkel (1984) and could easily be integrated into a model as a derived product.

The introduction of nested vertical grids, as well as the use of nested horizontal grids, raises concerns about the turbulent closure schemes used in the model. Particularly, the Mellor-Yamada closure scheme, while well-suited for the large first grid, is not designed for the fine horizontal grid spacing found in the model's third grid. Also, the Mellor-Yamada scheme has been found to have problems in stable simulations (Xue *et al.*, 1996). Unfortunately, because the various grids employ two-way feedback, only one turbulence scheme can be used or else the grids will share incompatible coefficients. While it seems that the model ran adequately with the Mellor-Yamada scheme, one would expect an improved simulation of boundary-layer turbulence and moisture fluxes if a better-suited closure scheme were employed in the model's third grid. This could be done in one of two ways. First, the model code could be modified to prevent the sharing of incompatible coefficients between grids. Doing so would allow one to run the Mellor-Yamada scheme for the first grid while using a more appropriate scheme for the finer grids. Another option would be to integrate a probability density function-based model for simulating boundary layer clouds, such as the one developed by Golaz *et al.* (2002a, 2002b). Such as scheme was designed to be flexible enough to represent a variety of cloudiness regimes without the need for case-specific adjustments. This would be quite beneficial in a fog model, as the fog model must be able to properly simulate atmospheric behavior in many different regimes.

Finally, I would suggest that this study be extended in two ways. First, while the two cases presented in this study were quite different, they would both be classified as radiation fogs. It would be of great value to simulate frontal fogs, marine fogs, and ice

fogs, and see if the model's results are similar to observations. Second, while the model handled these two cases rather well, this study does not give one an idea of how often the model would miss fog events altogether. One could gather useful statistics on the accuracy of a fog product by running the model in real-time. The third grid could either be moved on a daily basis to regions where fog is likely, or kept in one area where fog is commonly observed. Over the course of months, one could get a better picture of the fog product's operational value to military, government, and private sector forecasters.

CHAPTER SEVEN: WORKS CITED

Adams, M., 2003. Personal correspondence. Wisconsin Department of Transportation.

Ali, S.A., 2001: Potential use of fog as an alternative water resource in the dry and semi-arid mountain chains of northern and eastern Ethiopia. *Preprints, 2nd International Conference on Fog and Fog Collection,* St. John's, 215-218.

Ballard, S.P., B.W. Golding, and R.N.B. Smith, 1991: Mesoscale model experiment forecasts of the Harr of northeast Scotland. *Mon. Wea. Rev.*, **119**, 2107-2123.

Barker, E.H., 1977: A maritime boundary layer model for the prediction of fog. *Boundary-Layer Meteor.*, **11**, 267-294.

Bauer, H., H. Giebl, A. Kasper-Giebl, M. Löflund, B. Schuster, F. Zibuschka, R. Hitzenberger, G. Reischl, and H. Puxbaum, 2001: Bacteria and fungi in aerosols and clouds. *Preprints, 2nd International Conference on Fog and Fog Collection,*St. John's, 5-8.

Bluestein, H.B., 1993: *Synoptic-Dynamic Meteorology in Midlatitudes. Volume II: Observations and Theory of Weather Systems*. Oxford University Press, New York, USA.

Bott, A. and T. Trautmann, 2002: PAFOG-a new efficient forecast model of radiation fog and low-level stratiform clouds. *Atmos. Research*, **64**, 191-203.

Bott, A., U. Sievers, and W. Zdunkowski, 1990: A radiation fog model with a detailed treatment of the interaction between radiative transfer and fog microphysics. *J. Atmos. Sci.*, **47**, 2153-2166.

Brown, R., 1980: A numerical study of radation fog with an explicit formulation of the microphysics. *Quart. J. Roy. Meteor. Soc.*, **106**, 781-802.

Brown, R. and W.T. Roach, 1976: The physics of radiation fog: II-A numerical study. *Quart. J. Roy. Meteor. Soc.*, **102**, 335-354.

Clark, T.L., 1977: A small-scale dynamic model using a terrain-following coordinate transformation. *J. Comput. Phys.*, **24**, 186-215.

Clark, T.L. and R.D. Farley, 1984: Severe downslope windstorm calculations in two and three spatial dimensions using anelastic interactive grid nesting: a possible mechanism for gustiness. *J. Atmos. Sci.*, **41**, 329-350.

Clark, T.L. and W.D. Hall, 1991: Multi-domain simulations of the time dependent Navier-Stokes equations: benchmark error analysis of some nesting procedures. *J. Comput. Phys.*, **92**, 456-481.

Cotton, W.R. and R.A. Anthes, 1989: *Storm and cloud dynamics*. Academic Press, San Diego, USA.

Cotton, W.R., R.A. Pielke, Sr., R.L. Walko, G.E. Liston, C.J. Tremback, H. Jiang, R.L. McAnelly, J.Y. Harrington, M.E. Nicholls, G.G. Carrio, J.P. McFadden, 2003: RAMS 2001: Current status and future directions. *Meteor. Atmos. Phys.*, **82**, 5-29.

Cram, J.M., 1990: Numerical simulation and analysis of the propagation of a prefrontal squall line. PhD dissertation, Atmos. Sci. Paper No. 471, Colorado State University, Dept. of Atmos. Sci., Fort Collins, CO, 332 pp.

Croft, P.J., R.L. Pfost, J.M. Medlin, G.A. Johnson, 1997: Fog forecasting for the southern region: A conceptual model approach. *Wea. Forecasting,* **12**, 545-556.

Davies, H.C., 1976: A lateral boundary formulation for multi-level prediction models. *Quart. J. Roy. Meteor. Soc.*, **102**, 405-418.

Davies, H.C. and R.E. Turner, 1977: Updating prediction models by dynamical relaxation: An examination of technique. *Quart. J. Roy. Meteor. Soc.*, **103**, 225-245.

Ediang, O.A., 2001: Piracy and armed robbery against ships and aircraft in the Niger Delta: negative impact of fog in Nigeria. *Preprints, 2nd International Conference on Fog and Fog Collection,* St. John's, 421-425.

Feit, D.M., 1972: A study of numerical simulation of maritime fog. Monterey, California, Naval Postgraduate School.

Fisher, E.L. and P. Caplan, 1963: An experiment in the numerical prediction of fog and stratus. *J. Atmos. Sci.,* **20**, 425-437.

Fitzenberger, J., 2003: A way through the fog. *The Fresno Bee*, January 6, 2003.

Gal-Chen, T. and R.C.J. Somerville, 1975: On the use of a coordinate transformation for the solution of the Navier Stokes equations. *J. Comput. Phys.,* **17**, 209-228.

Glickman, T.S. (ed.), 2000: *Glossary of Meteorology*, *Second Ed*. American Meteorological Sociey, Boston, USA.

Golaz, J.C., V.E. Larson, and W.R. Cotton, 2002a: A PDF-based model for boundary layer clouds. Part I: Method and model description. *J. Atmos. Sci.*, **59**, 3540-3551.

Golaz, J.C., V.E. Larson, and W.R. Cotton, 2002b: A PDF-based model for boundary layer clouds. Part II: Model results. *J. Atmos. Sci.*, **59**, 3552-3571.

Harrington, J.Y., 1997: The effects of radiative and microphysical processes on simulated warm and transition season Arctic stratus. PhD Diss., Atmospheric Science Paper No. 637, Colorado State University, Department of Atmospheric Science, Fort Collins, CO 80523, 289 pp.

Herckes, P., M. Millet, P. Mirabel, and H. Wortham, 2001: Fogwater composition in Strasbourg (France) from 1990-1999 - a change in urban air quality? *Preprints, 2nd International Conference on Fog and Fog Collection,* St. John's, 77-80.

Herckes, P., T. Lee, L. Trenary, G. Kang, H. Chang, and J.L. Collett, Jr., 2002: Organic matter in central California radiation fogs. *Environ. Sci. Technol.*, **36**, 4777-4782.

Hill, G.E., 1974: Factors controlling the size and spacing of cumulus clouds as revealed by numerical experiments. *J. Atmos. Sci.*, **31**, 646-673.

Jaén, V.M., 2001: Fog: drinking water for rural zones. *Preprints, 2nd International Conference on Fog and Fog Collection,* St. John's, 247-250.

Johnson, A., 2002: Fog a common contributor to crashes, especially on I-43. *Milwaukee Journal Sentinel*, October 12, 2002.

Kidder, S.Q., D.W. Hillger, A.J. Mostek, and K.J. Schrab, 2000: Two simple GOES imager products for improved weather analysis and forecasting. *National Wea. Digest*, **24**, 25-30.

Kunkel, B.A., 1984: Parameterization of droplet terminal velocity and extinction coefficient in fog models. *J. Clim. Appl. Meteor.*, **23**, 34-41.

Larrain, H., 2001: Three years of zoological records at a fog-site at Alto Patache, south of Iquique (Chile), during "El Niño" and "La Niña" (1997-2001). *Preprints, 2nd International Conference on Fog and Fog Collection,* St. John's, 297-300.

Lilly, D.K., 1962: On the numerical simulation of buoyant convection. *Tellus*, **14**, 148-172.

Mahrer, Y. and R.A. Pielke, 1977: A numerical study of airflow over irregular terrain. *Beitrage zur Physik der Atmosphare*, **50**, 98-113.

Mellor, G.L. and T. Yamada, 1982: Development of a turbulence closure model for geophysical fluid problems. *Rev. Geophys. Space Phys.*, **20**, 851-875.

Mesinger, F. and A. Arakawa, 1976: Numerical methods used in atmospheric models. GARP Publication Series, No. 14, WMO/ICSU Joint Organizing Committee, 64 pp.

Mesinger, F., T.L. Black, and M.E. Baldwin, 1999: Impact of resolution and of the Eta coordinate on skill of the Eta model precipitation forecasts. *Numerical Methods in Atmospheric and Oceanic Modeling: the Andre J. Robert Memorial Volume*, 399-423.

Meyers, M.P., R.L. Walko, J.Y. Harrington, and W.R. Cotton, 1997: New RAMS cloud microphysics parameterization. Part II: The two-moment scheme. *Atmos. Research*, **45**, 3-39.

Musson-Genon, L., 1987: Numerical simulation of a fog event with a one-dimensional boundary layer model. *Mon. Wea. Rev.*, **115**, 592-607.

Oliver, D.A., W.S. Lewellen, and G.G. Williamson, 1978: The interaction between turbulent and radiative transport in the development of fog and low-level stratus. *J. Atmos. Sci.*, **35**, 301-316.

Olson, J.S., J.A. Watts, and L.J. Allison, 1985: Major World Ecosystem Complexes Ranked by Carbon in Live Vegetation: A Database. NDP-017. Carbon Dioxide Information Center, Oak Ridge National Laboratory, Oak Ridge, Tennessee.

Pielke, R.A., Sr., 2000: *Mesoscale Meteorological Modeling, 2nd Ed*. Academic Press, San Diego, USA.

Pielke, R.A., W.R. Cotton, R.L. Walko, C.J. Tremback, W.A. Lyons, L.D. Grasso, M.E. Nicholls, M.D. Moran, D.A. Wesley, T.J. Lee, and J.H. Copeland, 1992: A comprehensive modeling system - RAMS. *Meteor. and Atmos. Phys.*, **49**, 69-91.

Pilié, R.J., E.J. Mack, W.C. Kocmond, W.J. Eadie, and C.W. Rogers, 1975a: The life cycle of valley fog. Part I: Micrometeorological characteristics. *J. Appl. Meteor.*, **14**, 357-363.

Pilié, R.J., E.J. Mack, W.C. Kocmond, W.J. Eadie, and C.W. Rogers, 1975b: The life cycle of valley fog. Part II: Fog microphysics. *J. Appl. Meteor.*, **14**, 364-375.

Reynolds, R.W., N.A. Rayner, T.M. Smith, D.C. Stokes, and W. Wang, 2002: An improved in situ and satellite SST analysis for climate. *J. Climate.*, **1610**, 1609-1625.

Rodhe, B., 1962: The effect of turbulence on fog formation. *Tellus*, **14**, 49-86.

Rogers, E., T.L. Black, D.G. Deaven, G.J. DiMego, Q. Zhao, M.E. Baldwin, N.W. Junker, and Y. Lin, 1996: Changes to the operational Early Eta analysis/forecasting system at the National Centers for Environmental Prediction. *Wea. Forecasting*, **11**, 391-413.

Seagraves, M.A. and R. Szymber, 1995: Weather: a force multiplier. *Military Review,* **75**, 69-75.

Seinfeld, J.H. and S.N. Pandis, 1998: *Atmospheric chemistry and physics*. Wiley-Interscience, New York, USA.

Smagorinsky, J., 1963: General circulation experiments with the primitive equations. I. The basic experiment. *Mon. Wea. Rev.*, **91**, 99-164.

Tag, P.M. and J.E. Peak, 1996: Machine learning of maritime fog forecast rules. *J. Appl. Meteor.*, **35**, 714-724.

Teixeira, J., 1999: Simulation of fog with the ECMWF prognostic cloud scheme. *Quart. J. Roy. Meteor. Soc.*, **125**, 529-552.

Tremback, C.J., 1990: Numerical simulation of a mesoscale convective complex: Model development and numerical results. PhD Diss., Atmos. Sci. paper no. 465, Colorado State University, Department of Atmospheric Science, Fort Collins, CO 80523.

Tripoli, G.J. and W.R. Cotton, 1982: The Colorado State University three-dimensional cloud/mesoscale model-1982. Part I: General theoretical framework and sensitivity experiments. *J. Rech. Atmos.*, **16**, 185-220.

Tripoli, G.J. and W.R. Cotton, 1986: An intense, quasi-steady thunderstorm over mountainous terrain. Part IV: Three-dimensional numerical simulation. *J. Atmos. Sci.*, **43**, 896-914.

Verlinde, J., P.J. Flatau, and W.R. Cotton, 1990: Analytical solutions to the collection growth equation: Comparison with approximate methods and application to cloud microphysics parameterization schemes. *J. Atmos. Sci.*, **47**, 2871-2880.

Walko, R.L., W.R. Cotton, M.P. Meyers, J.Y. Harrington, 1995: New RAMS cloud microphysics parameterization, Part I: the single moment scheme. *Atmos. Research,* **38**, 29-62.

Walko, R.L., L.E. Band, J. Baron, T.G.F. Kittel, R. Lammers, T.J. Lee, D. Ojima, R.A. Pielke, Sr., C. Taylor, C. Tague, C.J. Tremback, and P.L. Vidale, 2000: Coupled atmosphere-biophysics-hydrology models for environmental modeling. *J. Appl. Meteor.*, **39**, 931-944.

Weathers, K.C., 1999: The importance of cloud and fog in the maintenance of ecosystems. *Trends in Ecology and Evoltuion*, **14**, 214-215.

Webb, R. S., C. E. Rosenzweig, and E. R. Levine, 1993: Specifying land surface characteristics in general circulation models: Soil profile data set and derived water-holding capacities. *Global Biogeochem. Cycles*, **7**, 97-108.

Whiffen, B., 2001: Fog: impact on aviation and goals for meteorological prediction. *Preprints, 2nd International Conference on Fog and Fog Collection,* St. John's, 525-528.

Xue, M., J. Zong, and K. K. Droegemeier, 1996: Parameterization of PBL turbulence in a multi-scale non-hydrostatic model. *Preprint, 11th AMS conference on Numerical Weather Prediction,* Amer. Meteor. Soc., Norfolk, VA., 363-365.

Zängl, G., 2002: An improved method for computing horizontal diffusion in a sigma-coordinate model and its application to simulations over mountainous topography. *Mon. Wea. Rev.*, **130**, 1423-1432.

Zdunkowski, W.G. and B.C. Nielsen, 1969: A preliminary prediction analysis of radiation fog, *Pure Appl. Geophys.*, **75**, 278-299.